Development of Methods for Element-Wise Assessment of Oscillatory Rotor Angle Stability

Müller, Daniel

Publication date:
2021

Document Version
Publisher's PDF, also known as Version of record

Center for Electric Power and Energy

Development of Methods for Element-Wise Assessment of Oscillatory Rotor Angle Stability

Daniel Müller

PhD Thesis, March 2021, Kongens Lyngby, Denmark

DANMARKS TEKNISKE UNIVERSITET
Center for Electric Power and Energy (CEE)
DTU Electrical Engineering

Development of Methods for Element-Wise Assessment of Oscillatory Rotor Angle Stability

Udvikling af metoder til elementvis vurdering af svingende rotorvinkelstabilitet

Dissertation, by Daniel Müller

Supervisors:
Arne Hejde Nielsen, Technical University of Denmark
Hjörtur Jóhannsson, Technical University of Denmark
Kjetil Uhlen, Norwegian University of Science and Technology

DTU - Technical University of Denmark, Kgs. Lyngby - April 2021

Development of Methods for Element-Wise Assessment of Oscillatory Rotor Angle Stability

This thesis was prepared by:
Daniel Müller

Supervisors:
Arne Hejde Nielsen, Technical University of Denmark
Hjörtur Jóhannsson, Technical University of Denmark
Kjetil Uhlen, Norwegian University of Science and Technology

Dissertation Examination Committee:
Examiner No. 1 (Chairman)
Department of Electrical Engineering, Technical University of Denmark, Denmark

Examiner No. 2
Department of XX, University of XX, Country

Examiner No. 3
Department of XY, Technical University of YY, Country

Center for Electric Power and Energy (CEE)
DTU Electrical Engineering
Elektrovej, Building 325
DK-2800 Kgs. Lyngby
Denmark

Tel: (+45) 4525 3500
Fax: (+45) 4588 6111
E-mail: cee@elektro.dtu.dk

Release date: 28.02.2021

Edition: 1

Class: Internal

Field: Electrical Engineering

Remarks: The dissertation is presented to the Department of Electrical Engineering of the Technical University of Denmark in partial fulfillment of the requirements for the degree of Doctor of Philosophy.

ISBN: 000-00-00000-00-0

Preface

This thesis is prepared at the Department of Electrical Engineering of the Technical University of Denmark in partial fulfillment of the requirements for acquiring the degree of Doctor of Philosophy in Engineering. The Ph.D. project was funded by a joint cooperative between the Technical University of Denmark (DTU) and the Norwegian University of Science and Technology (NTNU).

This dissertation summarizes the work carried out by the author during his Ph.D. project. It started on 01st November 2017, and it was completed on 28th February 2021. During this period, he was hired by the Technical University of Denmark as a Ph.D. student at the Center for Electric Power and Energy (CEE).

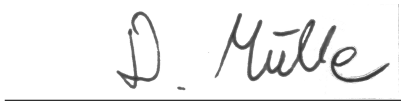

Daniel Müller
28.02.2021

Acknowledgements

First and foremost, I would like to thank my team of supervisors Hjörtur Jóhannsson, Arne Hejde Nielsen and Kjetil Uhlen for their consistent support and guidance throughout the project and for giving me the opportunity to pursue this PhD.

In my three years as a PhD at DTU I was lucky to meet numerous talented colleagues, who I really enjoyed working with. A special thanks to my long term roommates Mirza and Kanakesh, for creating a nice working environment and the entertaining breaks from work.

From May until November 2019 I had the pleasure to spend half a year at NTNU in Trondheim. I would like to express my thanks to all the nice colleagues and friends, that I met there, and who have made my external research stay such a great experience. Unfortunately, the circumstances prevented me from coming back in 2020 but I am sure, I will be visiting again some day. A special thanks goes out to Hallvar for the discussions and collaborations during the research project.

Finally I would like to thank my family for their continuous support throughout my studies and without whom, I would have never come thus far. My friends, both back home in Frankfurt, as well as here in Copenhagen who allowed me to take my mind off from work when needed and and enrich my life in so many ways. Last but not least, a very special thanks to Ana for her amazing and endless support.

Daniel Müller

Copenhagen, Denmark, 2021

Table of Contents

List of Figures

List of Tables

Abstract

This thesis concerns the development of methods that can detect emerging stability issues related to undamped low frequency power oscillations. Power oscillations are caused by interactions of the dynamic system components and are an inherent property of interconnected electric power systems. As such the occurrence of these oscillations cannot be prevented but as long as they are well damped they do not affect the stability of the system. Certain operating conditions, however, can lead to oscillations of increasing magnitude, which in the worst case can lead to a complete system blackout. It is therefore of interest to develop a method which can predict the operating conditions under which the damping becomes critical and provide margins that can help the operator to counteract emerging stability problems in due time.

The fundamental mechanisms that govern the characteristic of the oscillations were investigated. It was shown that the problem consists of two separate layers. The first layer concerns the dynamic properties of the system at the oscillatory frequency and the second is related to the steady state operating conditions that affect the dynamic performance of the system. In order to obtain a representative stability margin, the conditions that lead to instability of the dynamic system were determined. Furthermore, the interactions between the two layers were analyzed and a methodology, capable of identifying the steady state operating conditions which violate the instability condition of the dynamic system, was developed.

The stability boundary is determined by combining the sensitivity information of the steady state parameters at a given operating point with the derived sensitivities of the dynamic system. The relevant sensitivities are obtained as a result of the perturbation of the active power injection of a particular machine in the system. The resultant distance to the point of instability is therefore assessed on an element-wise basis providing an individual stability margin that is given as the maximum power a machine could inject into the system before instability occurs. To provide an informative measure of the distance to instability the maximum power that a machine could inject before the stability boundary is crossed is given as a percentage margin related to the loading of the machine.

The assessment method was implemented in an algorithm that efficiently performs the required steps for carrying out the stability assessment. The algorithm takes snapshots of the current system state provided by phasor measurement units or state estimators as input and analyzes the stability of the given operating point. With further optimization the developed algorithm should be suited to perform a stability assessment of large power systems close to real time.

The method was tested on a representation of the Nordic power system consisting of Norway, Sweden, Denmark and Finland. It was shown that the method was able to detect critical stability margins and relate the critical margin to specific system components and thereby already provides indicators for potential counter-measures. The method was capable of accurately predicting the distance to instability well away from the critical boundary and would therefore allow to apply suitable counter-measures in due time to prevent an emerging blackout.

Resumé

Nærværende afhandling vedrører udvikling af metoder til detektering af begyndende stabilitetsproblemer med udæmpede lavfrekvente effektsvingninger i elsystemet. Effektsvingninger opstår ved vekselvirkning mellem dynamiske systemkomponenter og er en naturlig egenskab i et større sammenkoblet elsystem. Effektsvingninger kan altså ikke undgås, men så længe de er tilstrækkeligt dæmpede påvirker de ikke stabiliteten i elsystemet. Imidlertid kan visse driftstilstande føre til svingninger med øgende amplitude, og i værste tilfælde føre til totalt blackout i elsystemet. Derfor er det af betydning at udvikle metoder til at detektere driftstilstande, hvor svingninger bliver kritiske og at udvikle sikkerhedsmarginer til hjælp for personale til at tidligt modvirke begyndende sikkerhedsproblemer.

De grundlæggende mekanismer, der bestemmer svingningernes karakteristik, er undersøgt. Det er påvist, at problemerne har to niveauer. Det første niveau vedrører systemets dynamiske egenskaber ved svingningernes frekvens, og det andet vedrører driftstilstande, der påvirker systemets dynamiske egenskaber. For at udvikle repræsentative sikkerhedsmarginer blev årsagerne til sikkerhedsproblemer bestemt. Yderligere blev vekselvirkningen mellem de to niveauer analyseret og der blev udviklet en metode til identifikation af de driftstilstande, der kan føre til ustabilitet i elsystemet.

Stabilitetsgrænsen blev bestemt ved at kombinere information om parameter sensivitet i driftstilstanden med sensivitet i det dynamiske system. Den relevante sensivitet blev bestemt ved pertubationer i effekttilførslen i en bestemt generator i systemet. Den resulterende sikkerhedsmargin er bestemt ved at maskine for maskine at bestemme en stabilitetsgrænse ved at bestemme den maksimale effekttilførsel for de individuelle maskiner. Stabilitetsmarginen for den enkelte maskine er angivet ved en maksimal effektforøgelse regnet i procent af den aktuelle tilførte effekt. Analysemetoden blev implementeret i en algoritme, der effektivt udfører de trin, der er nødvendige for stabilitetsanalysen. Algoritmen tager et øjebliksbillede at driftstilstanden ved faseværdier (PMU date) eller tilstandsestimatorer og finder stabiliteten i det aktuelle arbejdspunkt. Med yderligere optimeringer vil systemet være egnet til stabilitetsanalyse i store elsystemer i real tid.

Metoden blev testet på en model af det nordiske elnet bestående af Norge, Sverige, Danmark og Finland. Det blev vist, at metoden er i stand til at detektere kritiske stabilitetsgrænser og at pege på de kritiske komponenter og derved anvise metoder til at modvirke ustabilitet. Metoden var i stand til at forudsige en nøjagtig stabilitetsmargin selv ved stor afstand til ustabilitet og derved at hjælpe til at iværksætte modforanstaltninger for at undgå begyndende blackout.

CHAPTER 1

Introduction

1.1 Background

Power system oscillations involving large portions of the system are closely coupled to the flow of power over a set of transmission lines that connect individual subsystems. The damping ratio of such an oscillatory mode depends to a large portion on the strength of the interconnection, and an increasing power flow can weaken the system to an extend that undamped oscillations occur. Historically power system have been built with a national or regional focus with a limited amount of cross regional interconnectors since there was also not much incentive for trading large amounts electric power across borders. The strength of the internal system was therefore much larger than the strength of the system connecting different regions. The lines which represent the bottleneck in terms of oscillatory small signal stability are therefore quite often the interconnections between separate control areas. With an increasing amount of fluctuating renewable energy sources (RES) installed in the system the situation changes considerably. In times of high availability there is a large amount of production capacity available that can be exported if the local generation exceeds the demand. To fully exploit the capacity of RES it is of interest to allow power transfer from regions with high renewable availability to areas with low availability. Apart from constructing additional system interconnections it is beneficial to maximize the transmission capacity of the existing transmission corridors. This, however, requires operation of the system closer to its stability limit, and methods that can reliable determine the distance to instability based on on-line measurements are needed. Traditionally, transfer capacity limits have been set based on operational experience and off-line analysis. Methods that can exploit the observability provided by the increasing amount of phasor measurement units (PMU) installed in the system allow to provide system operators with a dynamic stability margin by continuously deriving the applicable stability boundary based on available measurements.

1.2 Project objective

The secure operation of electric power systems is challenged by various mechanisms of different physical nature that can cause the system to become unstable and therefore lead to the activation of emergency measures such as load shedding. An overview of these mechanisms as defined by a joint CIGRE and IEEE PES taskforce in 2004 [1] is presented in figure 1.1. To guarantee a stable supply of electricity it is imperative that the system is operating with a sufficiently large stability margin in respect to any of these mechanisms at all times. Providing awareness about existing margins in real-time can help to identify the most critical mechanism. This allows the operator to address emerging issues by applying suitable countermeasures in due time and avoid the need to activate drastic emergency measures.

Previous research has led to the development of a wide-area real-time software package that evaluates the overall stability of the system by employing a set of methods that address each

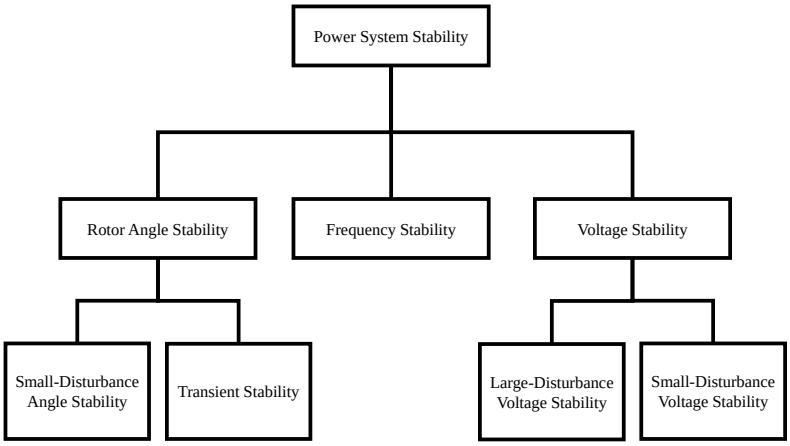

Figure 1.1: Classification of Power System Stability according to [1]

possible mechanisms leading to instability individually. The methods are executed in parallel and their results are then combined to provide an overall picture of the system state at any given time. The platform analyses snapshots of the system state provided by phasor measurement units and state estimators and determines the stability boundaries that apply for the mechanisms that can potentially cause instability. The currently implemented methods address voltage stability [4], aperiodic small signal rotor angle stability [5] and transient stability [6]. Further elements include a fast assessment of n-1 post fault operating points [7] and the derivation of proposed control actions based on the results of the stability assessment [8]. Each of the methods employs an element-wise approach that identifies the distance to instability related to a particular component or characteristic group of components and therefore allows to point out critical elements in the system. An overview of the software platform is presented in figure 1.2.

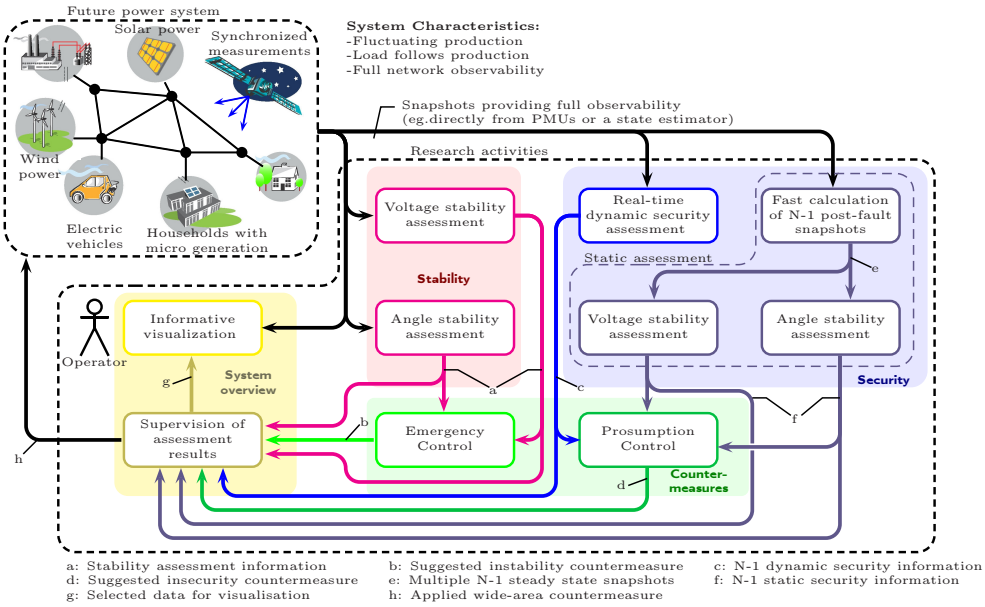

Figure 1.2: Overview of the envisioned software package

The method developed in this thesis aims at contributing to the overall package by addressing oscillatory small signal rotor angle stability. In the framework of the wide-area software package, the method contributes to stability assessment, where it is located along the methods addressing voltage and rotor angle stability. The envisioned method should:

- Be able to identify critical elements in the system
- Provide a meaningful stability margin associated with individual elements in the system
- Be able to operate in real- or near real-time to fully exploit the high update rate of PMUs in the system

For the stability margin to be meaningful it is important that it is evaluated in respect to parameters that provide value to the observer and are in the best case controllable. The natural choice for such a parameter in respect to generating units would be the active power injection, that is the loading of the machine at a given operating point. The envisioned method would therefore be able to derive the maximum power that an individual generating unit can inject into the system before the system becomes oscillatory unstable.

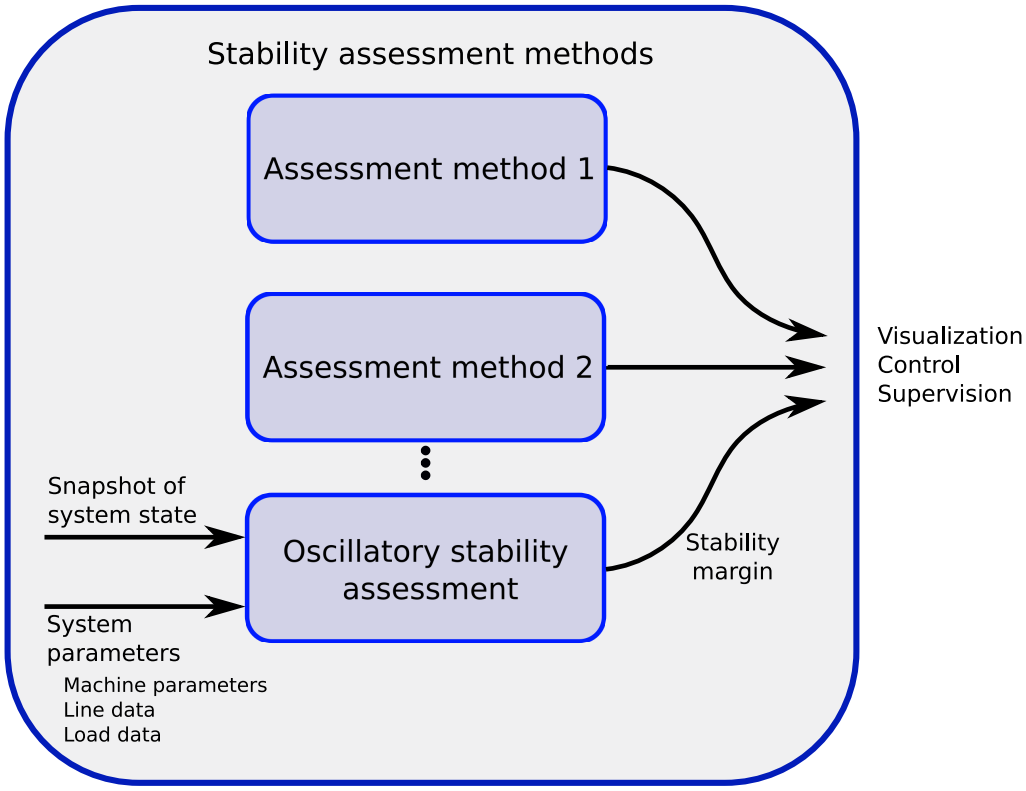

Figure 1.3: Overview of the proposed method

The proposed design of the method is illustrated in figure 1.3 The method:

1. Receives a snapshot of the system by state estimators and PMUs
2. Considers changes in the system structure or model parameters

3. Combines the system snapshot and model data to determine the stability margin
4. Relates the stability margin to active power injections of the machines
5. Provides an output that can be further processed by:
    - Visualizing the system state in an informative manner
    - Incorporating automated control schemes that are activated in the state of emergency
    - Forwarding numerical results for supervisory access

The output of the method is a percentage loading that evaluates the current active power injection against the maximum injection determined by the method. The outcome of the assessment is ready to be forwarded to subroutines of the platform providing informative visualizations that help the operator to quickly identify emerging stability issues and thereby contribute to an early warning system. Furthermore the results can be implemented in emergency control methods proposing optimal control actions that reestablish secure operation.

1.3 Contribution

The main contributions presented in this thesis are listed below:

- *An analysis of the mechanism that leads to oscillatory instability*: The mechanism leading to oscillatory instability is analysed based on the modal components of the electrical torque. The relationship between the oscillations observed in the speed of the machines and the damping contribution of individual machines is provided.
- *A method that allows an element-wise assessment of the damping contributions to the oscillatory modes*: A method is developed that allows to extract information regarding the contribution of particular areas in the system and individual devices to the system eigenvalue.
- *A method for real-time assessment of oscillatory stability*: A method that allows an element-wise assessment of oscillatory stability margins based on eigenvalue sensitivity is developed.
- *Analytical expressions for the derivatives of several device function are developed*: The explicit derivatives of the machine transfer functions in respect to modal frequency and the power flow dependent variables are developed. Derivatives for constant impedance, constant current and constant power loads are presented.
- *A framework for the visualization of the assessment is proposed*: An approach that allows informative visualization of the distance to instability for all machines in the system at once is proposed. Information regarding critical elements in the system is directly accessible and can be evaluated quickly to initiate countermeasures.
- *Development of fast algorithms that enable execution rates suitable for online application* A fast algorithm was developed that maximizes the synergies between the different sub-functions. A full assessment of a system with 29 machines, 179 busses and 263 unique branches could be performed in 35.8 ms.
- *A test that demonstrates the added value of the method was performed* A test of the method is performed on a representation of the Nordic power system. The method was able to detect emerging stability issues related to an inter-area mode while the damping ratio of the oscillation was well above any critical value.

1.4 Thesis organization

The thesis is structured into five different parts and a total of 9 chapters as follows:

- ***Part I:*** **Background and State of the Art**
  - *Chapter 2:* Introduces the reader to the oscillatory stability problem and describes countermeasures that address oscillatory stability on different instances in the operation of the power system.
  - *Chapter 3:* Serves as an introduction to phasor measurement units (PMU). The basic working principle and the application of data provided by PMUs relevant for the assessment of oscillatory stability assessment are discussed.
- ***Part II:*** **Method Development**
  - *Chapter 4:* Provides the mathematical and modeling background relevant for the developed method.
  - *Chapter 5:* Provides an analysis of the mechanism that causes oscillatory instability. Further a method is introduced that provides an element-wise assessment of damping contributions.
  - *Chapter 6:* Describes the method proposed for the assessment of oscillatory stability. The mathematical concepts of chapter 4 are extended and the process to obtain the distance to instability information is described.
- ***Part III:*** **Method Implementation and Performance Evaluation**
  - *Chapter 7:* The implementation of the method is discussed. The main algorithm and the individual functionalities are presented. The description is accompanied with an assessment of the computational performance of the main algorithm as well as the subroutines.
- ***Part IV:*** **Test of Method**
  - *Chapter 8:* Describes the test of the method on the example of the Nordic power system.
- ***Part V:*** **Conclusion and Perspective**
  - *Chapter 9:* Conclusion and topics for future research related to the developed method

1.5 List of publications

The publications prepared during the project period are listed in the following:

- Müller, D., Johannsson, H., & Uhlen, K. (2020). *Impact of Reduced Synchronous Machine Capacity on Damping and Phase of Inter-Area Oscillations*. In Proceedings of 2020 IEEE PES Innovative Smart Grid Technologies Europe (pp. 394-398). IEEE.
- Müller, D., Johannsson, H., Uhlen, K. & Nielsen, A. H. *A Method to Determine the Distance to the Critical Oscillatory Stability Limit in Terms of Active Power Injections*. IEEE PES PowerTech 2021. Accepted.

- Müller, D., Johannsson, H., Uhlen, K. & Nielsen, A. H. *Online Assessment and Awareness of Critical Oscillatory Staility Limits - Method, Implementation and Visualization*. Journal submission. Manuscript.

The author also had minor contributions in the following publication:

- Haugdal, H., Uhlen, K., Müller, D., & Johannsson, H. (2020). Estimation of Oscillatory Mode Activity from PMU Measurements. In Proceedings of 2020 IEEE PES Innovative Smart Grid Technologies Europe (pp. 201-205). IEEE.

Part I

Background and State of the Art

CHAPTER 2

Oscillatory stability of power systems

This chapter serves as an introduction to the oscillatory stability problem. Methods to address potential issues related to oscillatory stability are presented and some real-life examples of events caused by power system oscillations are provided.

2.1 Background

The problem addressed in this thesis concerns the damping of low frequency electromechanical oscillations in particular that of inter-area oscillations. Whenever the active power balance in an electric power system is disturbed, the additional energy flows through the system and is picked up by the machines where it is converted into kinetic energy. In case of a load reduction the excess energy causes the rotor to accelerate, leading to mismatches between the speeds in different areas of the system. Due to the governing principle of synchronous machines these speed differences are counteracted by a change in electrical power which aims at restoring synchronism in the system. The inertia of the rotating masses prevents the speed from changing instantaneously which results in an oscillatory motion of the system as machines in different parts of the system exchange energy back and forth. The resulting motion is characteristic for a specific system, as the machines align in a particular way, reflected by different magnitudes and phases of the speed variations in the separate parts. The oscillatory motion of the system can be further described in terms of its frequency and damping ratio. The frequency of the motion reflects the coupling strength of the machines; due to the underlying power-angle characteristic; as well as the involved inertia. The damping refers to the ability of the system to remove energy from the oscillation as it propagates through the system. The oscillation persists until all its initial energy is depleted. While a large positive damping causes the oscillation to vanish after a few cycles, zero or negative damping result in sustained oscillations with constant or even increasing magnitude. In a complex power system there are a large number of such system inherent oscillatory modes, termed the natural modes of the system and for the secure operation of electric power systems it has to be guaranteed that all the system modes are sufficiently damped at all times.

Each of the natural system modes involves a different configuration of machines located in different areas of the power system. These modes can either be confined to a small region of the power system and therefore be considered local or spread across large parts of the system called inter-area modes. Local modes of oscillation concern only a small amount of machines and due to the smaller amount of inertia and the relatively strong coupling between the participating machines the frequency is higher than that of the inter-area modes. The range of frequency of local modes is typically 1-3 Hz. Inter-area modes are characterized by the movement of large areas separated by

long distances against each other and are therefore located at much lower frequencies; typically in the range of 0.1-1 Hz.

The previously described mechanisms apply to a system that is excited internally by a displacement of the operating point as it is for example caused by minor disturbances such as small variations of the system load. Transient disturbances such as line outages or short circuits also tend to converge towards the natural oscillation modes after the initial nonlinearities of the system response have vanished. On certain occasions the system can as well be subject to an external force acting on the system typically related to some malfunctioning equipment which results in a forced oscillation. A short description of the two different mechanisms is given below.

- **Natural response**: The natural response of the system in the absence of a driving external force. The oscillations are characterized solely by the interaction of the dynamic components in the system. The resulting modes of oscillation are the natural frequencies of the system.
- **Forced response**: Oscillations are caused by an external force acting on the system. The resulting oscillatory behavior of the system depends on the interaction of the system with the external force. These types of oscillations are typically caused by some malfunctioning equipment.

The analysis and mitigation of the oscillatory stability problems related to these two different mechanisms vary substantially.

Forced oscillations occur as sustained oscillations that persist until the source is deactivated. The shape of the observed oscillation as well as its effect on the overall stability of the system depends on the interaction of the system with the external source. The stability of the system is particularly threatened if the frequency of the external source lies close to a natural mode of the system resulting in a resonance or near-resonance case [9]. If the frequency of the forced oscillation coincides with a low damped natural mode, the magnitude of the oscillation is amplified. An example of such an event is described in [10] where a forced oscillation due to a malfunctioning speed governor in a power plant in Florida resonated with a natural inter-area mode of the system causing sustained oscillations in the magnitude of several hundred megawatts. Since forced oscillations mostly occur quasi random due to equipment failure neither their shape nor the effect on system stability can be predicted ahead of time and therefore must be handled in real-time. The only way to mitigate forced oscillations is thus to correctly identify and eliminate the source of the oscillation. Since the topic of forced oscillations is out of the scope of this thesis, methods for locating sources of forced oscillations are not discussed in detail here. An overview of some of the methods used for the analysis of forced oscillations is provided in [11] and some of the currently implemented methods in the control rooms of transmission system operators are presented in [12].

In contrast to forced oscillations, the behavior of the natural system modes can, in theory, be predicted ahead in time if the particular operating conditions as well as the underlying dynamics of the systems are known. The common process involves the analysis of the dynamic state admittance matrix, linearized about a specific operating point, in respect to its eigenproperties. The general procedure of constructing the state matrix and deriving the relevant properties from it is well illustrated in [13]. The eigenvalues and eigenvectors obtained from performing an eigenanalysis provide insight into the dynamic properties of a system within a specific mode and allow to identify

potential stability issues. The main characteristic of an oscillatory mode are its natural frequency and damping which are contained in its eigenvalue.

$$\lambda = \sigma \pm j\omega \tag{2.1}$$

The time response of an oscillatory mode observed in some arbitrary state variable of the system x has the general form

$$x(t) = c\, e^{\lambda t} \tag{2.2}$$

Where c describes the initial magnitude in the mode related to the disturbance that excites the mode.

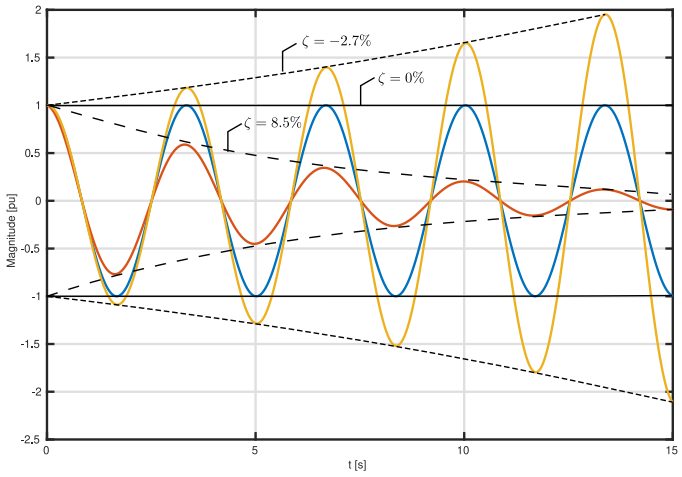

Figure 2.1: Oscillatory mode with different damping constants

For a complex eigenvalue, the time response in (2.2) oscillates with the frequency ω given by the imaginary part of the eigenvalue.The trajectory of the magnitude of the oscillation is related to the real part of the eigenvalue and is either

- constant: If the eigenvalue is purely imaginary. $\sigma = 0$
- increasing: If the real part of the eigenvalue is positive. $\sigma > 0$
- decreasing: If the real part of the eigenvalue is negative. $\sigma < 0$

The three different cases are illustrated in figure 2.1 showing the exemplary trajectories of the oscillatory magnitude over time for a $0.3\,\mathrm{Hz}$ mode. A system can be considered oscillatory stable as long as the real part of the eigenvalue, which indicates the rate of decay of the oscillation, is negative. From a practical perspective it is, however, desirable to operate the system with a certain damping margin to guarantee that oscillations die out in a limited amount of cycles. An overview of practical requirements in respect to damping of oscillatory modes reported by several utilities can be obtained from [14].

2.2 Addressing oscillatory stability on different time scales

Mitigation of stability issues related to the natural system modes can be addressed on a number of levels which can be generally related to a certain time frame as indicated in figure 2.2.

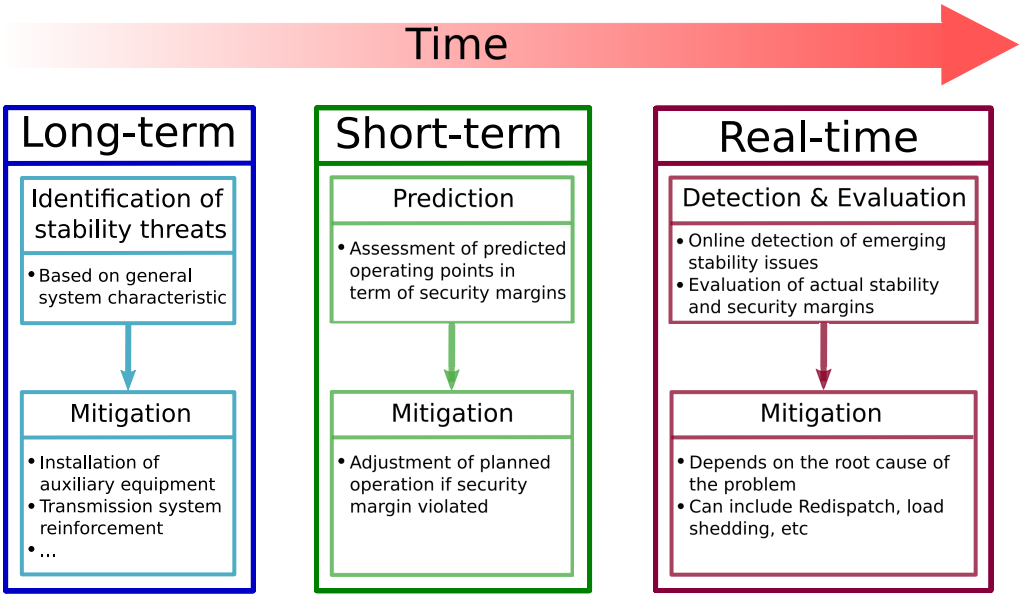

Figure 2.2: Oscillatory stability assessment of the power system and possible mitigation strategies at different levels

The first layer relates to the general observed or analytically obtained behavior of the system in respect to a variety of operating points. The second layer concerns the operational planning when the system load is predicted and generation capacity is allocated. In this stage the predicted operation is assessed against predetermined security margins which also consider possible contingencies. The third layer finally addresses the real-time operation where the stability of a given operating point needs to be evaluated against the actual security and stability margins in the system.

2.2.1 Oscillatory stability in the long-term

Global or local weaknesses with respect to the system dynamic performance can be addressed by adding additional equipment to improve its robustness in the long-term. Bottlenecks in the transmission system that occur due to stability imposed limitations can be eliminated by providing additional transfer capacity at the critical transmission corridors.
The most straightforward solution to damp power system oscillations is to address the problem at its source. Weakly damped oscillations became a prominent issue as soon as synchronous machines were equipped with fast acting excitation systems that helped to improve the transient stability of the system due to their improved voltage control capabilities. The improvement in respect to one mechanism of instability, however, came at the cost of a reduced damping of the characteristic system modes and special control systems that allowed to provide sufficient damping needed to be developed. Power system stabilizers (PSS) provide such a mean by generating a supplementary signal that modulates the excitation voltage of the machines [15]. In the ideal case the modulated voltage creates a torque component that counteracts the oscillation and improves the damping in the system over the whole frequency range of the system modes. The selection of optimal sites for PSS placement as well as the tuning procedure necessary to provide damping across a wide range of frequencies is not a trivial task but will not be discussed in detail here. An illustrative introduction to the tuning process of power system stabilizers can found in Graham Rodgers book

[16]. The coordinated tuning of PSS involving optimal placement and finding suitable control parameters is also addressed in a variety of publications such as [17], [18] and [19].
Another mean to improve system stability in the long-term is installing power oscillation damping devices at suitable locations in the system or implementing additional control loops for oscillation damping in existing devices. Any device that is capable of manipulating the power flow in the system in a controlled manner is, in principle, capable of providing such a service. The only strictly necessary condition is, that the oscillatory mode can be influenced by the output of the device. The controllability of a certain mode by a given output depends to a large extend on the location of the device in the system in respect to the characteristic of the mode. The input signal to the control can either be a local measurement or a remote signal, whichever is considered to be suitable in terms of performance and robustness. Typical examples for such devices include power electronically controlled flexible AC transmission system (FACTS) devices [20] or high voltage direct current (HVDC) systems. More information regarding the strategy in respect to tuning FACTS devices and their modeling for the purpose of small signal stability studies is provided in [21]. For details regarding HVDC systems and their prospects in terms of oscillation damping it is referred to [22] or [23].

2.2.2 Assessment of oscillatory stability in operational planning

All the aforementioned means to mitigate oscillatory stability problems concern the stability of the system in the long-term by generally improving the dynamic performance. The second stage in figure 2.2 relates to the scheduling of the power system operation where generation capacity is allocated depending on the predicted system load at a given time. The task here is to assess the stability of a planned operating point in terms of its security margins with respect to several stability mechanisms also considering a set of credible contingencies in order to make the system n-1 secure. Identified stability issues can be addressed by adapting the dispatch scenario until all security margins are considered sufficiently large. This can for example be achieved by incorporating small signal stability margins as a constraint in security constrained optimal power flow which is a topic addressed in numerous publications including [24],[25] and [26]. In [27] a contingency screening method is combined with eigenvalue sensitivity analysis to provide an optimal generator scheduling that maximizes the transmission capacity of the system. A general procedure to derive the smallest distance to instability of a scheduled operating point in a generalized parameter space is presented in [28].

2.2.3 Real-time assessment of oscillatory stability

A large power system consists of a multitude of individual elements and is subject to external influences such as e.g. prevailing weather conditions. Hence, it can never be entirely guaranteed that the system behaves exactly as predicted. Unforeseen outages or inadequate prediction of available generation capacity can lead to unforeseen operating conditions that are much closer to the actual stability limit than anticipated. These kind of situations can occur spontaneously and might require an immediate response from the system operator. To be able to mitigate stability issues occurring during operation of the power system, the first and most important step is to detect the emerging problems as soon as possible. If a potentially threatening operating condition goes undetected it can lead to severe consequences, which in the worst case can lead to a complete

system blackout. A precondition for the detection of immanent stability issues is that the process leading to instability can be observed from measurements of the system state. In this aspect the deployment of phasor measurement units, which will be further examined in chapter 3, plays a vital role due to the observability they can provide.
The second step is then associated with extracting the necessary information from the existing measurements. This process is related to the application of analytical tools that allow to assess the security of the observed operating point in respect to the mechanisms that cause instability. In terms of the oscillatory stability that includes an assessment of the damping and frequency of the dominant system modes.

At this stage, mitigation of stability issues has to be addressed in real-time and quick decision making is necessary to maintain stable operation. The actions that need to be taken to reestablish secure operation depend on the root cause of the problem and the current state of the system. They can range from a relatively simple redispatch to more drastic measures such as load shedding or islanding of certain system parts. To limit the amount of necessary intervention it is important to detect the emerging issue in due time as well as identify its root accurately. Some methods related to the identification of sources of forced oscillations were already mentioned in the beginning of this chapter. Some methods currently employed for real-time detection of oscillatory stability problems related to the natural system modes are further discussed in chapter 3.

Presently the assessment of the stability of the oscillatory stability of the system is based solely on the estimated damping. Several methods are proposed to provide the optimal redispatch when the detected damping ratio is low. In [29] a method that identifies the transmission lines that have the largest impact on the modal damping is presented. A method that aims at rescheduling the active power output to limit the minimum damping to a certain value is reported in [30]. The authors of [31] present a method to determine the small signal stability margin in respect to the loading of the system. Further methods dealing with the topic of finding the optimal redispatch action to achieve a certain damping ratio are reported in [32] and [33].

2.3 Oscillatory events in power systems

Perhaps the most prominent event, due to its severity, that can be linked to insufficient small signal oscillatory stability is the Western Systems Coordinating Council (WSCC) 1996 system outage [34]. The lack of sufficient damping and the resulting growing oscillations ultimately led to a split up of the system and a subsequent loss of more than 30 GW of load in the Western US. The incident which initiated the chain of event was a line outage that occurred during high power transfers. As the power was rerouted to other transmission lines more failures occurred to overloading of the lines. When one of the hydroelectric generating stations tripped due a malfunctioning protection system the power was picked up by other generators which further weakened the system. Ultimately, large undamped power oscillations started to occur which caused the protection system to split the system into smaller islands with inadequate generation capacity.

On February 19, 2011 and February 24, 2011 two very similar oscillation events took place in the Continental European (CE) system. The recordings from three different locations in Switzerland, Italy and Denmark in figure 2.3 show that the magnitude of the oscillations continued to increase for about 8 minutes until the damping became positive and the oscillation started to decline. In the report prepared by the European Network Transmission System Operators for Electricity (ENTSO-E) working group [2] that performed the post-event analysis it is stated that:

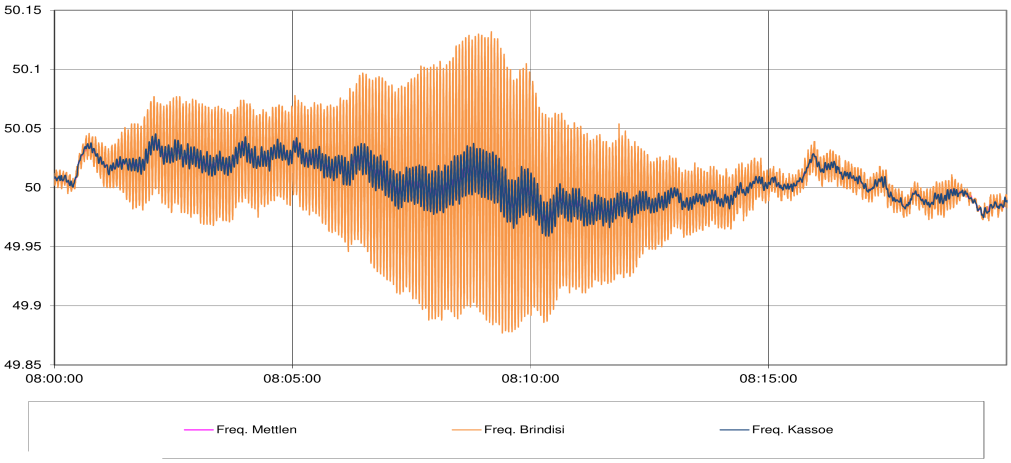

Figure 2.3: Oscillation event that occurred on February 19, 2011 in the synchronized European grid. The graph shows recordings of the system frequency from three different locations. The image is taken from the incident report prepared by the ENTSO-E working group [2]

> The oscillations started and finished without direct correlation to any known disturbances or forced outages of transmission lines, power plants or system loads. Only the fact that the oscillations started around the change of the hour and related changes of generation pattern within whole Europe due to schedule changes might have resulted in corresponding decrease of overall system damping.

The correlation of redispatch and the occurrence of the oscillation suggests that the event was related to certain power flow conditions. In particular since almost the same event could be observed a few days later.

On December 01, 2016 a transmission line connecting Spain to France unexpectedly opened while the power export from Spain into France was relatively high. The increased impedance triggered undamped oscillations that lasted for about 5 minutes until the power export was reduced. The conclusion of the report [35] states that:

> The event demonstrates that coincidence and combination of different factors can influence the system stability. Each factor may not normally be critical in itself, but in this particular case the combined effect decreased the general damping. The physical aspects and root causes of phenomena are clear and as demonstrated in the present report. In fact this event shows that power transport over long distances together with too high impedance can cause a too low system damping with respect to inter-area oscillations and should, therefore, be treated carefully.

Another incident that occurred on December 03, 2017 is described in [36] where undamped oscillations were observed in southern Italy. In the report of the event the system conditions leading to it were described as:

Very low consumption (decrease of load contribution to damping)

High voltage angle difference between inside Italy

Unavailability of some generators leading to a non-standard power flow in the system during a time of very low demand

Huge import in the southern part of the ENTSO-E system

Prior to the event no violations of standard operating parameters could be determined. The mode that became underdamped was a well known mode in the CE system, which is usually characterized by oscillations of the whole Southern European region against the Northern part. In this particular event the contribution of other areas apart from South Italy was negligible, such that the event was classified as local since the effect on the rest of the system was almost negligible.

2.4 Assessing the distance to instability

The events presented in the previous section illustrate the connection between the occurrence of low damped oscillations and certain power flow scenarios. In practice small signal stability limits are often imposed on critical transmission corridors, where the maximum transfer capacity has been determined based on offline eigenanalysis and transient simulations. The described events motivate research towards a method that can provide awareness about prevailing stability margins during operation. Awareness about existing stability margins can help to detect emerging problems, and identifying the critical elements that contribute the most allows to minimize the control action to mitigate emerging instability.

The proposed method is aiming at providing a continuous assessment of the distance to the oscillatory stability boundary by evaluating a given operating point at time t. The perspective is therefore different to most of the previously presented methods which approach the problem of emerging oscillatory instability from the perspective of finding the optimal redispatch which mitigates the problem. The method developed in this thesis aims at closing the gap between detection based on observing the current condition and mitigation by finding the solution to an optimization problem. The underlying idea is to supplement the information of the current damping with a estimate of the distance to the oscillatory stability limit. A fast assessment of the distance to instability can detect potential imminent threats when the damping of the system is considered sufficient but the damping ratio is relatively vulnerable to changes in operating conditions. Furthermore it allows a quick assessment of stability margins after an unexpected contingency.

CHAPTER 3

The role of PMUs in oscillatory stability assessment

The purpose of this chapter is to provide an overview of the potential and already implemented applications enabled by synchronized phasor measurements. The fundamental concept of phasor measurements is introduced and several potential applications relevant for the assessment of oscillatory stability are presented, where two applications are discussed in detail.

3.1 The concept of synchronized phasor measurements

Since Steinmetz introduced the concept of phasors in 1893, the analysis of AC circuits has been greatly simplified [37]. Expressing a time varying sinusoidal signal in terms of its phasors, i.e. magnitude and phase, is now the foundation of almost all analytical tools related to balanced three phase circuits. The angle of a phasor reflects the phase angle difference of a sinusoid in respect to a reference signal. Without this reference the particular phase angle in time of a time varying signal has no particular meaning. Considering that measurement devices are distributed in the system and record the waveform of a local signal they need to be provided with a common reference that allows to relate the measurements to each other. PMUs were developed to overcome this problem by synchronizing the measurements to a common time signal.

This principle is illustrated in figure 3.1 considering two PMUs at locations *a* and b. The left hand side represents the waveform of the measured signal while the right hand side reflects the reported phasor at the coordinated measurement time given by the time tag. According to the angle convention specified in the IEEE Standard C37.118-2005 [38] a zero angle is reported when the reporting instant coincides with the peak of the signal as in case *a)* of figure 3.1. The PMU in location *b)* reports a phase angle of $48°$ as the phase angle of the signal has progressed by $48°$ after passing the peak at the reporting time.

In order to comply with the IEEE standard the reporting rate of PMUs must be in the range of $10\,\mathrm{Hz}$ up to half the systems nominal frequency, i.e. $25\,\mathrm{Hz}$ or $30\,\mathrm{Hz}$, and have a total vector error (TVE) of less than 1%. The total vector error is defined as the difference of the reported phasor to the ideal phasor as:

$$TVE = \frac{|\bar{X_M} - \bar{X_I}|}{|\bar{X_I}|} \tag{3.1}$$

Where $\bar{X_M}$ is the measured phasor and $\bar{X_I}$ is the true or ideal phasor. This representation of the measurement accuracy takes into account errors related to the timing of the measurement as well as magnitude and angle errors of the measurement.

The high report rate and accuracy of PMUs have opened new opportunities for monitoring and control of electric power systems [39]. Some of them, particularly relevant for low frequency power oscillations are presented in the following sections.

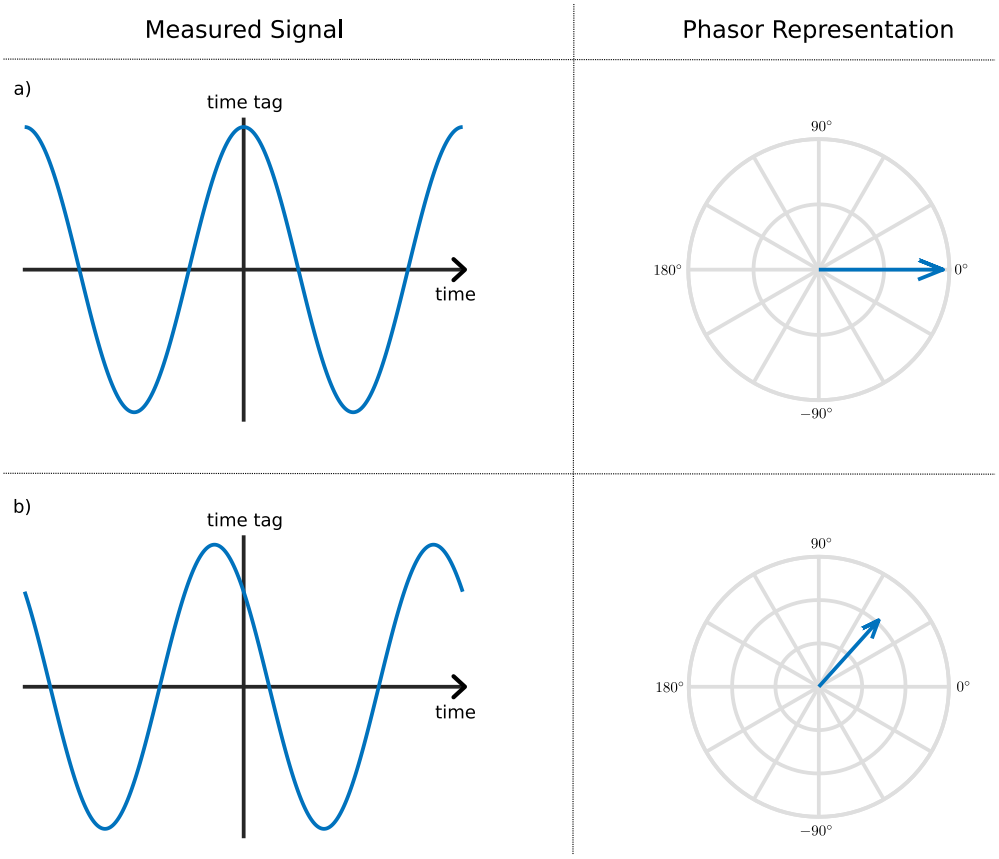

Figure 3.1: Phasor representation of a measurement signal taken at synchronized time at two different measurement points a) and b). Adopted from [3]

3.2 Added value of PMUs in respect to oscillatory stability assessment

Traditional Supervisory Control and Data Acquisition (SCADA) systems relied on local non-synchronized measurements provided by individual substations with an update rate in the range of 2-4 s. Due to the low resolution and the asynchronous nature of the measurements only an approximation of the steady state operation could be obtained. The high update rate of PMUs on the other hand allows to capture some of the dynamic processes in the system. According to the Nyquist theorem the maximum frequency of the dynamic process that can be accurately reflected is given as half the reporting rate of the PMU. Assuming the minimum reporting rate specified in the IEEE standard, the maximum frequency of a dynamic process that can be well captured by a PMU is $5\,\mathrm{Hz}$. That frequency is well above the typical frequency range of electromechanical oscillations. PMUs therefore provide a valuable tool for analyzing inter-area oscillations by extracting the modal content of the measured signal directly from the measurements. Comparing the system response with the expected response obtained from a simulation model further allows to validate and improve the accuracy of power system models that are used for power system planning and stability analysis.

In terms of power oscillation damping (POD) control, the availability of highly accurate distributed measurements allows to incorporate remote signals in closed or open loop controls. POD devices are typically placed at strategic locations where their output has a large effect on the damping of

an oscillatory mode. Local measurements are though not always suitable as an input to the control loop since they do not necessarily contain the information needed to modulate the output of an actuator in a way that provides the maximum positive effect. Having a large pool of potential measurements available allows to choose the most suitable signal that maximizes the efficiency of the power oscillation damper. In [40] and [41] the potential benefits from including wide area signals in damping controls to raise the transmission capacity on critical transmission corridors are presented. A common problem when relying on remote signals in closed loop controls is that of communication time delays that need to be accommodated in order to achieve the desired result. This problem is addressed in [42] and [43] by implementing a suitable predictor network that compensates for the time delay.
One particular application that benefits all stability assessment methods relying on the availability of the steady or quasi steady state operating point is the synergy between PMU measurements and state estimation [44]. State estimation aims at providing an estimate of the quantities that are not directly observable in the network to achieve full observability of the network states. With increasing PMU coverage of the network the number of unknown states is reduced and the quality of the prediction of the remaining states is increased [45].

3.2.1 Extracting modal parameters from measurements

The increased observability of the system led to the development of applications that allow to extract the essential properties of the dominant system modes directly from measurements distributed in the system. The type of system response that contains the modal information which is to be be extracted can be divided into two different categories related to the level of excitation.

- *Ambient:* The ambient response of the system stems from small random perturbations of the system operating points. These perturbations include the random fluctuations of load and generation in the system. The level of excitation of the mode is relatively low compared to the total response (low signal to noise ratio (SNR))
- *Transient:* The system response to a sudden disturbance such as a line trip or fault. The modal content is typically clearly visible in the system response (high SNR)

The distinctiveness of the modal properties in the transient system response typically allows to obtain a more accurate result and requires a shorter time window to obtain reasonably accurate estimations. Common methods used to extract modal information from transient system responses include Prony ([46],[47]) , Matrix Pencil [48] and Hankel Total Least Square [49]. Although they can provide an accurate estimate of the frequency and damping of a mode their application is limited by the requirement of a dominant oscillatory signal in the measurement. As such they are typically employed in post-event analysis or automatically triggered when a transient event is detected as proposed in [50].
To overcome this limitation, methods that were able to provide an estimate of the electromechanical modes from ambient data were developed. While they lack the accuracy of transient based identification methods they allow to continuously track the frequency and damping of the dominant system modes. The ambient response is characterized by small load variations which cause a random low-level excitation of the system modes [51]. There are numerous methods that aim at extracting the modal content from ambient data. Each of the algorithms is applied to data

samples which are either handled block-wise or recursively. While block processing algorithms are applied to the full data window and equally weigh each data point, recursive methods are updated for each new measurement sample considering the previous estimates where newer values are weighted more. Each of the algorithms typically requires a few minutes of data before they converge to a steady state solution. Depending on the strength of the signal typically 2-20 minutes of data are required [52] to achieve a reasonable accuracy. Prominent block processing methods are N4SID [53], Yule-Walker [54] and modified versions of the Yule-Walker method [52], [55]. Recursive methods include the least-mean squares method [56] and the regularized robust recursive least squares (R3LS) [57].
All of the above mentioned methods provide an estimate of the damping and the frequency of the most dominant modes. Further insights into the system dynamics can be obtained from an estimation of the mode shape, which describes the relative magnitude and phase of the oscillation observed in different locations in the system. An overview of methods that allow to estimate mode shapes based on ambient condition is provided in [58].

3.2.2 Validation and tuning of dynamic system models

Due to their rich information content, transient events are the perfect source for capturing the dynamic response of the system and the availability of high frequency synchronized measurements provided by PMUs allows to examine this response in detail. As early as 1996, coverage of high sample rate measurement data had progressed far enough to enable reconstruction of the events leading to the WSCC outage by fitting the recorded system response with the model response [34]. Engineers were able to pinpoint inadequate modeling assumptions in the existing models and adjust the dynamic model to fit the system trajectory observed during the event. Since then, the observability of the system has yet increased allowing to continuously adopt existing models to the observed system response.
Model validation is closely related to extracting the modal properties of the system from measurements and thus similar methodologies as the ones presented in section 3.2.1 are employed. A continuous verification of the underlying power system model can be obtained by comparing the modal parameters, such as frequency, damping and phase, obtained from the model with parameters estimated from ambient data [59]. Instead of relying on the quasi random excitation of oscillatory modes by natural events a dynamic response of the system can be triggered by artificially creating a disturbance using a suitable actuator. The probing signal can be either of a transient nature, such as the insertion of a large breaking resistor, or stem from an actuator that allows to modulate its output in a controllable manner. Recent advances in system identification allowed to use long term low level probing signals instead of intrusive transient signals [60] which allows to carry out tests more regularly. The design choices for such signals are described in [61] and [62]. For the probing tests described in [61] the Pacific HVDC Intertie was modulated with a multi-sine output signal with a maximum amplitude of 20 MW, which corresponds to an excitation of the system modes just above the regular ambient level.
While the main purpose of the previously described methods is to gain insights into the system characteristics and compare the system response to the expectation, the results also allow to improve existing dynamic models. Two different approaches for tuning model parameters to fit a measured response are reported in [63] and [64]. A framework for the validation of power system models relying on hybrid simulations that combine measurements and simulation is developed in [65], [66]. High resolution data provided by PMUs thus helps to develop and validate power

system models that reflect the dynamics of the real system close enough to predict the real system trajectory based on the model in most situations.

Part II

Method Development

CHAPTER 4

Mathematical concepts and equivalent models

The purpose of this chapter is to establish the mathematical concepts that serve as a foundation to the assessment method presented in chapter 6 of the thesis and introduce the equipment models that are used in the method.

4.1 The concept of modal torques

In order to explain the underlying physics of low frequency electromechanical oscillations it is convenient to analyze the forces that act during small disturbances in the system. In general electromechanical oscillations are caused by the interaction of the electrical system with the mechanical system represented by the large rotating masses of the generators. Any kind of small disturbance in the system as e.g. a small increase in system load disturbs the balance between the generated electrical torque and the mechanical torque applied to the shaft of the generating units. Depending on the direction of the load change the machine will either accelerate or decelerate according to the equation of motion.

$$M\frac{d}{dt}\omega = T_m - T_e \tag{4.1}$$

Where M is the inertia constant of the machine and T_m and T_e are the mechanical and electrical torque respectively. Since the disturbance is assumed to be small the equation of motion can be linearized about the current operating point to represent the dynamics that act at a specific frequency $s = \frac{d}{dt}$. The motion of a single machine at the modal frequency s can then be described by:

$$Ms\Delta\omega = \Delta T \tag{4.2}$$

The torque in equation (4.2) follows a dynamic power-angle curve which depends on the frequency of the mode as well as the speed perturbation. The time constant of the governor controlling the mechanical torque is relatively large, and assuming the mechanical torque as constant in the frequency range of the electromechanical modes has only little influence. Rewriting equation (4.2) by expressing the torque by its incremental component in respect to the speed perturbation yields the relationship described by (4.3).

$$Ms\Delta\omega = -\frac{\Delta T_e(s)}{\Delta\omega}\Delta\omega \tag{4.3}$$

For a single machine the speed perturbation $\Delta\omega$ can be eliminated and the eigenvalue of the electromechanical mode can be readily obtained by solving equation (4.3) for $s = \lambda$.

In a multimachine power system the dynamics of the individual machines are linked through the electrical system. The torque that a single machine generates is therefore not only related to the speed disturbance on its own shaft but also contains contributions due to speed changes at the remaining machines in the system. The resulting torque is therefore a linear combination of torque components related to speed changes of all the machines in the system. The torque generated at machine i due to a speed change at machine j can be represented by the relationship (4.4).

$$\Delta T_i\big|_{\Delta\omega_j} = \frac{\partial T_i}{\partial \omega_j}\Delta\omega_j \tag{4.4}$$

The sensitivities of all machines in respect to each other can be assembled into the single matrix $\boldsymbol{T_\omega}$ given by (4.5). Each entry describes the incremental torque of the machine associated with the row of the matrix when the speed of the machine associated with the column is perturbed by $1pu$.

$$\boldsymbol{T_\omega} = \begin{bmatrix} \frac{\partial T_1}{\partial \omega_1} & \frac{\partial T_1}{\partial \omega_2} & \cdots & \frac{\partial T_1}{\partial \omega_n} \\ \frac{\partial T_2}{\partial \omega_1} & \frac{\partial T_2}{\partial \omega_2} & \cdots & \frac{\partial T_2}{\partial \omega_n} \\ \vdots & \vdots & \ddots & \vdots \\ \frac{\partial T_n}{\partial \omega_1} & \frac{\partial T_n}{\partial \omega_2} & \cdots & \frac{\partial T_n}{\partial \omega_n} \end{bmatrix} \tag{4.5}$$

The diagonal elements that contain the elements of torque due to speed changes at the machines itself can be described as a self component of the electrical torque, while the off-diagonal elements represent the mutual torques that link the machines in the system. Using the information obtained from the machine coupling, the equation of motion of the single machine system in equation (4.3) can be extended to describe the dynamics in the multimachine power system.

$$(\boldsymbol{M}s + \boldsymbol{T_\omega})\Delta\boldsymbol{\omega} = \mathbf{0} \tag{4.6}$$

Where $\boldsymbol{M}$ is a diagonal matrix of machine inertia constants

$$\boldsymbol{M} = \begin{bmatrix} M_1 & & & \\ & M_2 & & \\ & & \ddots & \\ & & & M_n \end{bmatrix}$$

and $\Delta\boldsymbol{\omega}$ is a column vector containing the relative perturbations of the machine speeds.

$$\Delta\boldsymbol{\omega} = \begin{bmatrix} \Delta\omega_1 \\ \Delta\omega_2 \\ \vdots \\ \Delta\omega_n \end{bmatrix}$$

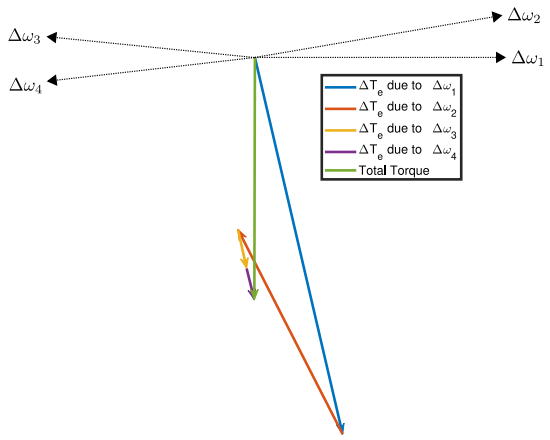

Figure 4.1: Phasor plot of the torque components of a machine. The total torque (green) is obtained as the sum of contributions of all the machines in the system

It is worth noting that the values $\Delta\boldsymbol{\omega}$, obtained as a solution of equation (4.6) for an electromechanical eigenvalue of the system $s = \lambda$, are equivalent to the right eigenvector of the speed states obtained from modal analysis. they describe the observability of the oscillations in the states associated with the machine speed.

The phasor plot in figure 4.1 exemplary illustrates how the torque of machine 1 in a four machine system is a result of contributions of all machines. The largest torque component (blue) is the self induced torque. The second largest component (orange) stems from a machine which is closely linked to machine 1 which counteracts the self generated torque. The two other components (yellow and purple), which are much smaller in magnitude but pointing in a similar direction as the torque of the machine itself, are the contributions of machines in another part of the system. The sensitivities are typically such that the off diagonal elements of (4.5) oppose the self induced torque. The resulting alignment in figure 4.1 is therefore mostly a result of the phase separation of the speed oscillations oberved in the different parts of the system. The individual torque components finally superimpose and result in a net torque, shown in green, which indicates the actual, measurable torque of the machine.

The relationship between the modal components of the electrical torque and the oscillatory stability of the system is investigated in more detail in the following chapter 5.

4.2 Representation of the synchronous machine dynamics

This section introduces the mathematical model of the synchronous machines that is used to determine the modal components of the electrical torque. For the purpose of studying the dynamic interactions between the machines embedded in a power system, it is convenient to express them in terms of frequency dependent transfer functions. The current and electrical torque of a machine can be expressed in terms of voltage and rotor speed changes.

$$\Delta I_g = G_{IV}(s)\Delta V_g + G_{I\omega}(s)\Delta\omega \tag{4.7}$$

$$\Delta T_e = G_{TV}(s)\Delta V_g + G_{T\omega}(s)\Delta\omega \tag{4.8}$$

Equation (4.7) relates the current injected into the system to the terminal voltage oscillations and the speed perturbations of the machine. The general form of the equation is such, that the machine is represented as a current source depending on the speed perturbations in parallel to a dynamic admittance. In the dynamic system each machine can therefore be represented by a Norton equivalent as illustrated in figure 4.2 with the equivalent parameters y_d and I_s as described in (4.9) and (4.10) respectively.

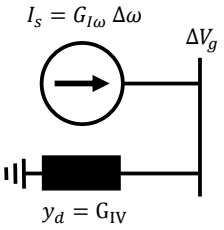

Figure 4.2: Norton equivalent representation of the synchronous machine

$$y_d = G_{IV} \tag{4.9}$$

$$I_s = G_{I\omega}\,\Delta\omega \tag{4.10}$$

When all the machines are represented by their respective Norton equivalent, the network equation of the dynamic system is given by (4.11).

$$\boldsymbol{I_s} = (\boldsymbol{Y} - \boldsymbol{Y_d})\,\Delta\boldsymbol{V} \tag{4.11}$$

Here, $\boldsymbol{Y}$ is the network admittance matrix with loads represented by their respective load admittance as described in section 4.4, and $\boldsymbol{Y_d}$ is a block diagonal matrix containing the individual device admittances.

Using (4.11) to eliminate the voltage term in (4.8), the torque can be expressed as function of the speed oscillations in the system:

$$\Delta\boldsymbol{T_e} = \boldsymbol{G_{TV}}(\boldsymbol{Y} - \boldsymbol{Y_d})^{-1}\boldsymbol{I_s} + \boldsymbol{G_{T\omega}}\Delta\boldsymbol{\omega} \tag{4.12}$$

The first term in (4.12) describes the component of the torque that is caused by the interaction of the current sources with the network due to the induced voltages at the terminal. The second term is a diagonal matrix containing the inherent torques that a machine generates independent of the external system. If (4.12) is evaluated element-wise, i.e. in respect to the contributions of each of the current sources to the torque, the sensitivity matrix in (4.5) is obtained.

4.3 Synchronous machine model

Equation (4.13) describes the operational impedance model of a synchronous machine [[13] which describes the machine by the efficient impedance identified based on the equivalent circuit illustrated in figure 4.3.

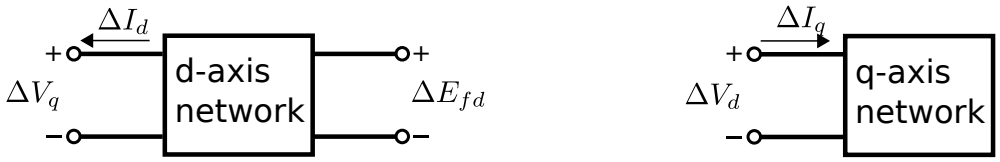

Figure 4.3: The d- and q-axis equivalent networks

The operational impedance model relies on determining the effective impedance of the machine and is often used to obtain the machine equivalent parameters by evaluating the frequency response based on an artificial probing signal. The incremental change in machine voltage in respect to current injection I_d and I_q and excitation voltage E_{fd} in the frequency domain are described by the relationship in (4.13).

$$\begin{bmatrix} \Delta V_d(s) \\ \Delta V_q(s) \end{bmatrix} = \begin{bmatrix} 0 & x_q(s) \\ -x_d(s) & 0 \end{bmatrix} \begin{bmatrix} \Delta I_d(s) \\ \Delta I_q(s) \end{bmatrix} + \begin{bmatrix} 0 \\ G_s(s) \end{bmatrix} \Delta E_{fd} \tag{4.13}$$

In (4.13) G_s is the open circuit field to voltage transfer function presented in (4.14).

$$G_s(s) = \left. \frac{\Delta \Psi_d(s)}{\Delta E_{fd}} \right|_{I_d=0} \tag{4.14}$$

The transfer function between the d-axis flux linkage and field voltage in (4.14) is obtained from the machine equivalent circuit as described in equation(4.37) within section 4.3.1.

The following simplifications are made in the employed model:

- The armature resistance r_a of the machines is assumed small and is neglected
- The speed perturbations are assumed small such that the approximations presented in equations (4.15) and (4.16) are valid.

$$V_d = -\Psi_q \tag{4.15}$$

$$V_q = \Psi_d \tag{4.16}$$

In the above described model the excitation voltage is treated as an input to the system. If the terminal voltage of the machine is controlled by means of an automatic voltage regulator (AVR), the applied field voltage depends on the control action of the AVR acting on the difference between the specified voltage setpoint V_r and the measured voltage V_t. After linearizing, the function of the field voltage in respect to the AVR is given by (4.17).

$$\Delta E_{fd} = G_{avr}(s)(\Delta V_r - \Delta V_t) \tag{4.17}$$

The voltage error consists of two components, namely the perturbation of the voltage magnitude given by (4.18) and the variation of the voltage setpoint supplied to the AVR. The voltage reference is expressed explicitly and contained as an input since it serves as connection point for the power system stabilizer (PSS).

$$\Delta V_t = \frac{V_{d_0}\Delta V_d + V_{q_0}\Delta V_q}{V_{t_0}} \tag{4.18}$$

In (4.13) the voltages and currents are given in the machine reference frame denoted by d and q. The internal reference frame of the machine and the reference frame of the external system denoted by D and Q are related by the transformation matrices in equations (4.19) and (4.20).

$$\begin{bmatrix} V_D \\ V_Q \end{bmatrix} = \begin{bmatrix} \sin\delta & \cos\delta \\ -\cos\delta & \sin\delta \end{bmatrix} \begin{bmatrix} V_d \\ V_q \end{bmatrix} \tag{4.19}$$

$$\begin{bmatrix} V_d \\ V_q \end{bmatrix} = \begin{bmatrix} \sin\delta & -\cos\delta \\ \cos\delta & \sin\delta \end{bmatrix} \begin{bmatrix} V_D \\ V_Q \end{bmatrix} \tag{4.20}$$

Linearizing the transformation matrices (4.19) and (4.20) in respect to angle and voltage, yields the transformation in respect to the incremental values of the rotor angle $\Delta\delta$ and voltage ΔV.

$$\begin{bmatrix} \Delta V_D \\ \Delta V_Q \end{bmatrix} = \begin{bmatrix} \sin\delta_0 & \cos\delta_0 \\ -\cos\delta_0 & \sin\delta_0 \end{bmatrix} \begin{bmatrix} \Delta V_d \\ \Delta V_q \end{bmatrix} + \begin{bmatrix} -V_{Q_0} \\ V_{D_0} \end{bmatrix} \Delta\delta \tag{4.21}$$

$$\begin{bmatrix} \Delta V_d \\ \Delta V_q \end{bmatrix} = \begin{bmatrix} \sin\delta_0 & -\cos\delta_0 \\ \cos\delta_0 & \sin\delta_0 \end{bmatrix} \begin{bmatrix} \Delta V_D \\ \Delta V_Q \end{bmatrix} + \begin{bmatrix} V_{q_0} \\ -V_{d_0} \end{bmatrix} \Delta\delta \tag{4.22}$$

Applying the linearized transformation (4.22) to both sides of equation (4.13) and solving for the machine current, yields a set of transfer functions in respect to perturbations of the rotor angle, voltage and the voltage reference applied to the AVR.

$$\begin{bmatrix} \Delta I_D \\ \Delta I_Q \end{bmatrix} = G_{I\delta}(s)\Delta\delta + G_{IV}(s) \begin{bmatrix} \Delta V_D \\ \Delta V_Q \end{bmatrix} + G_{IV_r}(s)\Delta V_r \tag{4.23}$$

The explicit expressions of the transfer functions are presented in equations (4.24) - (4.26).

$$G_{IV} = \begin{bmatrix} \frac{1}{2}dx\sin(2\delta_0) - \frac{K_1 V_{D_0}\sin\delta_0}{x_d} & -dx\cos^2\delta_0 - \frac{1+K_1 V_{Q_0}\sin\delta_0}{x_d} \\ dx\sin^2\delta_0 - \frac{1+K_1 V_{D_0}\cos\delta_0}{x_d} & -\frac{1}{2}dx\sin(2\delta_0) + \frac{K_1 V_{Q_0}\cos\delta_0}{x_d} \end{bmatrix} \tag{4.24}$$

$$G_{I\delta} = \begin{bmatrix} \frac{V_{d_0}\sin\delta_0}{x_d} + \frac{V_{q_0}\cos\delta_0}{x_q} - I_{Q_0} \\ -\frac{V_{d_0}\cos\delta_0}{x_d} + \frac{V_{q_0}\sin\delta_0}{x_q} - I_{D_0} \end{bmatrix} \tag{4.25}$$

$$G_{IV_r} = \frac{G_s G_{avr}}{x_d} \tag{4.26}$$

Where:

$$dx = \frac{1}{x_q} - \frac{1}{x_d}$$
$$K_1 = \frac{G_s G_{avr}}{V_{t_0}}$$

The linearized form of the torque is given by:

$$\Delta T_e = I_D \Delta V_D + I_Q \Delta V_Q + V_D \Delta I_D + V_Q \Delta I_Q \tag{4.27}$$

Using the incremental values of current and voltage, the torque can be obtained as (4.28).

$$\Delta T_e(s) = G_{TV}(s) \begin{bmatrix} \Delta V_D \\ \Delta V_Q \end{bmatrix} + G_{T\delta}(s)\Delta\delta + G_{TV_r}(s)\Delta V_r \tag{4.28}$$

The explicit transfer functions in (4.28) are given by equations (4.29) - (4.31).

$$G_{TV} = \begin{bmatrix} I_{D_0} + V_{q_0} dx \sin\delta_0 + \frac{V_{Q_0} - K_1 V_{D_0} V_{d_0}}{x_d} \\ I_{Q_0} - V_{q_0} dx \cos\delta_0 - \frac{V_{D_0} - K_1 V_{Q_0} V_{d_0}}{x_d} \end{bmatrix}^T \tag{4.29}$$

$$G_{T\delta} = \frac{V_{d_0}^2}{x_d} + \frac{V_{q_0}^2}{x_q} - V_{D_0} I_{Q_0} + V_{Q_0} I_{D_0} \tag{4.30}$$

$$G_{TV_r} = V_{d_0} \frac{G_s G_{avr}}{x_d} \tag{4.31}$$

Without a power system stabilizer, the transfer functions can be related to the ones presented in section 4.2 by using the relationship between the speed and angle oscillations as expressed by (4.32).

$$\Delta\delta = \frac{\omega_0}{s}\Delta\omega \tag{4.32}$$

Assuming a speed type PSS, the input to the voltage regulator becomes a function of the machine speed. The resulting expressions for the current and torque transfer functions are given in equations (4.33) and (4.34) respectively.

$$G_{I\omega} = G_{I\delta} \frac{\omega_0}{s} + G_{IV_r} G_{PSS} \tag{4.33}$$
$$G_{T\omega} = G_{T\delta} \frac{\omega_0}{s} + G_{TV_r} G_{PSS} \tag{4.34}$$

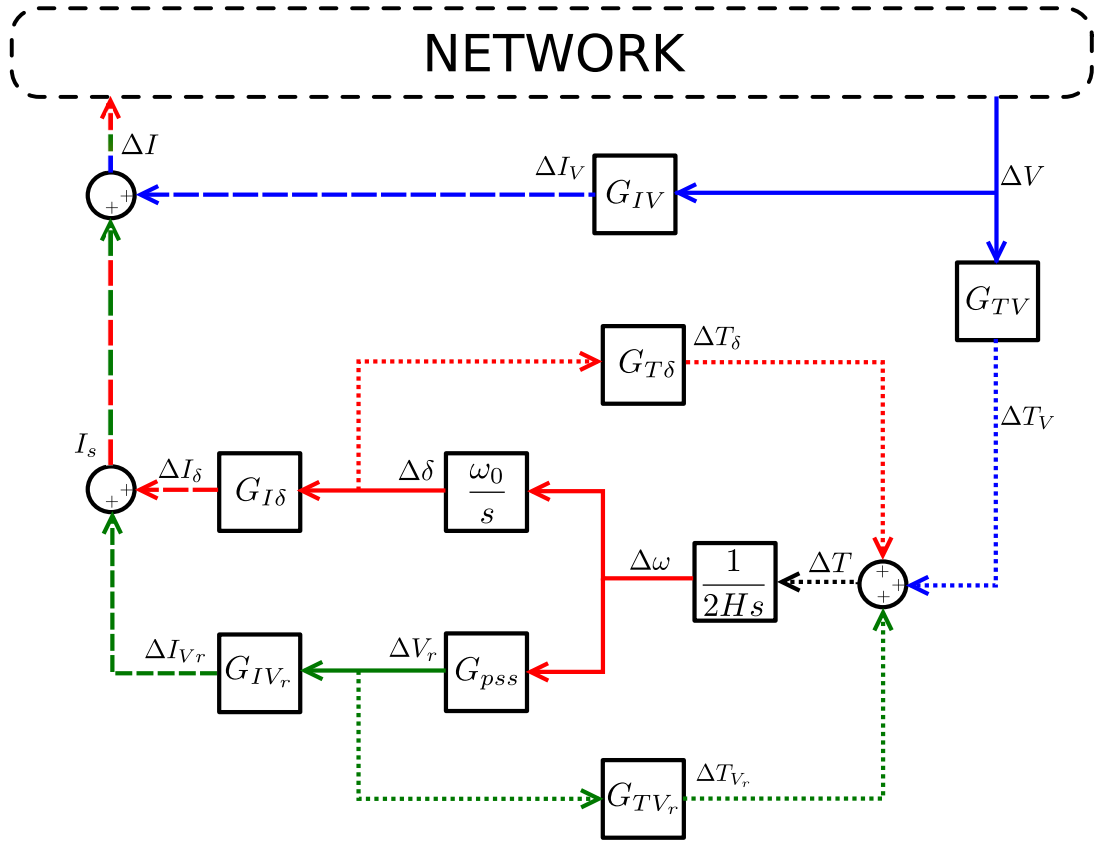

Figure 4.4: Block diagram of the machine transfer functions

The block diagram of the machine model represented by its transfer functions is presented in figure 4.4. The torque path is shown as the dotted lines while the path of the current is given by the dashed lines. The colors refer to the different signals where the speed/angle path is shown in red, blue refers to the voltage path and green highlights the path related to the PSS. The system loop is closed by the torque-speed interaction through the machine dynamics and the injected current - induced voltage relation determined by the system. Each of the signals related to speed, voltage and PSS consists of a feed-forward component that directly creates a torque and another component that interacts with the network. The torque components related to PSS and angle only link the machine itself, while the torque generated due to the perturbation of the terminal voltage contains the effect of voltages induced by other machines at the terminal. The direct feedback between the terminal voltage and the induced current though G_{IV} is equivalent to the dynamic admittance y_d shown in figure 4.2. The current source is represented by the sum of the angle and PSS dependent current shown as the green and red dashed lines.

4.3.1 Machine equivalent parameters

The parameters $x_d(s)$, $x_q(s)$ and $G_s(s)$ can be determined based on the time constants of the d- and q-axis equivalent circuits shown in figure 4.5 and 4.6 respectively. This commonly used model of the synchronous machine considers one damper winding in the direct axis and two damper windings in the quadrature axis.

From the equivalent circuit the set of characteristic time constants presented in table 4.1 can be derived.

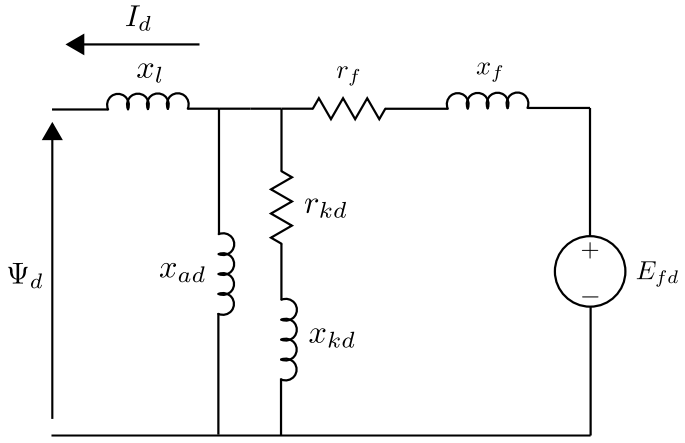

Figure 4.5: d-axis equivalent circuit

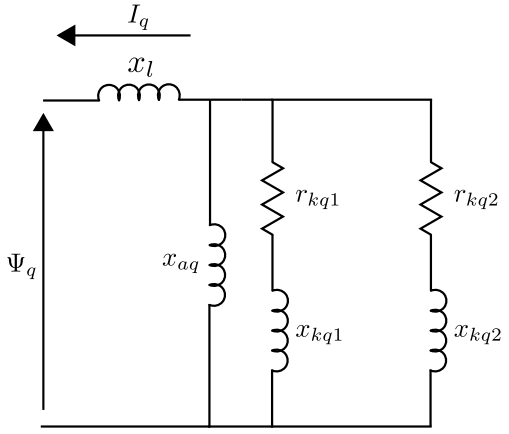

Figure 4.6: q-axis equivalent circuit

The operational impedances are given by equations (4.35) and (4.36). A detailed description regarding different approaches for expressing the time constants and the equivalent reactances can be found in chapter 7 of [67].

$$x_d(s) = x_d \, \frac{1 + s\,(T_{4d} + T_{5d}) + s^2\,(T_{4d} T_{6d})}{1 + s\,(T_{1d} + T_{2d}) + s^2\,(T_{1d} T_{3d})} \tag{4.35}$$

$$x_q(s) = x_q \, \frac{1 + s\,(T_{4q} + T_{5q}) + s^2\,(T_{4q} T_{6q})}{1 + s\,(T_{1q} + T_{2q}) + s^2\,(T_{1q} T_{3q})} \tag{4.36}$$

The open circuit transfer function expressed in terms of the machine time constants is given by (4.37)

$$G_s(s) = \frac{1 + s\,T_{kd}}{1 + s\,(T_{1d} + T_{2d}) + s^2\,(T_{1d} T_{3d})} \tag{4.37}$$

Table 4.1: d- and q- axis time constants based on equivalent circuit parameters

d-axis machine time constants	q-axis machine time constants:
$T_{1d} = (x_{ad} + x_f)\,\frac{1}{r_f}\,\frac{1}{\omega_0}$	$T_{1q} = (x_{aq} + x_{kq1})\frac{1}{r_{kq1}}\,\frac{1}{\omega_0}$
$T_{2d} = (x_{ad} + x_{kd})\,\frac{1}{r_{kd}}\,\frac{1}{\omega_0}$	$T_{2q} = (x_{aq} + x_{kq2})\frac{1}{r_{kq2}}\,\frac{1}{\omega_0}$
$T_{3d} = (x_{kd} + \frac{x_{ad}\,x_f}{x_{ad}+x_f})\,\frac{1}{r_{kd}}\,\frac{1}{\omega_0}$	$T_{3q} = (x_{kq2} + \frac{x_{aq}\,x_{kq1}}{x_{aq}+x_{kq1}})\,\frac{1}{r_{kq2}}\,\frac{1}{\omega_0}$
$T_{4d} = (x_f + \frac{x_{ad}\,x_l}{x_{ad}+x_l})\,\frac{1}{r_f}\,\frac{1}{\omega_0}$	$T_{4q} = (x_{kq1} + \frac{x_{aq}\,x_l}{x_{aq}+x_l})\,\frac{1}{r_{kq1}}\,\frac{1}{\omega_0}$
$T_{5d} = (x_{kd} + \frac{x_{ad}\,x_l}{x_{ad}+x_l})\,\frac{1}{r_{kd}}\,\frac{1}{\omega_0}$	$T_{5q} = (x_{kq2} + \frac{x_{aq}\,x_l}{x_{aq}+x_l})\,\frac{1}{r_{kq2}}\,\frac{1}{\omega_0}$
$T_{6d} = (x_{kd} + \frac{x_{ad}\,x_f\,x_l}{x_{ad}\,x_l+x_{ad}\,x_f+x_f\,x_l})\,\frac{1}{r_{kd}}\,\frac{1}{\omega_0}$	$T_{6q} = (x_{kq2} + \frac{x_{aq}\,x_{kq1}\,x_l}{x_{aq}\,x_l+x_{aq}\,x_{kq1}+x_{kq1}\,x_l})\,\frac{1}{r_{kq2}}\,\frac{1}{\omega_0}$

4.4 Representation of loads in the dynamic system

Loads are represented as a ZIP-loads with the general form of the load admittance:

$$\boldsymbol{Y_l} = \begin{bmatrix} Y_{DD} & Y_{DQ} \\ Y_{QD} & Y_{QQ} \end{bmatrix} \tag{4.38}$$

The total admittance of a load consists of a linear component $\boldsymbol{Y_{ll}}$ which contains the constant impedance characteristic of the load, which is the steady-state equivalent admittance of the load. The additional nonlinear component $\boldsymbol{Y_{nl}}$ is formed by the components of the load with constant current (cI) and constant power (cP) characteristic. The total load admittance is then obtained as the sum of the contributions of the linear and nonlinear load models.

$$\boldsymbol{Y_l} = \boldsymbol{Y_{ll}} + \boldsymbol{Y_{nl}} = \boldsymbol{Y_{cZ}} + \boldsymbol{Y_{cI}} + \boldsymbol{Y_{cP}} \tag{4.39}$$

The linear component of the load admittance is given by the constant impedance load with the elements given in (4.40) - (4.43).

$$Y_{DD,zZ} = \frac{P_l}{|V|^2} \tag{4.40}$$

$$Y_{DQ,cZ} = \frac{Q_l}{|V|^2} \tag{4.41}$$

$$Y_{QD,cZ} = -\frac{Q_l}{|V|^2} \tag{4.42}$$

$$Y_{QQ,cZ} = \frac{P_l}{|V|^2} \tag{4.43}$$

Additional nonlinear components are introduced when certain portions of the load are represented by either constant current or constant power characteristics. The admittance of a load with a certain constant active power (cP) and reactive power (cQ) component is determined by equations (4.44) - (4.47)

$$Y_{DD,cP} = -2V_D \frac{\text{cP}\, V_D + \text{cQ}\, V_Q}{|V|^4} \tag{4.44}$$

$$Y_{DQ,cP} = -2V_Q \frac{\text{cP}\, V_D + \text{cQ}\, V_Q}{|V|^4} \tag{4.45}$$

$$Y_{QD,cP} = -2V_D \frac{\text{cP}\, V_Q - \text{cQ}\, V_D}{|V|^4} \tag{4.46}$$

$$Y_{QQ,cP} = -2V_Q \frac{\text{cP}\, V_Q - \text{cQ}\, V_D}{|V|^4} \tag{4.47}$$

Similarly, the fraction of the load with constant current characteristic is given by equations (4.48) - (4.51).

$$Y_{DD,cI} = -V_D \frac{\text{cIP}\, V_D + \text{cIQ}\, V_Q}{|V|^4} \tag{4.48}$$

$$Y_{DQ,cI} = -V_Q \frac{\text{cIP}\, V_D + \text{cIQ}\, V_Q}{|V|^4} \tag{4.49}$$

$$Y_{QD,cI} = -V_D \frac{\text{cIP}\, V_Q - \text{cIQ}\, V_D}{|V|^4} \tag{4.50}$$

$$Y_{QQ,cI} = -V_Q \frac{\text{cIP}\, V_Q - \text{cIQ}\, V_D}{|V|^4} \tag{4.51}$$

The influence that the load has on the stability of the system depends to a large extend on the location of the loads in the system. The voltage magnitude oscillations are typically largest towards the center of oscillation while the voltage angle oscillations increase towards the outer parts of the system. While constant impedance loads depend solely on voltage magnitude oscillations, constant current and constant power loads additionally contain a component that depends on the angle oscillations. Constant power and constant current loads therefore contribute negatively to the damping of the oscillations when the angle oscillations of the load bus voltage is relatively large. A constant impedance load on the other hand has a less severe impact when subject to voltage angle oscillations but causes a deteriorating damping for large oscillations of the voltage magnitude.

A similar relationship holds for perturbations of the steady state operating conditions. While the non-linear load component is affected by variations of the voltage angle, impedance loads only depend on the impact of the perturbation on the voltage magnitude. The interaction of the steady-state characteristic and the sensitivity in respect to power flows perturbations can therefore be summarized as follows:

- The impact of constant impedance loads on the eigenvalue sensitivity will be largest if the load is located at a bus with significant voltage angle oscillations, i.e. close to the center of the oscillation, and the steady state voltage magnitude is sensitive to the steady state operating parameters.
- The effect of constant current and constant power loads will be significantly larger if the load bus is subject to relatively large angle oscillation and the steady state voltage angle is sensitive to perturbations of the steady state parameters.

When estimating the effect an additional power injection at a specific location has on the damping of a particular mode, it is therefore essential to consider the effect on the loads. The above described relationships are illustrated in figures 4.7 and 4.8.

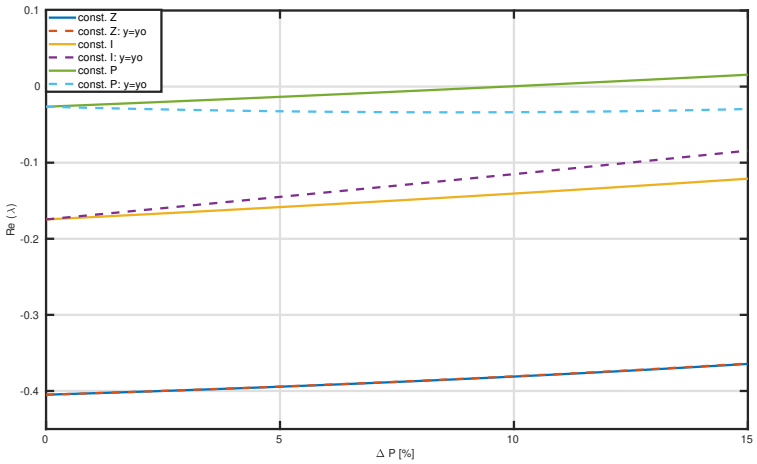

Figure 4.7: Examplary trajectory of the real part of the eigenvalue in respect to a redispatch involving two machines. The load is represented as 100 % constant power, constant current and constant impedance respectively, for both active and reactive power. The trajectory is compared to the case when the change in load admittance is not considered

The two figures relate to two different power systems with significantly different characteristic. The load centers of the system in figure 4.7 are to a large extend located close to the generators and in particular close to the machines with large participation in the oscillatory mode. The loads in the system depicted in figure 4.8 are on the other hand located in the center of the interconnection between two areas and therefore subject to large oscillations of the voltage magnitude. Note that the mode of the system in 4.8 is negatively damped. For the purpose of illustrating the impact of loads on the dynamic system, the initial value of the eigenvalue is not relevant and no attempt was made to stabilize the system.

Both figures show the effect of different load characteristics on one particular inter-area mode of oscillation. The trajectory of the curve refers to a percentage based redispatch of active power involving two machines that affect the inter-area power flow. The solid line shows the actual trajectory considering the fluctuations of the load admittance while the results illustrated by the dashed line were obtained assuming a constant load admittance.

There are several relevant observations. When comparing the general characteristic of the chosen load model, it becomes apparent that in the first case a constant impedance characteristic of the load introduces additional damping to the mode. Compared to the constant impedance load, constant current and constant power loads reduce the damping, where the effect of the constant power load is worse than the current load. The opposite is the case in the second system, where the real part of the eigenvalue increases when the load has a constant impedance characteristic, while the constant power load has the least detrimental effect on the damping. The linear component of the load related to the voltage magnitude is almost unaffected by the redispatch in the first system while in the second system it causes the largest deviation from the initial value. Constant power

and constant current loads deviate in all cases but their significance is larger in the first system. The observed effects correspond to the previously described relationships.

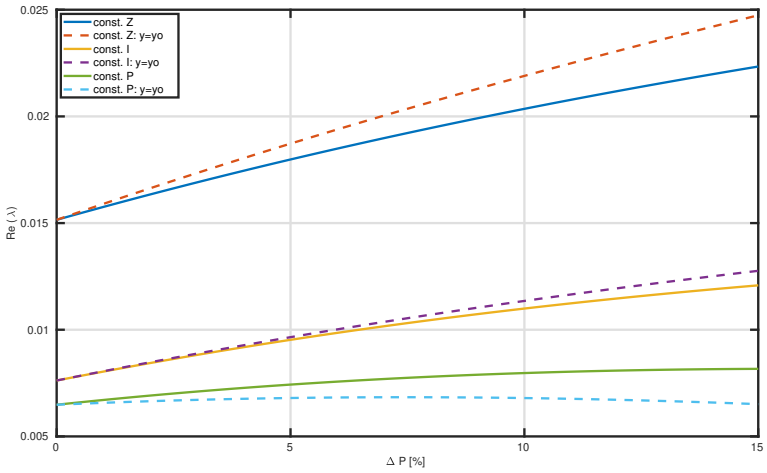

Figure 4.8: The same methodology as in 4.7 applied to a system where the loads are in the center of the interconnection and the load voltage magnitude is sensitive to the power flow

The nonlinear characteristic of the loads and their significance for the dynamic performance of the system is one of the main reasons why an analytical determination of the oscillatory stability boundary based on individual machine interactions alone is considered not feasible. An assessment based on quasi steady state properties of the power system needs to consider the interaction between machine injections and loads to provide a accurate representation of the system trajectory.

4.5 Eigenvalue sensitivity analysis based on modal torques

The influence a specific operating parameter has on a dynamic system mode can be assessed by performing a sensitivity analysis. The least computationally intensive way to perform this kind of analysis assumes that the relationship between the eigenvalue shift and the change of the studied parameter is linear. In the following, the procedure of obtaining the eigenvalue sensitivity from a linearization of the characteristic torque equation is illustrated.

The eigenproperties of the system are given as the eigenvalues and eigenvectors of the oscillatory modes of the system. The general eigenvalue problem can be formulated based on the torque sensitivity matrix $\boldsymbol{T_\omega}$ in (4.5) as:

$$\boldsymbol{M}s\boldsymbol{u} = -\boldsymbol{T_\omega}\boldsymbol{u} \tag{4.52}$$

Where u is the right eigenvector containing the speed perturbations of the machines. The left eigenvector w of the system is then obtained from:

$$\boldsymbol{w}^T\boldsymbol{M}s = -\boldsymbol{w}^T\boldsymbol{T_\omega} \tag{4.53}$$

Assuming that an arbitrary parameter ϵ in the system is perturbed by $\Delta\epsilon$, and linearizing equation (4.6) in respect to s and the parameter change $\Delta\epsilon$ yields:

$$\left[\left(\boldsymbol{M}+\frac{\partial \boldsymbol{T_\omega}}{\partial s}\right)u+(\boldsymbol{M}s+\boldsymbol{T_\omega})\frac{\partial u}{\partial s}\right]\Delta s=-\left[\frac{\partial \boldsymbol{T_\omega}}{\partial \epsilon}u+(\boldsymbol{M}s+\boldsymbol{T_\omega})\frac{\partial u}{\partial \epsilon}\right]\Delta\epsilon \tag{4.54}$$

Premultiplying equation (4.54) with $\boldsymbol{w}^T$ the derivatives of the right eigenvector can be eliminated by using the identity given in equation (4.53). The linear sensitivity of the eigenvalue in respect to a parameter change is therefore:

$$\frac{\Delta s}{\Delta \epsilon}=-\frac{\boldsymbol{w}^T\frac{\partial \boldsymbol{T_\omega}}{\partial \epsilon}\boldsymbol{u}}{\boldsymbol{w}^T(\boldsymbol{M}+\frac{\partial \boldsymbol{T_\omega}}{\partial s})\boldsymbol{u}} \tag{4.55}$$

Equation (4.55) relates the eigenvalue shift to a perturbation of a single operational parameter. In most of the relevant use cases the perturbed quantity p is not directly an operational parameter but will implicitly affect a number of operational parameters. In this case the parameter changes are given as set $\boldsymbol{\epsilon}=[\epsilon_1,\ldots,\epsilon_n]$ that are derived from the perturbed value, i.e. $\boldsymbol{\epsilon}=f(p)$. In respect to the first order sensitivity of the eigenvalue, the effect of the individual parameter changes are independent. The total eigenvalue shift can therefore be obtained from the linear combination of the individual parameter sensitivities. Assuming that the relationship $\partial\epsilon_i/\partial p$ is known for each ϵ, the resulting eigenvalue sensitivity in respect to the perturbed value Δp is:

$$\frac{\Delta s}{\Delta p}=\frac{-\boldsymbol{w}^T(\sum_{i=1}^{n}\frac{\partial \boldsymbol{T_\omega}}{\partial \epsilon_i}\frac{\partial \epsilon_i}{\partial p})\boldsymbol{u}}{\boldsymbol{w}^T(\boldsymbol{M}+\frac{\partial \boldsymbol{T_\omega}}{\partial s})\boldsymbol{u}} \tag{4.56}$$

Equation (4.56) allows to determine the linear approximation of the eigenvalue sensitivity in respect to an arbitrary change of a particular quantity p when the interaction between the perturbed quantity and all the other relevant operational parameters can be determined adequately.

CHAPTER 5

The mechanism leading to oscillatory instability

This chapter provides some basic insights into the processes that lead to oscillatory instability and introduces a method that can identify locations that contribute negatively to the damping of an oscillatory mode.

5.1 Relationship of modal torques and system stability

The stability boundary of an oscillatory mode is defined as operating condition where the mode becomes undamped, which is the case when the eigenvalue shifts to the right half of the complex plane. In terms of the machine torques, this condition is achieved if the effective torque of the machine in phase with the speed component is zero. For any machine in the system this relationship is obtained by relating the induced torques to the speed of the machine in question. Seperating the torque component that the machine generates by itself and the torque due to the other machines in the system, gives the following description of the stability boundary.

$$\Re(T_{\omega_{ii}} + \sum_{j,j\neq i} T_{\omega_{ij}} \frac{\Delta\omega_j}{\Delta\omega_i}) = 0 \tag{5.1}$$

The first component is the torque component generated by the machine if all other sources of oscillation are inactive. This is equivalent to the torque that would be generated if the speeds of all other machines in the system were fixed and only the speed of machine i was perturbed. The second component describes the torque that is generated due to the speed perturbations at other machines projected onto the speed oscillation of the machine i. Since the eigenvalue is a system wide parameter, equation (5.1) must be fulfilled for all machines. It is therefore not possible to draw any conclusions regarding the impact an individual element in the system has, by simply analyzing the resulting torque. Hence, the following applies for the decomposition of the torque into individual components:

- A machine that generates less damping than the damping of the system mode requires damping to be provided by the system
- The relative oscillation magnitude and phase observed in the machine speeds determine to which extend the torque sensitivity impacts the damping
- The relative speed oscillations are dependent on the torque sensitivities according to (4.6)

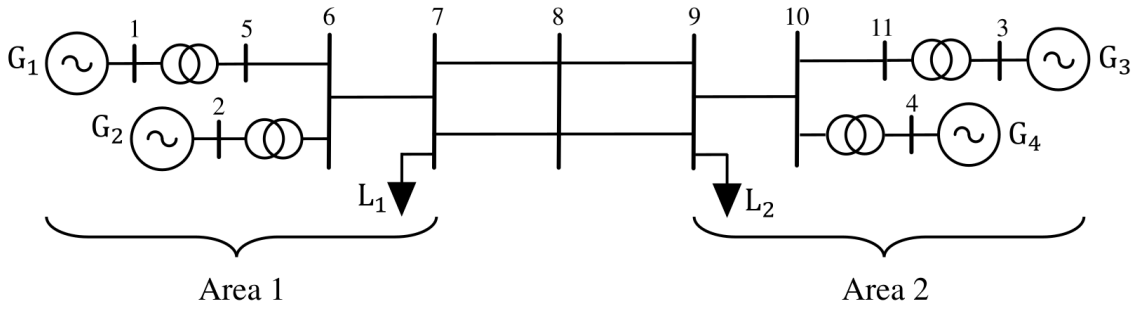

Figure 5.1: Structure of the system used to illustrate the method

5.1.1 Small test system

To illustrate the mechanism that causes oscillatory instability a small two area system is used. The system first presented in [68] contains all the features of a large multi-machine system. The general structure of the system is presented in figure 5.1 and the initial operating point is given in table 5.1.

By running multiple power flows and in turn increasing the power of a single machine, it can be determined that generator 1, followed by generator 2, has the most detrimental effect on the damping of the inter-area mode. Initially area 1 exports 400 MW into area 2 and it can be concluded that increasing the power export generally weakens the damping of the inter-area mode.

Table 5.1: System data

Machine	P	$\|V\|$	Load	P	Q
G_1	550 MW %	1.03 pu	L_1	700 MW	-100 MVAr
G_2	550 MW %	1.01 pu	L_2	1500 MW	-250 MVAr
G_3	600 MW %	1.03 pu			
G_4	557 MW %	1.01 pu			

5.1.2 Two machine example

To illustrate the relationship between the system eigenvalue and the modal torque components a two machine example can be employed. The torque sensitivity matrix of a two machine system can be written as:

$$\boldsymbol{T_\omega} = \begin{bmatrix} T_{11} & T_{12} \\ T_{21} & T_{22} \end{bmatrix} \tag{5.2}$$

Choosing machine 1 as reference for the speed oscillations by setting the speed perturbation $\Delta\omega_1$ to 1 pu the following equations apply for a natural mode of the system:

$$M_1 s + T_{11} + T_{12}\Delta\omega_2 = 0 \tag{5.3}$$

$$(M_2 s + T_{22})\Delta\omega_2 + T_{21} = 0 \tag{5.4}$$

If there is no explicit dependency of the torque to changes in the absolute value of angle and torque, an equivalent change $\Delta\omega_1 = \Delta\omega_2$ results in a zero net torque. In this case the relationships described by (5.5) and (5.6) apply to the incremental torque components.

$$T_{12} = -T_{11} \tag{5.5}$$

$$T_{21} = -T_{22} \tag{5.6}$$

Using the above described conditions and eliminating s in equation (5.3) using (5.4), yields the relationship described by (5.7) for the speed oscillations observed at machine 2.

$$\Delta\omega_2 = -\frac{M_1}{M_2}\frac{T_{22}}{T_{11}} \tag{5.7}$$

Similarly, the eigenvalue of the system can be obtained by replacing the speed perturbation, which results in (5.8).

$$s = -\left(\frac{T_{11}}{M_1} + \frac{T_{22}}{M_2}\right) \tag{5.8}$$

In this simple system the speed oscillation can be directly linked to the relation of the self generated torques and the resulting eigenvalue. The eigenvalue of the system is given as the sum of the self induced torques normalized by the machine inertia. The relationship between the speed oscillations indicates the relation between the normalized torques. The stability of the system can be directly linked to the individual components in (5.8) as each of them contributes in a specific way to the system eigenvalue. The system is on the stability boundary when the real part of either both torque components are zero, or both components compensate each other.

The previously described analysis applies for a particular steady state operating point. When the system moves from one steady state operating point to another, the trajectory of the damping depends on the evolution of the torque components. Considering a situation where the system is initially stable, the trajectory points towards instability when one torque components reduces to a larger extend than the other one increases.

To demonstrate the evolution of the eigenvalue and the individual contributions, the system presented in section 5.1.1 is modified such, that the remote of both areas (G_1 and G_2) are incorporated into the machines closer to the interconnection (G_2 and G_4). The torque sensitivity matrix of the inital operating point is given by:

$$\begin{aligned}\mathbf{T}_\omega &= \begin{bmatrix} 11.92 - j448.54 & -11.92 + j448.54 \\ -35.78 + j494.39 & 35.78 - j494.39 \end{bmatrix} \\ &= \begin{bmatrix} 448.6945\angle -88.47° & -448.6945\angle -88.47° \\ -495.6853\angle -85.86° & 495.6853\angle -85.86° \end{bmatrix}\end{aligned} \tag{5.9}$$

The eigenvalue contribution of each machine is determined by:

$$\begin{aligned} s &= -\left(\frac{11.92 - j448.54}{2 \cdot 6.5s \cdot 1800\text{MVA}} + \frac{35.78 - j494.39}{2 \cdot 6.175s \cdot 1800\text{MVA}}\right) \\ &= -(0.051 - j1.917) - (0.161 - j2.224) \\ &= -0.212 + j4.141i \end{aligned} \tag{5.10}$$

From these results it can be concluded that at the initial operating point G_1 contributes less to the damping of the mode than G_2, which was to be expected due to the power transfer from area 1 to area 2.

The magnitude and phase of the oscillation observed in the speed component of machine 2 is obtained from (5.7) as:

$$\begin{aligned} \Delta\omega_2 &= -\frac{495.6853}{448.6945}\frac{6.5s}{6.175s} \angle(-85.86 + 88.47)^\circ \\ &= 1.1629 \angle -177.3833^\circ \end{aligned} \tag{5.11}$$

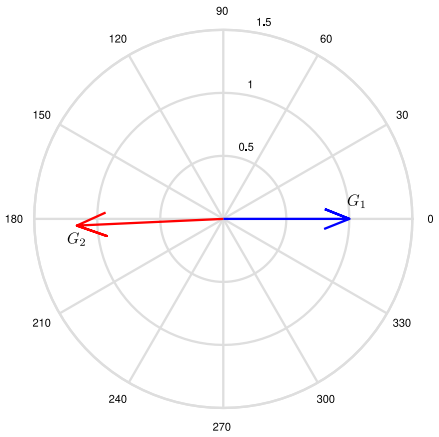

Figure 5.2: Phase and magnitude of the speed oscillations

The magnitude of the speed oscillation depends on the relation of the machine inertia constants and the magnitude of the torque. The torque magnitude is predominantly determined by the synchronizing torque component in phase with the angle changes, which is normally much larger than the component in phase with the speed. The angle between the speed oscillations observed at the two machines solely depends on the angle of the torque components. When none of the machines produces any damping torque, both torque components have an angle of -90°. The relative angle between the speed oscillations would thus be 180°. The same is observed when both of the torque angles are equal. The angle of the torque is given by:

$$\theta_T = \arctan\left(\frac{Im(T_\omega)}{Re(T_\omega)}\right) \tag{5.12}$$

Which can also be expressed in terms of the share of the damping torque component on the magnitude of the torque as:

$$\theta_T = \arccos\left(\frac{Re(T_\omega)}{|T_\omega|}\right) \tag{5.13}$$

For modes with relatively low damping, the imaginary part of the torque is a good approximation of the synchronizing torque component. The angle of the torque in (5.12) is thus a result of the ratio of the damping and synchronizing torque component generated by a machine. A large angle difference between the torques of the two machines will shift the angle of the speed oscillations closer to each other. The direction of the shift indicates which machine generates a larger share of damping torque. The machine that generates less damping torque will lead the angle of the other machine by less than $180°$, which is illustrated for the given example in figure 5.2. Here, machine 1 is the machine which generates less damping torque, which also agrees with the results obtained from the eigenvalue contribution.

The presented analysis only involves a particular steady state operating point. Considering an increase of power of G_1 followed by a reduction of power at G_2, it can be expected that the damping contribution of G_2 increases while the damping that G_1 provides decreases. The specific effect on the damping of the whole system depends on the slope of both components. This effect is illustrated in figure 5.3, where the contribution of each machine to the eigenvalue in (5.8) is evaluated individually for increasing and decreasing the power export from area 1 into area 2. The steeper slope of the machine in area 1 causes the real part of the eigenvalue, represented by the green line, to approach zero when the power export is increased. The damping would eventually become zero when the absolute values of both area contributions are equal.

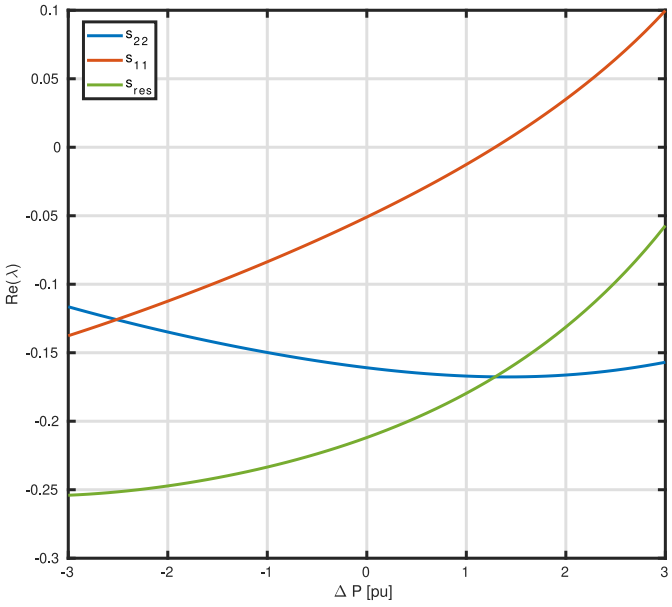

Figure 5.3: Individual contributions to the system eigenvalue

The effect on the active power dispatch on the speed oscillations observed in area 2 is shown in figure 5.4. The initial situation is represented by the solid blue arrow. Increasing the power export by 300 MW results in speed oscillations characterized by the dashed green arrow, while decreasing the power by 300 MW results in the situation shown by the dotted green arrow. As the damping

provided by area 1 becomes less the oscillation phase moves towards area 1 and the magnitude of the oscillations in area 2 increases. This indicates that the torque in area 1 compared to area 2 is reduced in both, magnitude, as well as damping torque.

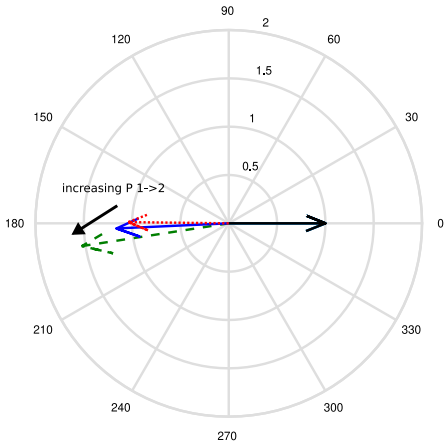

Figure 5.4: Phase and magnitude of the speed oscillations for variation of the active power flow

The given example illustrates the relationship between eigenvalue, oscillation phase and individual machine contributions to the damping of an oscillatory mode based on a two machine example. While the analysis of multi-machine systems is much more complex, some of the observed phenomenons are preserved. To ease the analysis of a large system it is desirable to reduce the complexity of the system, while preserving the main characteristics. In order to derive a reduced representation of the system that reflects the essential dynamics it is necessary to understand some of the key characteristics of inter-area oscillations.

5.2 Machine coupling in dynamic modes

Once excited, the energy contained in an oscillatory mode is not dissipated immediately but is exchanged between the machines in the system, where it is converted from electrical energy into kinetic energy and back. The specific pattern by which the machines exchange energy manifests in their relative phase of oscillation as they will form two characteristic groups with approximately opposing phase similar to the two machine case presented in the previous section. Before coming back to the two area system the essential characteristics of an inter-area mode are illustrated on a larger system.
Figure 5.5 exemplary shows the magnitude and phase of the speed oscillations observed in the inter-area mode of a 18 machine power system [69] which is described in more detail in chapter IV. The group located on the right hand side of figure 5.5 consists of machines 7 - 13 while the remainder of the machines, $1-6$ and $14-18$ are located on the left hand side.

Basis for the formation of the groups is the strength of the interaction between the machines. Machines within the same group exhibit a strong interaction while the interaction with the machines in the other group is much weaker. The strength of the interaction between two machines can be linked to the sensitivity of the electrical torque of one machine in respect to the speed of the other. This type of interaction is characterized by the torque sensitivity matrix introduced in equation (4.5). Figure 5.6 shows the magnitude of the torques linking the machines for the same system as

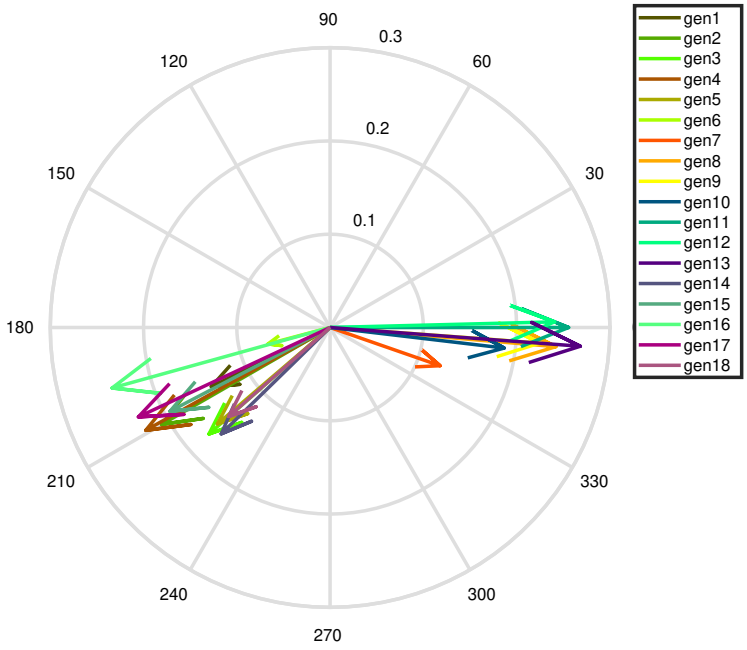

Figure 5.5: Speed oscillations observed in a 18 machine power system

in figure 5.5. The diagonal components that link the machines to themselves are excluded here and the maximum element within each row is normalized to one. Rows indicate the influence of the machines distributed in the system on a particular machine while the columns relate to the impact the machine has on the system.

The colored boxes indicate the partitioning of the matrix into different sections. The elements within the light blue and light green boxes link the machines within the groups, which are determined based on their phase relationship. The dark green and blue boxes on the other hand are the torque components that link the groups. It is apparent that the groups appear as blocks with large torque sensitivities. A visual inspection further reveals which machines are located at the boundaries of the groups and are therefore electrically close to the interface of the oscillation. In the given case, machines 6 and 7 could be identified as the machines close to the boundary as they show a considerable interaction with each of the groups.

Analyzing the coupling strength within the individual oscillatory groups can reveal further information in terms of the dynamic performance in the system. Despite belonging to the same group, machines are not necessarily electrically close and groups can consist of subgroups that only exhibit weak interactions with each other. This kind of information cannot be obtained by solely relying on the phase relationships. An analysis based on coupling strength on the other hand allows to identify these coherent subgroups.

5.3 Assessing individual damping contributions

In chapter 4.1, the relation between eigenvalue, speed oscillation and modal torque components was established. The interaction of a pair of machines within a mode is determined by the relative

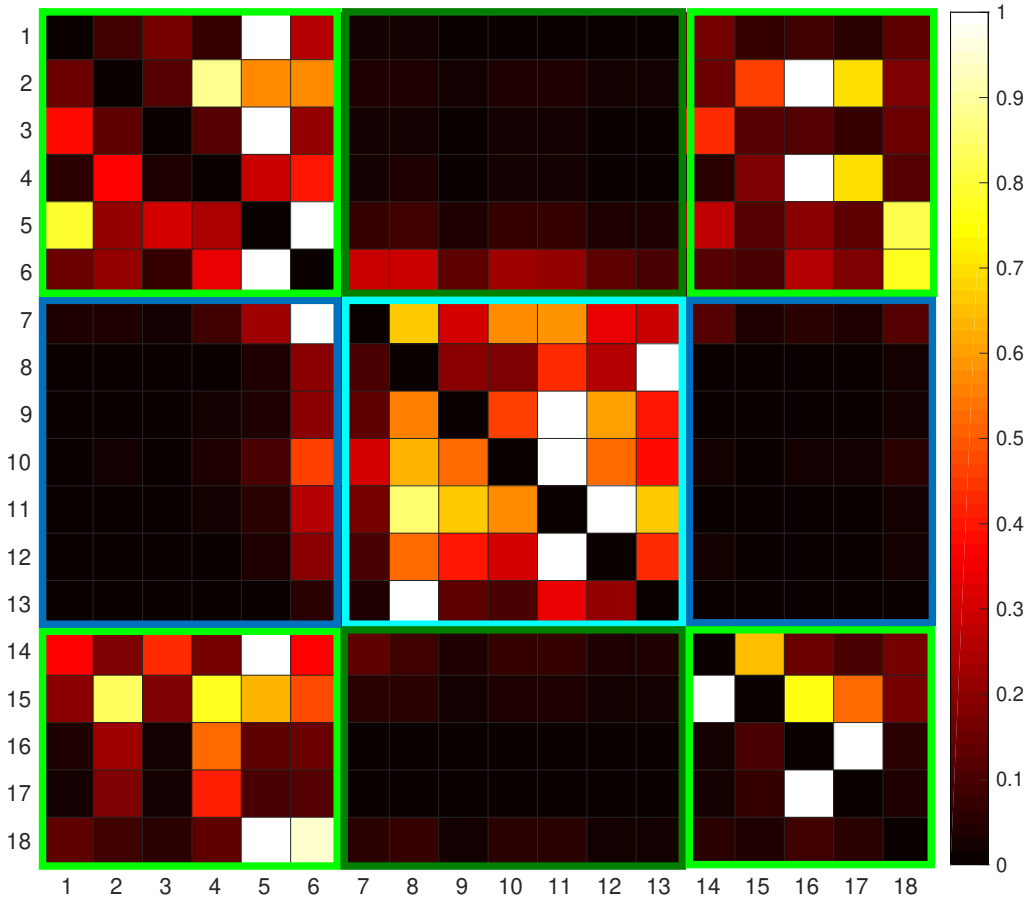

Figure 5.6: Magnitude of the torques linking the machines

phase difference of the speed oscillations and the electrical coupling described by the respective incremental torque components. Due to the opposing phase of the groups, there is a fundamental difference how the torque sensitivities within the groups and the torque sensitivities linking the groups affect the machines. The off-diagonal elements of the torque sensitivity matrix, in particular within a group, are typically negative as the machines counteract the generated torque of the machine where the speed disturbance is applied. For machines with opposing phase, this negative component finally materializes as a positive torque component in phase with its own speed change, while the effect on machines belonging to the same group is such, that the induced torque is negative in relation to their speed. Machines in the same area therefore typically affect their damping negatively while the effect on the other group is positive.

Undamped oscillations involving large groups of machines often occur not as a result of a particularly low damping torque component that a single machine provides for itself but rather as a result of the alignment within the groups and of the groups in respect to each other. In order to assess the performance of a group, a modal equivalent that allows to determine the net effect of the contributions of machines in an area is developed in the following.

The torque sensitivity matrix can be partitioned in terms of the groups such that:

$$\boldsymbol{T_\omega} = \begin{bmatrix} \boldsymbol{T_{A_{11}}} & \boldsymbol{T_{A_{12}}} \\ \boldsymbol{T_{A_{21}}} & \boldsymbol{T_{A_{22}}} \end{bmatrix} \tag{5.14}$$

In order to represent the dynamics in terms of the effective torque that the areas generate for themselves and the torques linking the areas, the submatrices in equation (5.14) need to be mapped in a specific way that preserves the dynamics of the original system. This process can be seen as defining an equivalent machine that contains the dynamics of each of the machines in the area. For an eigenvalue of the system the equation of motion of the equivalent machines need to fulfill:

$$(M_{eq1}s + T_{A_{11}})\Delta\omega_{eq1} + T_{A_{12}}\Delta\omega_{eq2} = 0 \tag{5.15}$$

$$(M_{eq2}s + T_{A_{22}})\Delta\omega_{eq2} + T_{A_{21}}\Delta\omega_{eq1} = 0 \tag{5.16}$$

Relating equations (5.15) and (5.16) to the equation describing the original system (4.6), the conditions that need to be satisfied can be expressed as:

$$M_{eq1}\Delta\omega_{eq1} = \sum_i M_i\Delta\omega_i \tag{5.17}$$

$$M_{eq2}\Delta\omega_{eq2} = \sum_k M_k\Delta\omega_k \tag{5.18}$$

$$T_{A_{11}}\Delta\omega_{eq1} = \sum_i\sum_j T_{ij}\Delta\omega_j \tag{5.19}$$

$$T_{A_{12}}\Delta\omega_{eq2} = \sum_i\sum_k T_{ik}\Delta\omega_k \tag{5.20}$$

$$T_{A_{21}}\Delta\omega_{eq1} = \sum_k\sum_l T_{kl}\Delta\omega_l \tag{5.21}$$

$$T_{A_{22}}\Delta\omega_{eq1} = \sum_k\sum_j T_{kj}\Delta\omega_j \tag{5.22}$$

Where i and j represent the indices of the machines in area 1 while k and l contain the indices of the machines in area 2.

There is a degree of freedom in choosing the equivalent representation of inertia and speed oscillation of the area. Defining the equivalent inertia of an area as total inertia in the area gives:

$$M_{eq1} = \sum_i M_i \tag{5.23}$$

$$M_{eq2} = \sum_j M_k \tag{5.24}$$

The equivalent speed changes of the areas then become:

$$\omega_{eq1} = \frac{\sum_i M_i\Delta\omega_i}{M_{eq1}} \tag{5.25}$$

$$\omega_{eq2} = \frac{\sum_k M_k\Delta\omega_k}{M_{eq2}} \tag{5.26}$$

Equations (5.25) and (5.26) reflect the movement of the center of inertia of the areas in the oscillation.

Since the system is fully determined the eigenvalue can be obtained for each system individually by (5.15) and (5.16):

$$s_{A1} = -(\frac{T_{A_{11}}}{M_{eq1}} + \frac{T_{A_{12}}}{M_{eq1}}\frac{\Delta\omega_{eq2}}{\Delta\omega_{eq1}}) \tag{5.27}$$

$$s_{A2} = -(\frac{T_{A_{22}}}{M_{eq2}} + \frac{T_{A_{21}}}{M_{eq2}}\frac{\Delta\omega_{eq1}}{\Delta\omega_{eq2}}) \tag{5.28}$$

The resulting eigenvalues in both areas are the same, since they both represent the eigenvalue of the whole system. Each of the eigenvalues is characterized by two separate contributions. One represents the contribution of the area itself, while the other reflects the contribution of the external system to the eigenvalue. Simplifying the notation in (5.27) and (5.28) in terms of the two components results in:

$$s_{A1} = s_{A1}\big|_{A_1} + s_{A1}\big|_{A_2} \tag{5.29}$$

$$s_{A2} = s_{A2}\big|_{A_2} + s_{A2}\big|_{A_1} \tag{5.30}$$

The performance of an area within a mode can be assessed on the basis of equations (5.29) and (5.30). If the real part of the contribution of an area to itself is negative, this particular area reduces the damping of the mode and can be identified as the critical area. In order to gain insights into the dynamics within the groups the contribution of the individual machines to the group performance can be assessed. The effect of the oscillation source at a machine is determined by the torque component that it induces in other machines. The contribution of machine 1 to the eigenvalue of area 1 can be obtained by:

$$s_{A1}\big|_1 = -\frac{\sum_i T_{i,1}\Delta\omega_1}{\Delta\omega_{eq1}} \tag{5.31}$$

Assessing all machines in the area that have been identified as critical in such a way, allows to narrow down the cause for the relatively bad performance of the group. The machine that has the largest positive contribution to the real part of the eigenvalue can be considered as the component which has the largest negative effect on the damping. When the negative contribution can be linked to the particular operating condition of the system, identifying the most critical machine can also help to determine location where an increase in power injection has the most detrimental effect on system stability. The coupling strength in the dynamic system provides an indication how coherent a set of machine acts in an oscillatory mode and therefore indicates which machines will be most affected by a perturbation of the steady state state operating point at specific machine. An indication of what could be the critical subgroup can therefore be obtained by assessing the coupling strength in relation to the machine that has been identified as critical.

To illustrate the process a numerical example based on the two area system presented in section 5.1.1 will be provided in the following:

$$\boldsymbol{T_\omega} = \begin{bmatrix} 176.56 - j641.93 & -167.78 + 500.16 & -0.43 + j73.57 & -8.35 + j68.20 \\ -199.71 + j449.25 & 194.31 - j727.67 & 12.13 + j134.60 & -6.73 + j143.82 \\ 13.34 + j108.14 & -3.98 + j122.96 & 156.86 - j700.11 & -166.21 + j469.00 \\ -7.28 + j115.24 & -31.47 + j138.24 & -176.75 + j472.59 & 215.49 - j726.06 \end{bmatrix} \tag{5.32}$$

$$= \begin{bmatrix} 665.76\angle -74.62° & 527.5482\angle 108.54° & 73.5739\angle 90.33° & 68.70\angle 96.98° \\ 491.64\angle 113.96° & 753.16\angle -75.04° & 135.14\angle 84.85° & 143.97\angle 92.67° \\ 108.95\angle 82.96° & 123.02\angle 91.85° & 717.46\angle -77.37° & 497.58\angle 109.51° \\ 115.46\angle 93.61° & 141.77\angle 102.82° & 504.55\angle 110.50° & 757.36\angle -73.46° \end{bmatrix}$$

The right eigenvector with machine 3 as a reference is given as:

$$\Delta\boldsymbol{\omega} = \begin{bmatrix} 0.92\angle 170.00° \\ 0.66\angle -178.10° \\ 1.00\angle 0° \\ 0.91\angle -4.28° \end{bmatrix} \tag{5.33}$$

After determining the equivalent parameter ω_{eq} and M_{eq}, the contributions to the eigenvalue in (5.29), written in form of coefficients, are obtained as

$$\begin{bmatrix} s_{11} & s_{12} \\ s_{21} & s_{22} \end{bmatrix} = \begin{bmatrix} 0.0056 + j1.7495 & -0.1249 + j2.1889 \\ -0.0059 + j1.7529 & -0.1134 + j2.1855 \end{bmatrix} \tag{5.34}$$

From inspection of (5.34) it can be concluded that area 1 clearly contributes negatively to the damping of the inter-area mode since it affects the eigenvalue in both areas negatively, while the machines in area 2 provide damping to both areas. Employing (5.31) to identify the individual contributions of machines 1 and 2 to the eigenvalue of area 1 yields (5.35).

$$\begin{bmatrix} s_{11}\big|_1 \\ s_{11}\big|_2 \end{bmatrix} = \begin{bmatrix} 0.1988 + j0.9498 \\ -0.0010 + j0.6970 \end{bmatrix} \tag{5.35}$$

By inspection it can be determined that machine 1 increases the real part of the eigenvalue and could therefore be determined as the machine which destabilizes the system the most.

To illustrate the trajectory of the eigenvalue contributions a similar approach as in section 5.1.2 is taken. The power change is equally distributed among the machine in each area. The effect on the eigenvalue contributions of each area is illustrated in figure 5.7. The general characteristic resembles the one from the two machine system where the contribution of area 1 to the real part of the eigenvalue is steeper than the negative contribution of area 2, which leads to a degrading damping. For this system the initial guess that increasing the power of the already weak area 1 further degrades the damping therefore applies.

The assessment presented in this chapter allows to identify areas as well as machines within the areas that contribute the least to the damping of an oscillatory mode. Although the result also yields a relatively good projection regarding the expected trajectory related to changes in active

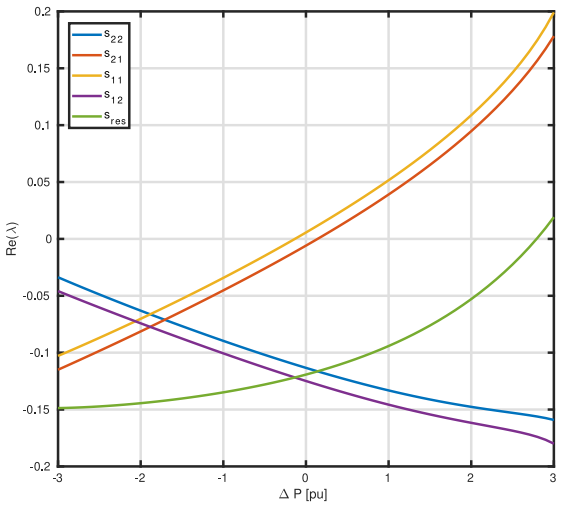

Figure 5.7: Individual contributions to the system eigenvalue

power dispatch in the presented case, these have to be taken with care. It should be noted that the analyzed system did not contain any power system stabilizers. As stabilizers can be idealized as an offset to the real part of the eigenvalue they can influence the result quite considerably. The offset that stabilizers produce is relatively independent of the power flow and a concentration of damping devices in one area might lead to the conclusion that increasing the export from that area has a positive effect. When power oscillation damping devices are relatively equal distributed in the system the relative assessment could become relevant again. Furthermore, the method cannot provide any kind of meaningful distance to instability. Such a method is presented in the following chapters.

CHAPTER 6

Derivation of oscillatory stability margins

This chapter introduces the thoughts and considerations in the development process of the proposed assessment method. The concept and the method are introduced and the individual steps for obtaining the oscillatory stability margin are illustrated.

6.1 Oscillatory stability as a global phenomenon

While the root cause for unstable oscillations might be due to specific operating conditions related to a subset of the complete system, the eigenvalue of the unstable mode is a global parameter. The torque per unit speed change normalized by the inertia is the same for all the machines in system. From an assessment of the total modal torque of a machine no conclusions can be drawn regarding the individual performance. Furthermore, there exists only one stability boundary for the whole system and all machines cross the boundary at exactly the same instant in time. The solution of the eigenvalue is a function of the incremental torque sensitivities in the system but deriving direct conclusions from the sensitivities alone is difficult since the resulting alignment in respect to magnitude and phase of the speed oscillations needs to be taken into account.

It could be argued that the torque component that links the machine to itself would be a good measure of performance within a mode. While it is certainly true that a positive component of the self generated damping torque improves the stability of the system, it neither helps to identify the critical margin nor does it relate to the root cause of a particularly low or high damping. Consider the case when a particular machine is equipped with a PSS. Idealized, the action of the PSS can be represented as an additional damping at the generator shaft equivalent to a damping constant D. This damping constant will increase the damping torque component linked with the machine itself and appear as a positive contribution to the system performance. The decision which machines are equipped with power system stabilizers and which not is however a design choice and is not linked to any specific operating condition.

Power system oscillations, as characteristic property of individual systems, by nature involve certain machines that participate more in the oscillations than others. A negative impact of these machines is therefore expected and considered when operating the system. The analysis of the performance of individual elements in the system therefore needs to consider a reference with which a studied case can be compared to. To assess the impact of changing operating conditions on the system, the parameter changes between different scenarios and their effect on system stability has to be evaluated.

6.2 Stability boundary represented as a redispatch scenario

Taking into account the considerations presented in section 6.1, it was decided to assess the performance of an individual element in the system by formulating the problem as a potential redispatch scenario involving a pair of machines. The objective is to find the worst possible redispatch for each machine which then yields the maximum power that can be injected into the system at a given load.

The small signal stability of an operating scenario can be assessed by performing a load flow, considering a given system load, and a given active power injection of the synchronous machines. The stability of the balanced system is then assessed by linearizing the system around the obtained operating point and performing a modal analysis, to assess whether all system modes are sufficiently damped. Theoretically, there is an infinite amount of scenarios considering all possible combinations of load and generation and the most credible and critical scenarios need to be determined. Considering the assessment of the stability of a given operating point in regards to the possible system trajectories away from the current point, the following simplifying assumptions are made.

- The assessment considers operation in steady or quasi steady state
- The system needs to be balanced and generation must match demand at all times
- Any increase in power injection by a single machine must therefore be compensated somewhere else
- The system load is considered constant during the assessment
- If the assessment is performed continuously for each operating point, the change of system loading is reflected in the assessment of the updated operating point
- Any kind of redispatch involving a number of machines can be considered as a linear combination of redispatches involving machine pairs

Let ΔP_1 an increase in power injection at machine 1 which is compensated by machines 2 and 3. Assuming that the system is balanced and neglecting losses, this can be written as (6.1)

$$\Delta P_1 + \Delta P_2 + \Delta P_3 = 0 \tag{6.1}$$

$$\Delta P_1 = -\left(\Delta P_2 + \Delta P_3\right) \tag{6.2}$$

If the small signal stability of the new operating point was to be analyzed, a change in eigenvalue due to the altered steady state operating point could be observed. The resulting eigenvalue shift is a result of the redispatch action and if the redispatch is sufficiently small, a linear relationship between dispatch and eigenvalue shift can be assumed. The effective eigenvalue shift can then be represented as a linear combination of the contributions of the individual machines involved.

$$\Delta s = \frac{\partial s}{\partial P_1}\Delta P_1 + \frac{\partial s}{\partial P_2}\Delta P_2 + \frac{\partial s}{\partial P_3}\Delta P_3 \tag{6.3}$$

Assuming that the additional power that machine 1 injects is related to the power changes at machines 2 and 3 by k_2 and k_3, where k_2 and k_3 indicate the share of ΔP_1 that is compensated by the respective machine as indicated in (6.4).

$$\Delta P_2 = -k_2 \Delta P_1 \tag{6.4}$$

$$\Delta P_3 = -k_3 \Delta P_1 \tag{6.5}$$

$$1 = k_2 + k_3 \tag{6.6}$$

The total redispatch can then be described as two seperate redispatches of smaller magnitude occuring simultaneously. The magnitudes of the individual redispatches are described by k_2 and k_3. The effect of the redispatch action can then as well be reformulated into two seperate problems, each involving a characteristic pair of machines. Defining $P_{12} = k_2 \Delta P_1$ as the amount of power shifted from generator 2 to generator 1, the contribution of the redispatch to the eigenvalue can be assessed from (6.7).

$$\Delta s|_{\Delta P_{12}} = \left(\frac{\partial s}{\partial P_1} - \frac{\partial s}{\partial P_2} \right) \Delta P_{12} \tag{6.7}$$

Similarly, the redispatch related to machine 3 can be evaluated by (6.8).

$$\Delta s|_{\Delta P_{13}} = \left(\frac{\partial s}{\partial P_1} - \frac{\partial s}{\partial P_3} \right) \Delta P_{13} \tag{6.8}$$

The total eigenvalue shift due to the whole dispatch scenario is then obtained as the linear combination of the solutions of the two smaller partial dispatch scenarios as (6.9).

$$\Delta s = \Delta s|_{\Delta P_{12}} + \Delta s|_{\Delta P_{13}} \tag{6.9}$$

The relationships described by equations (6.7) and (6.8) allow to express the stability of the system in relation to a fictive power flow between pairs of machines. A large magnitude of $\Delta s|_{\Delta P_{12}}$ in (6.7) would indicate that this pair of machines is particularly sensitive to perturbations of the active power. A large positive value would indicate that increasing the active power injection at machine 1 would destabilize the system. The problem can therefore be viewed as an inverse redispatch problem where the aim is not to assess the stability of a given scenario assuming known injections but rather find the amount of redispatch involving a pair of machines that would cause the system to become unstable.

The distance to instability can be derived considering that the eigenvalue at a given operating s_0 point is known. Considering that the current operating point is oscillatory stable, the eigenvalue shift that would cause a mode to become undamped, i.e. $Re(s) = 0$, is given as the solution to (6.10). Δs_{12} is given as the sensitivity of the eigenvalue in relation to ΔP_{12} obtained from (6.7) for a power disturbance ΔP_{12} equal to $1pu$.

$$0 = Re\left(s_0\right) + Re\left(\Delta s_{12}\right) \Delta P_{12,max} \tag{6.10}$$

The maximum additional power shift between the two machines is then obtained from (6.11).

$$\Delta P_{12,max} = -\frac{Re\left(s_0\right)}{Re\left(\Delta s_{12}\right)} \tag{6.11}$$

The active power flow change in (6.11) considers a direction of the flow $1 \rightarrow 2$. The derived maximum power change can be either negative or positive depending on the sign of the additional power injection. The reverse problem seen from the point of view of machine 2 is related to (6.11) by $\Delta P_{21,max} = -\Delta P_{12,max}$. The magnitude of the critical power margin is thus the same while the direction is reversed.

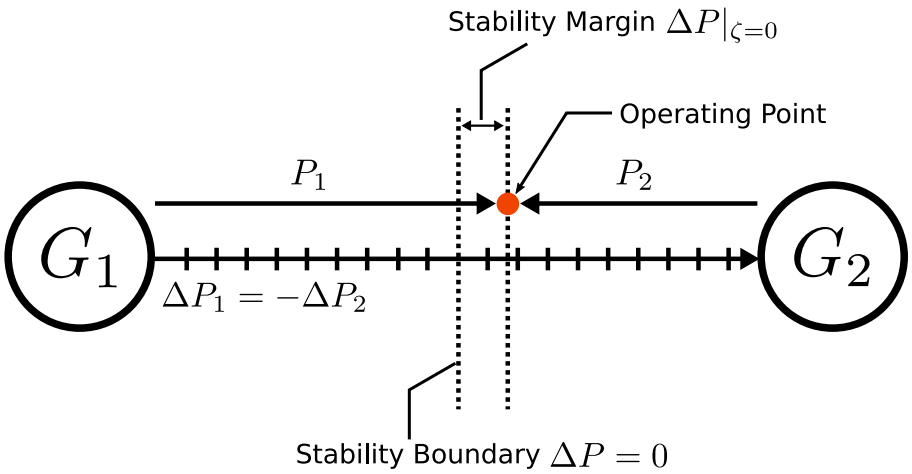

Figure 6.1: Illustration of the stability boundary as redispatch limit involving two machines

An equivalent representation of the provided assessment is presented in figure 6.1. The axis represents the distance to the stability boundary expressed in terms of active power which is located in the center. The stability boundary represents the point where an evaluation of (6.11) yields $\Delta P_{12,max} = 0$. The active power injections of the two machines are represented as phasors along the axis of active power margins, indicating that the sum of both injections is constant. The current operating point is represented by the orange dot which is a certain distance away from the center, where the distance indicates the current stability margin. In the illustrated example an increase of power by machine 2 would increase the length of the phasor P_2. P_1 would reduce by the same amount and the operating point would therefore move closer to the stability boundary.

Considering a system with n machines assessed in respect to machine 1 would result in $n-1$ two machine equivalents, similar to 6.1. In order to obtain a full picture of the system state each machine would have to be evaluated against each other. Even if symmetry is considered, assuming that the reverse solution can be obtained by changing the sign, the amount of necessary power flow evaluations would still amount to $n\ (n-1)\ /\ 2$, which is of quadratic complexity.

In order to reduce the number of redispatch scenarios, it can be considered that the evaluation of two seperate machines 1 and 2 against a common reference r can be written as (6.12).

$$\begin{aligned} 0 &= \Delta P_1 + \Delta P_{r_1} \\ 0 &= \Delta P_2 + \Delta P_{r_1} \end{aligned} \tag{6.12}$$

The power change of the reference machine consists of a component that opposes the applied power disturbance and an additional component that accommodates additional losses ΔP_l caused by the variation of the power flow pattern. Decomposing ΔP_r into the individual components (6.12) can be expressed as (6.13).

$$\begin{aligned} \Delta P_{r_1} &= -\Delta P_1 + \Delta P_{l_1} \\ \Delta P_{r_2} &= -\Delta P_2 + \Delta P_{l_2} \end{aligned} \tag{6.13}$$

Assuming the same size of the perturbation ΔP in respect to the reference, the eigenvalue shift due to a shift of power from machine 1 to 2 is obtained as

$$\begin{aligned} \Delta s_{12} &= \left(\frac{\partial s}{\partial P_1} - \frac{\partial s}{\partial P_r}\right)\Delta P - \left(\frac{\partial s}{\partial P_2} - \frac{\partial s}{\partial P_r}\right)\Delta P + \frac{\partial s}{\partial P_r}\left(\Delta P_{l_1} - \Delta P_{l_2}\right) \\ &= \left(\frac{\partial s}{\partial P_1} - \frac{\partial s}{\partial P_2}\right)\Delta P + \frac{\partial s}{\partial P_r}\left(\Delta P_{l_1} - \Delta P_{l_2}\right) \end{aligned} \tag{6.14}$$

The term related to the additional losses will typically be small compared to the power disturbance. The relative eigenvalue sensitivity of a pair of machine can then be uniquely determined based on a power flow assessment against a common reference. Additionally, choosing a reference which is known to have little participation in the critical modes, and therefore a low sensitivity, $\frac{\partial s}{\partial P_r}$ can help to further minimize the contribution of the additional system losses to the result of the assessment. Neglecting the contribution of the reference, the eigenvalue shift involving machines 1 and 2 is given by (6.15).

$$\Delta s_{12} = \Delta s_{1r} - \Delta s_{2r} \tag{6.15}$$

Where Δs_{1r} and Δs_{2r} are the results of the assessment of machines 1 and 2 against the reference machine. Here Δs_{12} represents the eigenvalue shift for a $1pu$ increase at G_1.

Applying the above mentioned methodology for all possible machine pairs allows to reduce the amount of necessary scenarios to describe the whole system to $n-1$, scaling linearly with the amount of machines in the system. The presented method therefore provides an efficient mean to obtain the two machine equivalents of the whole system.

6.3 Interpreting and visualizing the stability margin

The stability margin expressed in terms of an active power perturbation allows to illustrate the stability boundary by imposing an active power balance constraint on the two machine equivalent model. This allows the current injections, and changes applied to the injections, to be represented on a common scale. Interpreting a stability margin expressed in terms of absolute power can be difficult to interpret since the implications on a given machine might not be directly visible. How critical the margin is depends on the installed capacity in the system and the size of the machine. The active power of a machine typically does not fluctuate a lot within a short time frame. Relating the stability margin to a percentage increase or decrease in active power is therefore a

good measure of how close the machine is in fact operating to the boundary. The percentage based stability margin is obtained from (6.16) by normalizing the active power margin with the currently generated power.

$$P_{margin}\,[\%] = \frac{\Delta P_{max}}{P_g} \cdot 100\% \tag{6.16}$$

In contrast to the stability margin expressed in per unit power the percentage margin of a pair of machines depends on which machine it is related to. The percentage margin has the same sign as the margin expressed in total power indicating the direction of the flow that causes instability. In terms of visualizing occurring stability problems a percentage based assessment is more useful since it provides the opportunity to issue automated warnings when a certain threshold is surpassed.

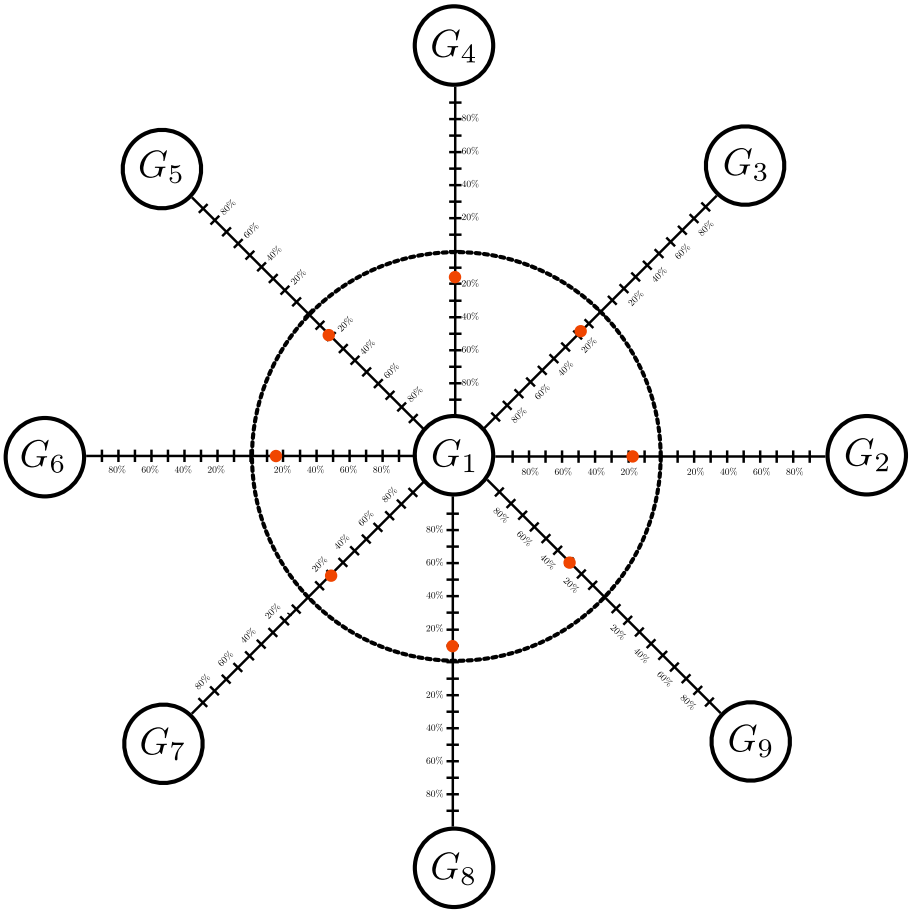

Figure 6.2: Visualization of the stability margin in respect to machine 1 as an extension of 6.1

Extending the visualization of the two machine system in 6.1 by combining several two-machine equivalents involving machine 1 and arranging them circularly gives a representation of the system as in 6.2. The assessed machine is connected to other machines by an axis similar to figure 6.1 and the stability boundary can now be represented as a circle around the assessed machine. The operating point of each of the two machine equivalents is given as a phasor, where the magnitude indicates the percentage margin in respect to the stability margin. Operation inside of the circle indicates that instability occurs for increasing injections of machine 1, while operation outside of

the circle relates to approaching instability in case of power reduction. The directional element of the phasor indicates the equivalent counterpart of the respective two machine equivalent system.

The directional element provides useful indicators in respect to power flow direction and magnitude. By clustering the machines of certain areas in the power system together in predefined sectors stability problems related to inter-area power flow can be quickly identified. An attempt of such a visualization is shown in figure 6.3. The percentage margin is now represented as multiple circles around the origin. The red circle is related to the stability boundary and the yellow circles are the 10% margin lines which here serves as example of an early warning threshold. The directional element of the operating point relates to the geographical location of the machines in the system, which was here loosely inspired by the Nordic system. Such a visualization could help to identify the critical elements quickly, and directly point out their location within the system. In the presented example the generators in regions SE1 and SE2 which would be associated with the Swedish system could be identified as the critical elements in relation to machine 1. Assuming that the currently assessed machine is located in Norway, the power flow from Norway into Sweden could be identified as a potential threat for oscillatory stability and reducing the flow would increase the margin.

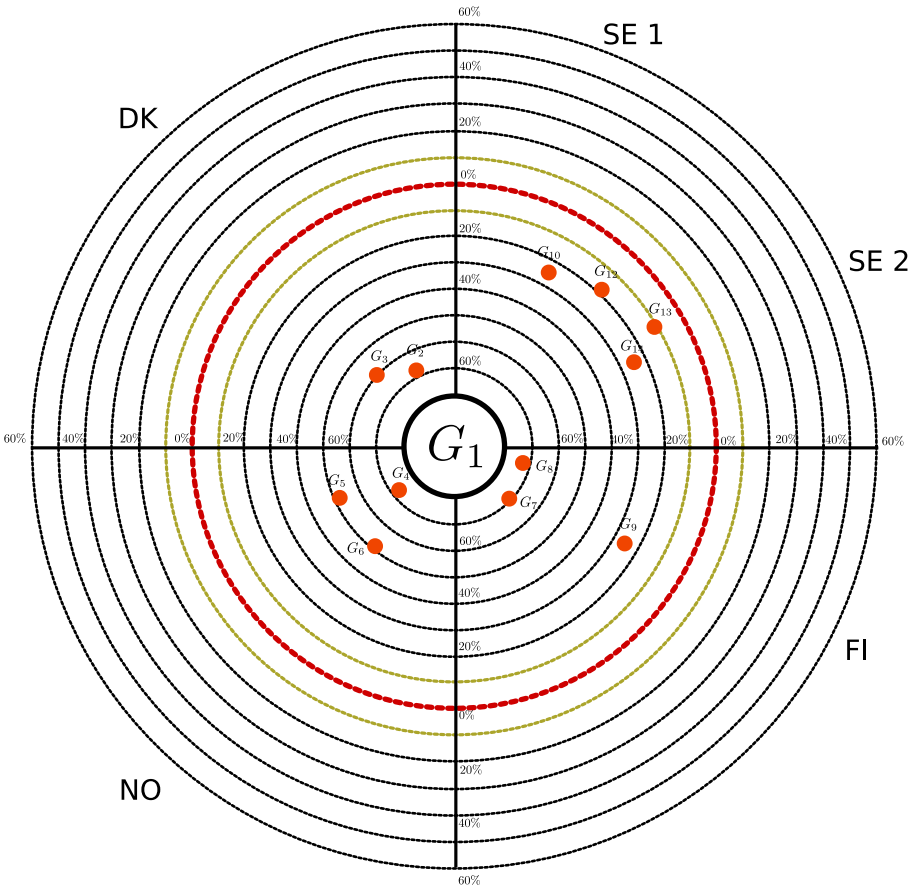

Figure 6.3: Visualization of the stability margin in respect to machine 1 where the margins are represented as circles around the the assessed machine. The angle of the operating point is associated with the location of the corresponding machine in the system and the magnitude represents the stability margin

Since the method only assesses distance and direction to the stability boundary it does not directly

provide an indication whether the current operation is stable or unstable. Only when the current operating point is directly on the boundary can the absolute stability be derived from the calculated margins. In case the current operating point is oscillatory unstable, the derived margin would in fact indicate the distance to stability. The stability of the current operating point is directly obtained from the real part of the eigenvalue and could be included in the visualization. The distance to stability on the other hand also provides useful information since it indicates the right actions to be taken in order to restore stability.

Figure 6.2 and 6.3 only represent the partial stability assessment related to a specific machine. Such a representation is convenient when determining the effect of a single machine in detail. It is, however, desirable to provide a mean to assess the state of the whole system at once. To achieve this the number of operating points of each machine is reduced from $n-1$ to the single most critical margin.

Considering that the eigenvalue shift can be expressed by (6.15) the critical shift is obtained by finding the machines which have the maximum and minimum sensitivity in respect to the real part of the eigenvalue. This is equivalent to finding the set of critical machines which have the largest contributions to the real part of the eigenvalue. A redispatch involving this machine pair would be expected to have the biggest impact. Defining $\boldsymbol{s_r}$ as the vector that contains the sensitivities of all the machines against the reference, the maximum and minimum sensitivity are obtained by (6.17) and (6.18) respectively.

$$\Delta s_{max} = \max\left[\, Re\left(\Delta \boldsymbol{s_r}\right)\right] \tag{6.17}$$

$$\Delta s_{min} = \min\left[\, Re\left(\Delta \boldsymbol{s_r}\right)\right] \tag{6.18}$$

Normalizing s_r in respect to the obtained maximum and minimum values gives two vectors Δs_+ and Δs_- that contain the maximum eigenvalue change for additional injections in positive and negative direction respectively.

$$\Delta s_+ = Re\left(\Delta \boldsymbol{s_r}\right) - \Delta s_{min} \tag{6.19}$$

$$\Delta s_- = \Delta s_{max} - Re\left(\Delta \boldsymbol{s_r}\right) \tag{6.20}$$

For machine i the critical eigenvalue sensitivity is evaluated by considering the closes distance to instability by applying the criterion given in (6.21).

$$\Delta s_{crit} = Re\left(\Delta s_i\right) \begin{cases} +\Delta s_+ & \forall\, \Delta s_+ > \Delta s_- \\ -\Delta s_- & \forall\, \Delta s_- > \Delta s_+ \end{cases} \tag{6.21}$$

The critical active power percentage margin is then derived by (6.22).

$$P_{crit}\,[\%] = \frac{-Re\left(s_0\right)}{Re\left(\,\Delta s_{crit}\right) \cdot P_g} \cdot 100\% \tag{6.22}$$

The result of visualizing all the machines in one diagram is illustrated in figure 6.4. The operating points are now always located on both sides of the stability boundary, corresponding to direction of the additional power injection that causes instability. The directions are chosen such, that increasing power moves the operating point outwards while a power reduction drags it towards the center. When the damping of a mode becomes zero, the operating point of all the machines are located exactly on the stability boundary, i.e. all machines are distributed along the red circle. In the illustrated example, the machines in the area indicated by NO^S are the machines for which the stability boundary is in the direction of increasing power. The machines with the smallest opposite margin are distributed among the other areas, indicating that the stability is primarily linked to the power flow from NO^S into the rest of the system.

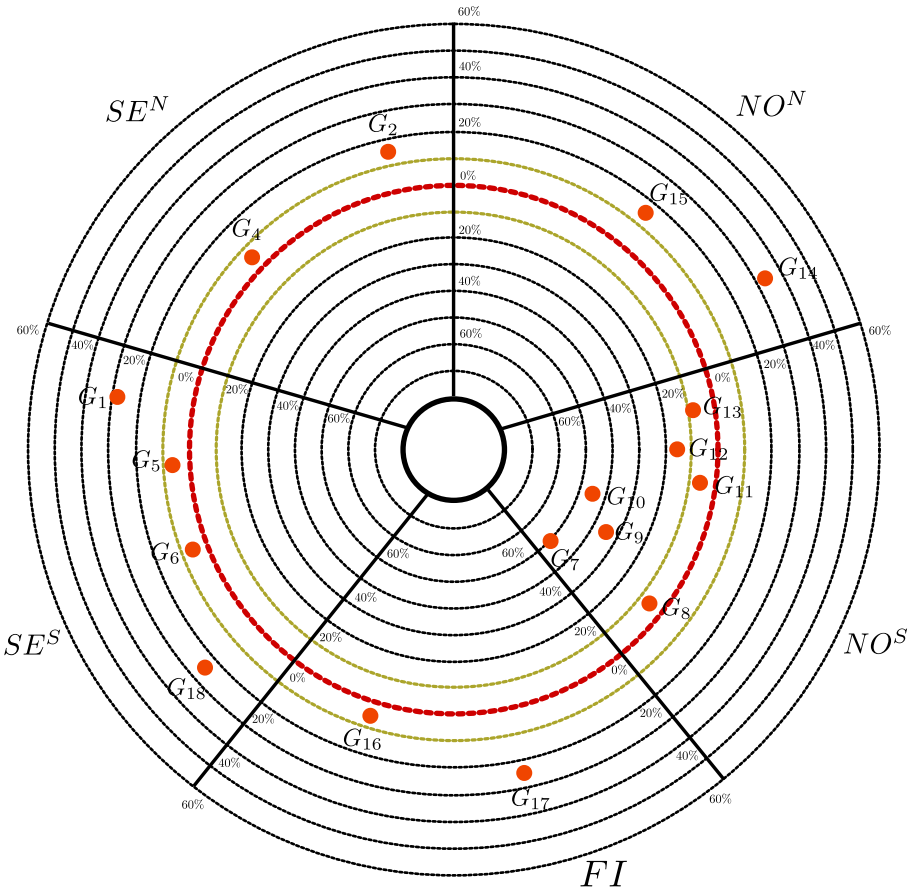

Figure 6.4: Visualization of the critical margins in the system. Instead of a specific machine located in the center the margins are now expressed for each machine in respect of their most critical counterpart.

The diagrams in figures 6.1 - 6.4 show the evolution from a two machine equivalent representation towards a visualization of the system state that allows to include all machine with their respective margins. These visualizations were developed as a mean to ease the interpretation of the results obtained from the assessment method. Currently there is automated mean for visualization of the results available in the assessment program. If such a visualization could be implemented it would help to quickly identify emerging stability problems and, at the same time, provide indicators for their root cause.

6.3.1 Margins of predetermined sub-systems

Considering a geographical distribution of the machines in the system, as indicated by the different areas partitioning the circles in figure 6.4, it might be useful to determine the stability of each of the individual subsystem as a whole, rather than for each element individually. To account for the different capacities of the machines in the subsystem participation factors, representing the share of the individual machine capacity on the total area capacity, are introduced.

$$\lambda_i = \frac{S_{b,i}}{\sum_j S_{b,A}} \tag{6.23}$$

Where A contains all the machines in the subsystem and $j \epsilon A$.
The obtained participation factor is then used to weigh the contribution of a machine on the eigenvalue sensitivity of the whole area:

$$\Delta s_{area} = \sum_j \lambda_i \, \Delta s_{ir} \tag{6.24}$$

The eigenvalue sensitivity obtained from(6.24), which is the sensitivity evaluated against the reference machine, can be handled in the same fashion as the individual machine sensitivities. That is, the maximum power injection in respect to another area can be obtained by replacing the machine sensitivities in (6.15) and (6.11) by the area sensitivities derived from (6.24). In systems where multiple sub-systems are involved to a different extent in an inter-area mode an area based assessment can help to quickly identify critical power flows in the system.

6.4 Calculation of steady state sensitivities

The following section provides the background for obtaining the relevant parameters that allow an assessment of the eigenvalue shift due to a potential increase in power injection stemming from a single machine. The parameter sensitivities that are needed to accurately determine the interaction of the steady state operation with the dynamic system are presented and the method for calculating the steady state sensitivity as well as the parameter sensitivities derived thereof are presented. The relevant parameters that fluctuate depending on the initial operating point and fully determine the dynamic system are presented in table 6.1 .

6.4.1 Deriving steady state sensitivities by means of the power flow Jacobian

The dynamic equivalent model is obtained from a linearization of the power system at a given operating point. The sensitivity of the dynamic model therefore depends on a set of parameters which link the steady state system with the dynamic equivalent. In terms of the synchronous machines these parameters are the steady state voltages and currents, as well as the initial rotor angles. The steady state voltage sensitivity in respect to perturbations of active power is obtained by evaluating the power flow Jacobian of a given operating point by applying (6.25).

Table 6.1: Parameters of the dynamic system that depend on steady state initial conditions

Parameter	Description
V_{D_g},V_{Q_g}	Terminal voltage at the machine buses in the system reference frame
V_{D_l},V_{Q_l}	Load voltages in the system reference frame
V_{d_g},V_{q_g}	Terminal voltage at the machine buses in the machine reference frame
I_{D_g},I_{D_g}	Current injections the machines in the system reference frame
δ	Machine rotor angles

$$\boldsymbol{J}\begin{bmatrix}\Delta V_{D_{pv}}\\ \Delta V_{Q_{pv}}\\ \Delta V_{D_{pq}}\\ \Delta V_{Q_{pq}}\end{bmatrix}=\begin{bmatrix}\Delta P_{pv}\\ \Delta|V|_{pv}\\ \Delta P_{pq}\\ \Delta Q_{pq}\end{bmatrix} \tag{6.25}$$

The general structure of the power flow Jacobian in (6.25) is shown in (6.26).

$$\boldsymbol{J}=\begin{bmatrix}\frac{\partial P_{pv}}{\partial V_{D_{pv}}} & \frac{\partial P_{pv}}{\partial V_{Q_{pv}}} & \frac{\partial P_{pv}}{\partial V_{D_{pq}}} & \frac{\partial P_{pv}}{\partial V_{Q_{pq}}}\\ \frac{\partial |V|_{pv}}{\partial V_{D_{pv}}} & \frac{\partial |V|_{pv}}{\partial V_{Q_{pv}}} & \mathbf{0} & \mathbf{0}\\ \frac{\partial P_{pq}}{\partial V_{D_{pv}}} & \frac{\partial P_{pq}}{\partial V_{Q_{pv}}} & \frac{\partial P_{pq}}{\partial V_{D_{pq}}} & \frac{\partial P_{pq}}{\partial V_{Q_{pq}}}\\ \frac{\partial Q_{pq}}{\partial V_{D_{pv}}} & \frac{\partial Q_{pq}}{\partial V_{Q_{pv}}} & \frac{\partial Q_{pq}}{\partial V_{D_{pq}}} & \frac{\partial Q_{pq}}{\partial V_{Q_{pq}}}\end{bmatrix} \tag{6.26}$$

For an arbitrary bus i the active and reactive power and voltage magnitude sensitivities are obtained from:

$$\Delta P_i=\begin{bmatrix}V_{D_i} & V_{Q_i}\end{bmatrix}\begin{bmatrix}\Delta I_{D_i}\\ \Delta I_{Q_i}\end{bmatrix}+\begin{bmatrix}I_{D_i} & I_{Q_i}\end{bmatrix}\begin{bmatrix}\Delta V_{D_i}\\ \Delta V_{Q_i}\end{bmatrix} \tag{6.27}$$

$$\Delta Q_i=\begin{bmatrix}V_{Q_i} & -V_{D_i}\end{bmatrix}\begin{bmatrix}\Delta I_{D_i}\\ \Delta I_{Q_i}\end{bmatrix}+\begin{bmatrix}-I_{Q_i} & I_{D_i}\end{bmatrix}\begin{bmatrix}\Delta V_{D_i}\\ \Delta V_{Q_i}\end{bmatrix} \tag{6.28}$$

$$\Delta|V|_i=\frac{1}{|V|_i}\begin{bmatrix}V_{D_i} & V_{Q_i}\end{bmatrix}\begin{bmatrix}\Delta V_{D_i}\\ \Delta V_{Q_i}\end{bmatrix} \tag{6.29}$$

The current injections are related to the voltage changes by:

$$\Delta\boldsymbol{I}=\boldsymbol{Y}\Delta\boldsymbol{V} \tag{6.30}$$

Assembling equations (6.27) - (6.29) in matrix form and using the admittance matrix to eliminate the currents yields:

$$\Delta\boldsymbol{P}=(\boldsymbol{V_{Pm}Y}+\boldsymbol{I_{Pm}})\Delta\boldsymbol{V} \tag{6.31}$$

$$\Delta\boldsymbol{Q}=(\boldsymbol{V_{Qm}Y}+\boldsymbol{I_{Qm}})\Delta\boldsymbol{V} \tag{6.32}$$

$$\Delta|\boldsymbol{V}|=\boldsymbol{V_{Vm}}\Delta\boldsymbol{V} \tag{6.33}$$

The matrices $\boldsymbol{V_{Pm}}$,$\boldsymbol{I_{Pm}}$,$\boldsymbol{V_{Qm}}$ and $\boldsymbol{I_{Qm}}$ collect the preceding factors in equations (6.31) and (6.32), where each row only contains the voltages and currents of the associated bus. Determining the leading coefficient matrix (6.31) with the proper bus ordering directly yields the entries of the Jacobian associated with active power changes. The Jacobian entries associated with reactive power are obtained by only considering the rows related to pq-buses $\boldsymbol{V_{Qm}}$, $\boldsymbol{I_{Qm}}$ as well as the admittance matrix. The entries of the Jacobian related to the voltage magnitude $\boldsymbol{V_{Vm}}$ are the subset of $\boldsymbol{V_{Pm}}$ associated with the pv-buses.

Apart from the elements related to the voltage magnitude and the elimination of the reference machine, the Jacobian has the same sparsity pattern as the admittance matrix of the system. For the purpose of obtaining the voltage sensitivities in respect to perturbations of the active power injections of single machines, the Jacobian needs to be evaluated for one right hand side per assessed machine. Each column of the right hand side is very sparse, since the only nonzero entry is related to the active power of the perturbed machine. The process can therefore be efficiently implemented using solution techniques that can exploit the sparsity of the Jacobian matrix.

The elements of the Jacobian associated with the voltage magnitudes at pv-buses can be eliminated by introducing the dependency in (6.34), obtained from the condition that the voltage magnitude at pv-buses is considered constant, i.e. $\Delta|V|_{pv} = 0$.

$$\Delta V_{D_{pv}} = -\frac{V_{Q_{pv}}}{V_{D_{pv}}} \Delta V_{Q_{pv}} \tag{6.34}$$

Using (6.34) to eliminate the D-axis voltage of the pv-buses reduces the number of nonzero entries in the Jacobian by $2\,n_{pv}$, where n_{pv} is the number of pv-nodes in the system. The elimination however introduces additional computational steps related to the elimination process and the efficient gain is very small.

6.4.2 Parameters derived from the steady state sensitivity

The rotor angle sensitivity is obtained from the active power perturbation and the reactive power sensitivity by (6.35).

$$\Delta\Theta_l = \frac{(-r_a\Delta Q_g - x_q\Delta P_g)\cos^2\Theta_l - (r_a\Delta P_g + x_q\Delta Q_g)\sin(\Theta_l)\cos(\Theta_l))}{r_aP_g + x_qQ_g + |V|} \tag{6.35}$$

The active power perturbation is nonzero only for the perturbed and the reference machine. The sensitivity $\Delta Q/\Delta P$ of the machines is obtained by applying the subset of (6.32) related to the machine buses to the calculated voltage sensitvities. The resulting rotor angle sensitivity is obtained as the linear combination of the load and voltage angle sensitivities.

$$\Delta\delta = \Delta\Theta + \Delta\Theta_l \tag{6.36}$$

Where $\Delta\Theta$ is obtained from:

$$\Delta\Theta = \frac{V_D \Delta V_Q - V_Q \Delta V_D}{|V|^2} \tag{6.37}$$

The effect of the voltage sensitivity of the load buses on the components of the load admittance is obtained by differentiating the linear load admittance $\boldsymbol{Y_{ll}}$ and the non-linear load admittance $\boldsymbol{Y_{nl}}$ presented in equations (4.44)-(4.47) and (4.48)-(4.51) in section 4.4 in respect to the D- and Q- axis voltages.

$$\Delta \boldsymbol{Y_{ll}} = \frac{\partial \boldsymbol{Y_{ll}}}{\partial \boldsymbol{V}} \Delta \boldsymbol{V} \tag{6.38}$$

$$\Delta \boldsymbol{Y_{nl}} = \frac{\partial \boldsymbol{Y_{nl}}}{\partial \boldsymbol{V}} \Delta \boldsymbol{V} \tag{6.39}$$

The derivatives needed to obtain the load sensitivities in (6.38) and (6.39) are presented in appendix A. The total change of the load admittance in respect to the perturbation of the steady state operating point is given as:

$$\Delta \boldsymbol{Y_{ld}} = \Delta \boldsymbol{Y_{ll}} + \Delta \boldsymbol{Y_{nl}} \tag{6.40}$$

6.5 Determining eigenvalues and eigenvectors based on an initial eigenvalue estimation

There already exist a variety of methods that aim at extracting information regarding the frequency and damping of electromechanical oscillations in the system. In the following it will therefore be assumed that such an estimate is available and can be used to provide a starting point for the method. The purpose of the method is to initialize the model of the power system with the corresponding critical eigenvalue that is observed in the system. Efficient methods that determine the eigenvalue based on the electrical torque of the machines were reported in [70], [71]. The application of such a method is discussed in the following.

The current and torque injections of a synchronous machine in an oscillatory mode can be described by:

$$\Delta I_g = G_{IV} \Delta V + G_{I\omega} \Delta\omega \tag{6.41}$$

$$\Delta T = (Ms + D + G_{T\omega})\Delta\omega + G_{TV} \Delta V \tag{6.42}$$

These expressions are essentially the same as presented in section 4.2 but are repeated here for convenience. When s is equal to a natural system eigenvalue the torque disturbance ΔT is zero for all machines in the system. This can be exploited by applying a speed perturbation of $1pu$ to a selected reference machine dg and determining the torque mismatch for an initial estimate of the eigenvalue s_0. The torque disturbance at all other machines is zero and the speed oscillations at these machines are unknown. The current sources of the non-disturbed (ng) machines are eliminated by defining an equivalent device admittance obtained from eliminating the speed in (6.41) by (6.42) using that $\Delta T = 0$ for the non-disturbed machines:

$$\Delta\omega_{ng} = -\frac{G_{TV_{ng}}\Delta V_{ng}}{M_{ng}s + D_{ng} + G_{T\omega_{ng}}} \tag{6.43}$$

And

$$Y_{ng} = G_{IV_{ng}} - \hat{Y}_{ng} \tag{6.44}$$

$$\hat{Y}_{ng} = \frac{G_{I\omega_{ng}}G_{TV_{ng}}}{M_{ng}s + D_{ng} + G_{T\omega_{ng}}}$$

The device admittance of the disturbed machine is:

$$Y_{dg} = G_{IV_{dg}} \tag{6.45}$$

Collecting the manipulated device admittances in $\boldsymbol{Y_g}$, the nodal equation of the dynamic system is expressed as:

$$\boldsymbol{I_s} = (\boldsymbol{Y} - \boldsymbol{Y_g})\Delta\boldsymbol{V} \tag{6.46}$$

The current injections I_s are zero, except for the disturbed machine, where $I_s = G_{I\omega_{dg}}$. After solving (6.46) for the device voltage of the perturbed machine, the torque mismatch can be calculated from (6.42). In order to obtain a new estimate of the eigenvalue, the derivative of the torque mismatch in equation (6.42) is explicitly obtained by analytically deriving the transfer functions of the machines. The equation for the perturbed machine (6.42) then becomes (6.47)

$$\frac{\partial\Delta T}{\partial s} = \frac{\partial G_{TV_{dg}}}{\partial s}\Delta V_{dg} + G_{TV_{dg}}\frac{\partial\Delta V_{dg}}{\partial s} + M_{dg} + \frac{\partial G_{T\omega_{dg}}}{\partial s} \tag{6.47}$$

While (6.47) involves only the perturbed machine, the voltage sensitivity obtained by (6.48) needs to consider the sensitivity of the device admittances and therefore involves the transfer function derivatives of all machines.

$$\frac{\partial\boldsymbol{I_s}}{\partial s} + \frac{\partial\boldsymbol{Y_g}}{\partial s}\Delta\boldsymbol{V} = (\boldsymbol{Y} - \boldsymbol{Y_g})\frac{\partial\Delta\boldsymbol{V}}{\partial s} \tag{6.48}$$

The derivative of the current source is determined by (6.49).

$$\frac{\partial\boldsymbol{I_s}}{\partial s} = \frac{\partial G_{I\omega_{dg}}}{\partial s} \tag{6.49}$$

The derivatives of the equivalent device admittance of the perturbed and nonperturbed machines are given by (6.50) and (6.51) respectively.

$$\frac{\partial Y_{g_{dg}}}{\partial s} = \frac{G_{IV_{dg}}}{\partial s} \tag{6.50}$$

$$\frac{\partial Y_{g_{dg}}}{\partial s} = \frac{G_{IV_{ng}}}{\partial s} - \frac{\partial\hat{Y}_{ng}}{ds} \tag{6.51}$$

(6.52)

Where:

$$\frac{\partial \hat{Y}_{ng}}{ds} = \frac{-\hat{Y}_{ng}\left(M_{ng} + \frac{\partial G_{T\omega_{ng}}}{\partial s}\right) + \frac{\partial G_{I\omega_{ng}}}{\partial s} G_{TV_{ng}} + G_{I\omega_{ng}} \frac{\partial G_{TV_{ng}}}{\partial s}}{M_{ng}s + D_{ng} + G_{T\omega_{ng}}}$$

After the voltage change ΔV_{dg} of the reference machine has been obtained from (6.48) the torque sensitivity in (6.47) can be evaluated. Combining the torque mismatch and the sensitivity information determined at iteration i allows to obtain a new estimate of the eigenvalue from (6.53).

$$s_{i+1} = s_i - \frac{\Delta T}{\frac{\partial \Delta T}{\partial s}} \tag{6.53}$$

This procedure is repeated until the eigenvalue change between subsequent iterations becomes smaller than a predefined threshold.

When the eigenvalue of the model has been correctly identified, the corresponding right eigenvector components of the nondisturbed machines can be directly obtained from equation (6.43). The explicit derivatives of the device transfer functions used in this section can be found in appendix B.1.

6.6 Eigenvalue sensitivity in respect to active power injection

Let $\boldsymbol{p}$ be the parameters affected by the perturbation of the steady state power injection that interact with the dynamic system. The sum of the eigenvalue sensitivity in respect to multiple parameter changes in (4.56) then relates to the linear combination of the torque sensitivity in respect to each of the parameters. Instead of determining each of the torques seperately each of the machine transfer function can be derived in respect to the parameters and be evaluated individually for all parameters. An overview of the parameters was provided in table 6.1 in section 6.4. The derivatives of the machine transfer function in respect to the applicable parameters can be found in appendix B.2. Rewriting (4.56) in terms of active power of machine i gives (6.54)

$$\frac{\Delta s}{\Delta P_i} = \frac{-\boldsymbol{w}^T \frac{\partial \boldsymbol{T_\omega}}{\partial P_i} \boldsymbol{u}}{\boldsymbol{w}^T (\boldsymbol{M} + \frac{\partial \boldsymbol{T_\omega}}{\partial s}) \boldsymbol{u}} \tag{6.54}$$

Where $\frac{\partial \boldsymbol{T_\omega}}{\partial P_i}$ is obtained from the machine transfer functions and their derivatives as (6.55).

$$\frac{\boldsymbol{T_\omega}}{\partial P_i} = \frac{\partial \boldsymbol{G_{T\omega}}}{\partial P_i} + \frac{\partial \boldsymbol{G_{TV}}}{\partial P_i} \Delta \boldsymbol{V} + \boldsymbol{G_{TV}} \frac{\partial \Delta \boldsymbol{V}}{\partial P_i} \tag{6.55}$$

The device voltage changes in (6.55) are obtained from the nodal equation (6.56)

$$(\boldsymbol{Y} - \boldsymbol{G_{IV}}) \frac{\partial \Delta \boldsymbol{V}}{\partial P_i} = \frac{\partial \boldsymbol{G_{I\omega}}}{\partial P_i} + \left(\frac{\partial \boldsymbol{G_{IV}}}{\partial P_i} - \frac{\partial \boldsymbol{Y_{ld}}}{\partial P}\right) \Delta \boldsymbol{V} \tag{6.56}$$

Equation (6.56) can be solved after approximating the partial derivatives $\frac{\partial \boldsymbol{p}}{\partial P_i}$ by the parameter sensitivities obtained from the steady state analysis $\frac{\Delta \boldsymbol{p}}{\Delta P}$, and evaluating the transfer functions. Note that $\frac{\partial \boldsymbol{T_\omega}}{\partial P_i}$ has dimensions $n \times n$, where n is the number of machines in the system. $\Delta \boldsymbol{V}$ in this case has dimensions $2n \times n$ and gives the contributions of each dynamic device to the voltage of each bus. The voltage obtained in (6.46) already contains the directional component caused by the eigenvector and therefore represents the resulting device voltages given as a column vector. This voltage represents the dynamic voltages at the current operating point which are the same as the voltages on the right hand side of (6.56). The current sensitivity in (6.56), however, has dimensions $2n \times n$ with nonzero elements at matrix indices related to the D- and Q-axis currents injected by the current sources at the generator buses. To transform $\boldsymbol{dI_s} = \frac{\partial \boldsymbol{G_{I\omega}}}{\partial P_i}$ into a column vector, the submatrix of $\boldsymbol{dI_s}$ related to the machine buses gb need to be multiplied with the right eigenvector.

$$\boldsymbol{dI_{s_{\omega,gb}}} = \boldsymbol{dI_{s_{gb}}}\, \boldsymbol{u} \tag{6.57}$$

The solution to (6.56) obtained this way also already considers the magnitude and phase of the oscillation and after multiplying $\frac{\partial \boldsymbol{G_{T\omega}}}{\partial P_i}$ with the right eigenvector the solution to (6.55) becomes $\frac{\boldsymbol{T_\omega}}{\boldsymbol{\partial P_i}}\, \boldsymbol{u}$. The nominator of the eigenvalue sensitivity formula (6.54) is then obtained by multiplying the previously obtained torque sensitivity with the left eigenvector. The illustrated process needs to be repeated for each machine in the system but the reference machine (related to power flow) to obtain the $n-1$ eigenvalue sensitivities of the machines.

The denominator in the eigenvalue sensitivity (6.54) represents the system response to a change in modal frequency. Most of the controlling devices in the system as well as the machine admittances are frequency responsive and therefore change their behaviour depending on the frequency. The sensitivity, in contrast to the active power sensitivity, does not depend on any particular location since the frequency is a global parameter. The sensitivity in respect to frequency therefore only needs to be determined once for each operating point.

The transfer function sensitivities were already determined in section 6.5 to determine the updated value of the eigenvalue due to the torque mismatch at the reference machine. The process here is slightly different since the eigenvalue shift needs to be related to any kind of torque change in the system instead of a torque change at a single location. In general the process of obtaining the denominator in (6.54) is the same the previously described process for obtaining the sensitivity in respect to P. Exchanging the transfer function derivatives with their respective counterpart related to frequency readily yields the torque derivative.

$$\frac{\boldsymbol{T_\omega}}{\partial s} = \frac{\partial \boldsymbol{G_{T\omega}}}{\partial s} + \frac{\partial \boldsymbol{G_{TV}}}{\partial s}\Delta \boldsymbol{V} + \boldsymbol{G_{TV}}\frac{\partial \Delta \boldsymbol{V}}{\partial s} \tag{6.58}$$

The device voltage changes in (6.58) are obtained from the nodal equation (6.59) which is similar to (6.56) except that the load admittance is constant in respect to the modal frequency s and thus does not appear on the right hand side of (6.59).

$$(\boldsymbol{Y} - \boldsymbol{G_{IV}})\frac{\partial \Delta \boldsymbol{V}}{\partial s} = \frac{\partial \boldsymbol{G_{I\omega}}}{\partial s} + \left(\frac{\partial \boldsymbol{G_{IV}}}{\partial s}\right)\Delta \boldsymbol{V} \tag{6.59}$$

Considering the additional solution for obtaining the information regarding the frequency response of the system, the shift in eigenvalue due to a shift of $1pu$ active power from the reference to each other machine can be assessed by solving n nodal equations.

Part III

Method Implementation and Performance Evaluation

CHAPTER 7

Implementation of the stability assessment method

In chapters 4 - 6, a method for assessing the distance to instability in respect to small signal oscillatory stability was presented. The following chapter concerns the implementations and computational optimizations of the method. Where applicable the performance of each block is evaluated individually in terms of speed and accuracy. All calculations are performed on an INTEL Core i7 - 6820 HQ *2.7 GHz CPU.* .

7.1 Overview of the proposed algorithm

The principal structure of the algorithm is outlined in figure 7.1 where each of the blocks in the figure relate to the different functionalities presented in part II of the thesis. The algorithm analyses snapshots of the system state given representing steady or quasi steady state operating points and provides stability margins for each assessed element. The algorithm is implemented in *MATLAB*. The main reason for choosing the proprietary *MATLAB* over the free *PYTHON* was that during the development phase the models and functionalities of the software were continuously evaluated using the *POWER SYSTEM TOOLBOX* [72]. The software is currently still in the development phase and does not yet have an interface to a PMU data stream. At the time being the input to the method are individual power flow snapshots emulating filtered PMU measurements.

Table 7.1 provides a short description of the functionalities of each of the seperate blocks in figure 7.1 and links the content of each block to the chapters in the thesis.

Algorithm 1: Overview of the main loop calling the subroutines associated with the different elements of the assessment method

```
Input: Snapshot of the system state
foreach snapshot do
    foreach machine except the reference do
        Calculate steady state sensitivity 7.4 ;
    end
    foreach critical eigenvalue do
        Determine model eigenvalue and eigenvectors 7.3;
        Calculate eigenvalue sensitivities 7.5;
        Derive stability margin 7.5;
    end
end
```

The performance of the algorithm is optimized by means of exploiting the sparsity pattern of the systems admittance matrix and by sharing relevant data across the different methods to avoid repeated calculations.

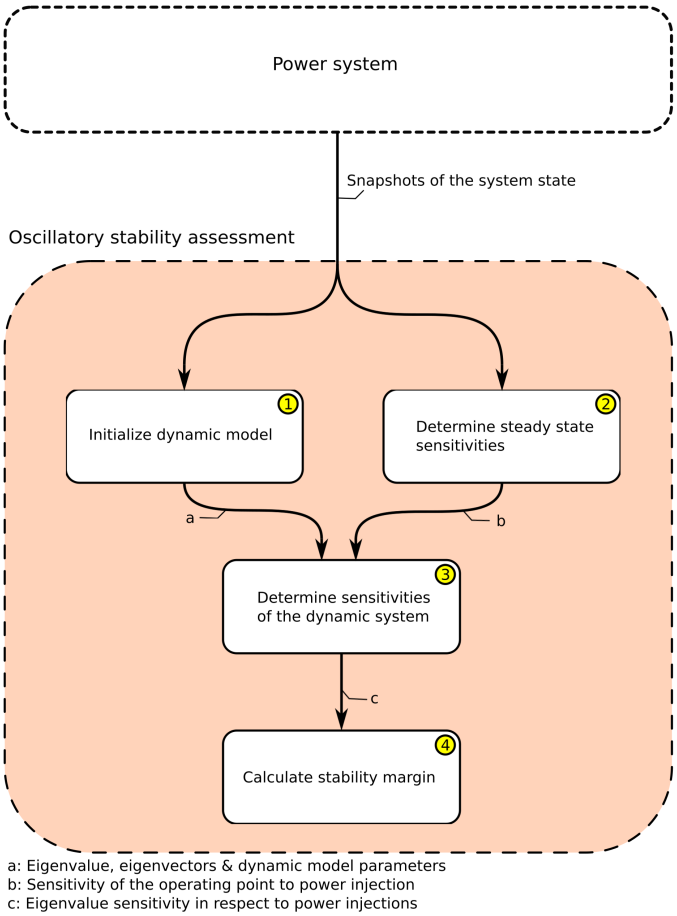

Figure 7.1: Overview of the proposed algorithm

7.2 Exploiting sparsity by factorization

The LU-factorization with partial pivoting is given by the factors $\boldsymbol{L}$, $\boldsymbol{U}$ and $\boldsymbol{P}$ that decompose a matrix $\boldsymbol{A}$ into the lower triangular matrix $\boldsymbol{L}$ and the upper triangular matrix $\boldsymbol{U}$. Partial pivoting allows to exchange the rows of the original matrix $\boldsymbol{A}$ to improve the sparsity of the resulting factors. The row interchanges, performed during the factorization, are contained in the permutation matrix P. The factors are related to the original matrix by (7.1)

$$\boldsymbol{P}\,\boldsymbol{L}\,\boldsymbol{U} = \boldsymbol{A} \tag{7.1}$$

$$\boldsymbol{L} = \begin{bmatrix} 1 & & & & \\ l_{21} & 1 & & & \\ l_{31} & l_{32} & 1 & & \\ \vdots & \vdots & \vdots & \ddots & \\ l_{n1} & l_{n2} & l_{n3} & \cdots & 1 \end{bmatrix} \qquad \boldsymbol{U} = \begin{bmatrix} u_{11} & u_{12} & u_{13} & \cdots & u_{1n} \\ & u_{22} & u_{23} & \cdots & u_{2n} \\ & & u_{33} & \cdots & u_{3n} \\ & & & \ddots & \vdots \\ & & & & u_{nn} \end{bmatrix}$$

The solution to the linear problem $\boldsymbol{LU}\boldsymbol{x} = \boldsymbol{b}$ is then obtained by first solving $\boldsymbol{L}\boldsymbol{y} = \boldsymbol{b}$ for $\boldsymbol{y}$ by forward substitution and use the solution $\boldsymbol{y}$ to solve $\boldsymbol{U}\boldsymbol{x} = \boldsymbol{y}$ for $\boldsymbol{x}$ using backwards substitution. The process is illustrated in (7.2).

Table 7.1: Description of the different blocks in figure 7.1 and their relation to the theory and implementation in the thesis

Block	Description	Theory	Algorithm
1	Combines the snapshot of the system and power system model data to determine the eigenvalue of the model. Determines eigenvectors and provides the device transfer functions as well as their derivative in respect to the eigenvalue	6.5	7.3
2	Constructs and evaluates the power flow Jacobian and provides the steady state sensitivities of the relevant parameters	6.4	7.4
3	Combines the dynamic model information from block 1 and the power flow sensitivities of block 2 to determine the eigenvalue sensitivity in respect to injection changes	4.5	7.5
4	Determines the applicable stability margins based on the ouput of block 3	6.2	7.5

$$\begin{aligned} Ly &= P^T b \leftarrow \text{solve for } y \\ Ux &= y \leftarrow \text{solve for } x \end{aligned} \tag{7.2}$$

The number on nonzero elements in $\boldsymbol{L}$ and $\boldsymbol{U}$ can be significantly reduced if the initial matrix $\boldsymbol{A}$ is reordered by applying an approximate minimum degree (AMD) ordering scheme [73] prior to the calculation of the matrix factors. AMD ordering aims at minimizing the amount of fill ins, that is additional nonzero elements in $\boldsymbol{L}$ and $\boldsymbol{U}$, generated during the elimination process. This optimizes the factorization and reduces the time as well as the amount of nonzero elements in the resultant matrix. The effect of the reordering on the sparsity of the resulting matrix factor is illustrated in figure 7.2. The AMD ordering method relies on an structural analysis of the matrix and is therefore independent of the numerical values within the matrix. This can be exploited by reordering the matrix only if either new elements are added to the matrix or existing elements are removed. In case of the admittance matrix this would indicate that either a new bus is connected to the system or a connection between two existing buses is added or removed.

After reordering the initial matrix *(i)*, matrix *(ii)* is obtained by moving elements from their initial position (i,i) to the new position (j,j), where the optimal position is determined by the AMD algorithm. The resulting sparsity pattern of the $\boldsymbol{L}$ matrix is shown in *(iii)* for the initial ordering, and in *(iv)* for the optimized ordering. The number of nonzero elements is less than half when the optimized ordering is applied. The reduction of fill ins also reduces the computational time of the matrix factorization obtained with partial pivoting. In this example calculating the matrix factors of the original matrix took $0.1132\,\mathrm{ms}$ while factorization with the improved ordering was completed in $0.0606\,\mathrm{ms}$ which corresponds to a speedup of approximately 53%. This includes the time needed for reordering the matrix elements of 0.0122, which only needs to performed once. Additionally the number of nonzero elements in matrix (iii) is more than twice as compared to the preconditioned matrix (iv), which reduces the efficiency of the calculation involving the LU factors.

Factorization methods are useful in almost all applications relying on the solution of large linear problems that involve highly sparse matrices. The potential of precalculating the relevant

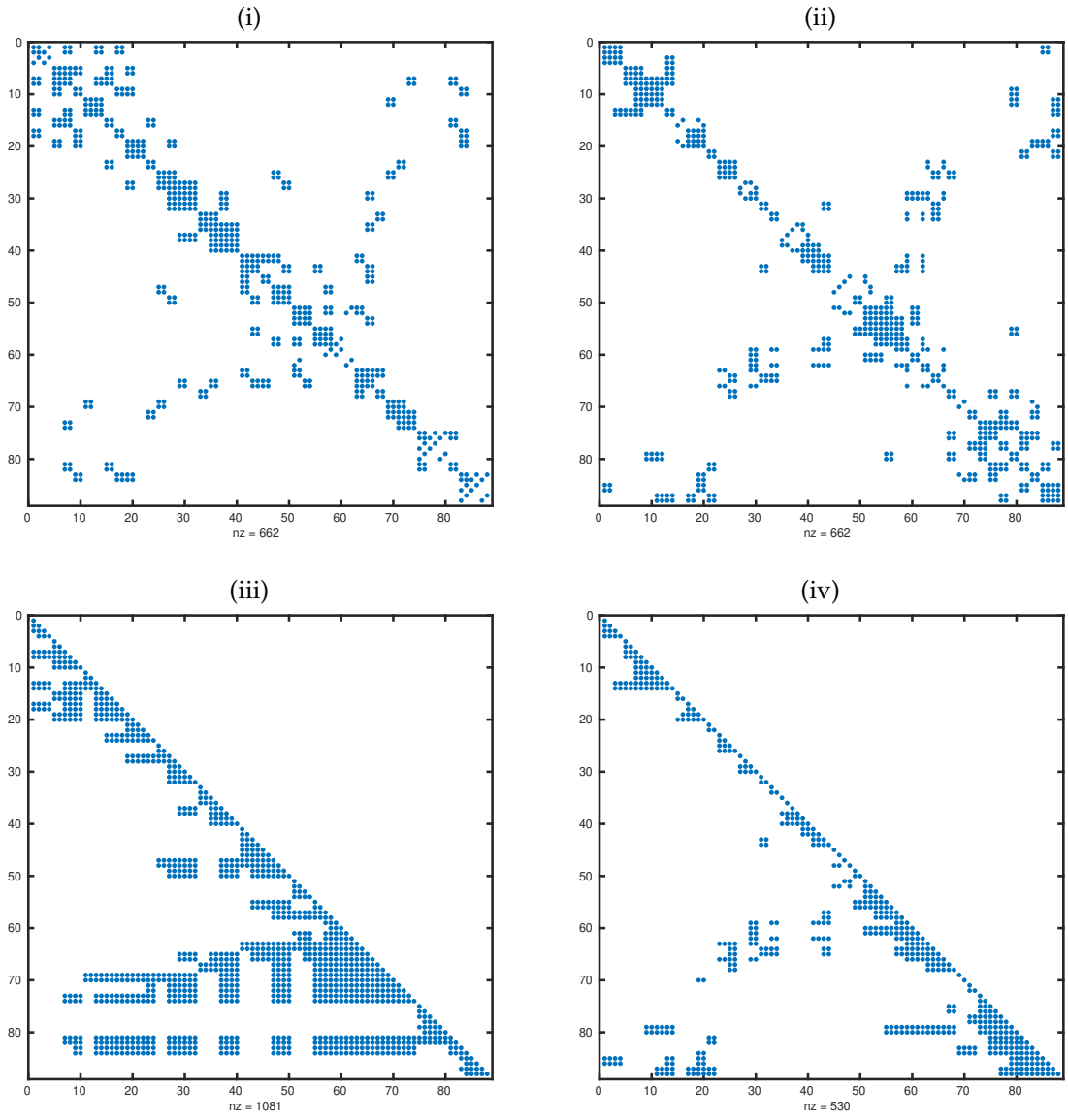

Figure 7.2: Matrix structure and number of nonzero entries of (i) the initial admittance matrix, (ii) the admittance matrix after reordering according to AMD, (iii) matrix factor $\boldsymbol{L}$ obtained from an LU factorization of (i) and (iv) the matrix factor $\boldsymbol{L}$ obtained after reordering

factorization prior to attempting to solve the problem can be fully exploited if repeated calculations relying on the same coefficient matrix but different right hand sides need to be performed. The proposed method presented relies on solving the augmented dynamic admittance matrix (4.11) once for each machine. The method can therefore greatly benefit from using sparse matrix methods to optimize the numerical performance.

7.3 Eigenvalue iteration algorithm

The purpose of this function is to initialize the model of the power system which the assessment is based upon with the correct eigenvalue. Input to the function are the system admittance matrix augmented with the linearized loads, an initial estimate of the eigenvalue and the dynamic

equivalent data of the machines and associated control systems. Furthermore a reference machine needs to be defined for which the torque mismatch and resulting eigenvalue change is calculated. The theory behind the algorithm is described in section 6.5. The eigenvalue is obtained through an iterative procedure following the procedure described in algorithm 2. The admittance matrix provided to the algorithm is the reordered system matrix including the regular load admittances as well as the linearized representation of the nonlinear loads.

Algorithm 2: The algorithm used to initialize the model with the correct eigenvalue

Input: Eigenvalue estimate s_0, admittance matrix $\boldsymbol{Y}$, reference machine dg, machine data

Output: Model eigenvalue s, eigenvectors u, w, transfer functions $\boldsymbol{TF}$ and derivatives $\frac{\partial \boldsymbol{TF}}{\partial s}$, device voltages ΔV

```
foreach Eigenvalue do
    while Δs > threshold do
        Calculate machine transfer functions TF at s ;
        Calculate equivalent device admittances of the nondisturbed machines Y_gng;
        Factorize (Y − Y_g) into L and U;
        Solve nodal equation for the device voltages ΔV;
        Calculate Torque mismatch ΔT;
        Determine transfer function derivatives ∂TF/∂s;
        Solve nodal equation for the derivative ∂ΔV/∂s;
        Calculate eigenvalue shift Δs;
        Determine s;
    end
    if eigenvalue converged then
        Determine right eigenvector u;
        Calculate left eigenvector w;
    end
end
```

The reference machine is considered as the only current source in the system while all other machines are represented as passive devices by modifying their device admittance according to (6.45) and (6.44). The obtained admittance matrix differs from the regular dynamic admittance matrix, due to the modification of the device admittance. The structure of the admittance matrix is unaltered and the factorization can still benefit from the improved ordering. The device admittance depends on the frequency s and the matrix factors therefore need to be recalculated for each eigenvalue estimate.

The eigenvalue is obtained through an iterative procedure aiming at minimizing the torque mismatch at the reference machine. The current injection vector contains only two entries associated with the d- and q- axis current of the reference machine and the admittance matrix is typically very sparse as well. When multiple eigenvalues are to be obtained the algorithm can easily be parallelized by assigning seperate eigenvalues to different cores.

7.3.1 Choice of reference machine

The performance of the iterative procedure of determining the eigenvalue depends on how well the chosen reference machine is suited for calculating a given eigenvalue. In order for the machine to converge to the desired mode the initial estimate must be such that the system gets attracted to the desired solution. If the selected reference machine has only minor participation in the mode of interest it will most certainly be attracted to a solution where the machine is more dominant.

An indicator of which machines are suitable for the assessment can be the magnitude of the speed or angle oscillations which can be estimated from system measurements. The principal characteristic of most of the dominant oscillatory modes is typically well known and locations suitable for perturbation can be determined based on experience from offline model studies or operation.

The dependency of the estimation on the choice of reference machine is illustrated in figure 7.3 at the example of the Nordic 44 system, which is described in chapter 8.1. The algorithm is applied considering that the initial eigenvalue estimate contains an error of 20%. Zero values indicate that the eigenvalue did not converge to the desired mode. The number of iteration until successful convergence shown in (i) ranges from $4-7$ for the machine that converged to the actual eigenvalue.

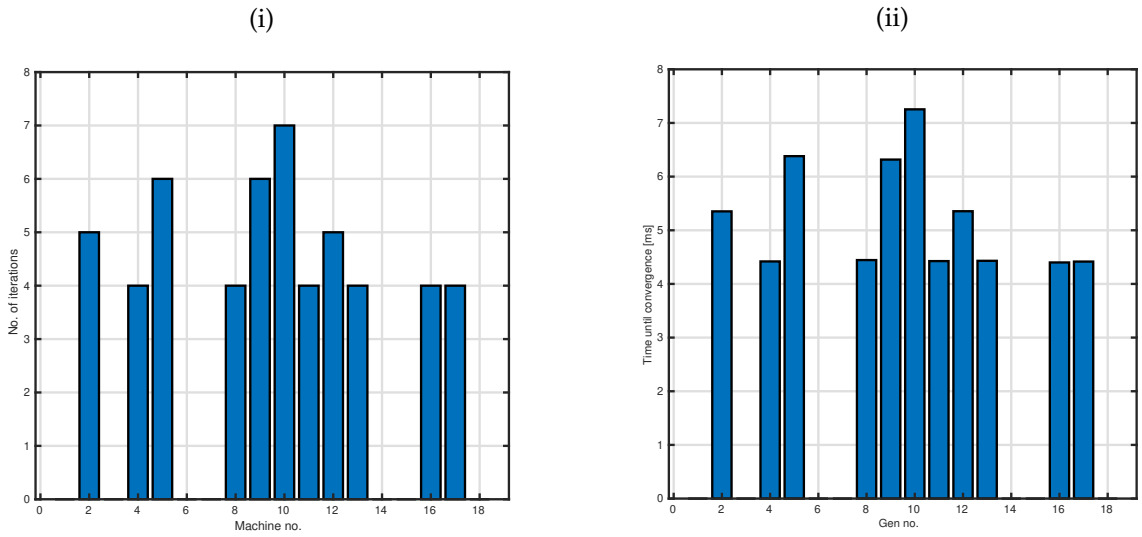

Figure 7.3: Number of iterations (i) and time (ii) until convergence depending on choice of reference when an error of 20% is imposed on both real and imaginary part of the initial eigenvalue. Zero values indicate that the respective machine did not converge to the correct eigenvalue. The eigenvalue tolerance is set to 10^{-4}

Apart from the successful convergence, the choice of the reference also impacts the runtime as the number of iterations until convergence shown in (i) in 7.3 varies from $4-7$. The minimum time to determine the eigenvalue from the given estimate is $4.4\,\mathrm{ms}$ obtained as the average of 1000 independent function calls with the same initial conditions. The average time for each iteration determined based on the iterations exceeding 4 compared to the average of the machines needing the minimum of 4 iterations is $0.95\,\mathrm{ms}$. Considering that the method is aiming at a continuous evaluation of the operating conditions, the problem of finding the eigenvalue rather becomes a problem of tracking the eigenvalue between subsequent system snapshots. The eigenvalue

between subsequent iteration will typically vary only little and if the eigenvalue from the previous time step is used as an input the mismatch can be expected small such that a result can be expected in very few iterations.

7.3.2 Efficient calculation of the left eigenvector

From the regular iterative procedure of the algorithm only the right eigenvector is obtained right away as a byproduct of the solution process. In the following, a method that efficiently calculates the left eigenvector is presented. The process reuses the factorization and the system model determined during the last iteration of the iterative loop.

Transposing the eigenvalue problem related to the left eigenvector given by (4.53) in section 4.5, results in (7.3).

$$\left(\boldsymbol{M}s + \boldsymbol{T_\omega}\right)^T \boldsymbol{w} = \boldsymbol{0} \tag{7.3}$$

Equation (7.3) can be expressed in terms of the machine transfer functions in matrix form by (7.4), which is derived from (4.12) in section 4.2.

$$\boldsymbol{0} = \left[\left(\boldsymbol{M}s + \boldsymbol{G_{T\omega}}\right) + \boldsymbol{G}_{\boldsymbol{I\omega}}^T \left(\boldsymbol{Y}^T - \boldsymbol{Y}_{\boldsymbol{d}}^T\right)^{-1} \boldsymbol{G}_{\boldsymbol{TV}}^T\right] \boldsymbol{w} \tag{7.4}$$

The term $\left(\boldsymbol{Y}^T - \boldsymbol{Y}_{\boldsymbol{d}}^T\right)^{-1} \boldsymbol{G}_{\boldsymbol{TV}}^T$ in (7.4) can be obtained by solving (7.5) for $\boldsymbol{x}$.

$$\left(\boldsymbol{Y} - \boldsymbol{Y_d}\right)^T \boldsymbol{x} = \boldsymbol{G}_{\boldsymbol{TV}}^T \tag{7.5}$$

The sparse matrix factors of the non transposed problem have already been determined in the process of calculating the eigenvalue. The existing factors are given by the lower triangular matrix $\boldsymbol{L}$, the upper triangular matrix $\boldsymbol{U}$ and the permutation matrix $\boldsymbol{P}$. The matrix factors relate to an arbitrary sparse initial matrix $\boldsymbol{S}$ by (7.6). The transpose of the initial matrix is then obtained by (7.7).

$$\boldsymbol{P}^T \boldsymbol{L}\boldsymbol{U} = \boldsymbol{S} \tag{7.6}$$

$$\boldsymbol{U}^T \boldsymbol{L}^T \boldsymbol{P} = \boldsymbol{S}^T \tag{7.7}$$

Equation (7.5) can therefore be efficiently be solved reusing the matrix factors from the last iteration of the eigenvalue algorithm. The transposed factors $\boldsymbol{L}^T$ and $\boldsymbol{U}^T$ become upper respective lower triangular and the transposed problem $\boldsymbol{S}^T\boldsymbol{x} = \boldsymbol{b}$ is then solved by the sequence described in (7.8)

$$\begin{aligned} \boldsymbol{U}^T \boldsymbol{y} &= \boldsymbol{b} \\ \boldsymbol{L}^T \boldsymbol{z} &= \boldsymbol{y} \\ \boldsymbol{P}\boldsymbol{x} &= \boldsymbol{z} \\ \boldsymbol{x} &= \boldsymbol{P}^T \boldsymbol{z} \end{aligned} \tag{7.8}$$

The left eigenvector can therefore be obtained by reusing the initial factorization of the augmented admittance matrix by solving (7.9) for $\boldsymbol{s}$.

$$\boldsymbol{U}^T \boldsymbol{L}^T \boldsymbol{P} \boldsymbol{x} = \boldsymbol{G}_{\boldsymbol{TV}}^T \tag{7.9}$$

Using the same approach as in the main loop the left eigenvector of the reference machine is set to 1 and the remaining components are derived from (7.10)

$$w_{ng} = -\frac{G_{I\omega}^T \, x_{ng}}{M_{ng} s + G_{T\omega}} \tag{7.10}$$

7.4 Power flow sensitivity algorithm

The purpose of the power flow sensitivity algorithm is to construct and evaluate the Jacobian matrix for each assessed machine considering a perturbation of the power injection of $1pu$. The input to the algorithm is the snapshot of the steady state operating conditions in the system. The outline of the algorithm is summarized in algorithm 3.

Algorithm 3: Illustration of the algorithm assessing steady state sensitivities

Input: Admittance matrix $\boldsymbol{Y}$, bus Voltages $\boldsymbol{V}$, power injections $\boldsymbol{S_g}$,$\boldsymbol{S_l}$

Output: Steady state voltage sensitivity $\frac{\Delta \boldsymbol{V_{ss}}}{\boldsymbol{P}}$, machine current sensitivity $\frac{\Delta \boldsymbol{I_g}}{\boldsymbol{P}}$, rotor angle sensitivity $\frac{\Delta \boldsymbol{\delta}}{\Delta \boldsymbol{P}}$ stored in $\boldsymbol{p}$

foreach *snapshot* **do**

- Construct the Jacobian matrix $\boldsymbol{J}$ 6.4.1;
- Determine the LU-factorization of $\boldsymbol{J} = \boldsymbol{PLU}$;
- Evaluate $\boldsymbol{PLU} \Delta \boldsymbol{V_{ss}} = \boldsymbol{d}$ for each machine;
- Calculate $\Delta \boldsymbol{\theta_g}$, $\Delta \boldsymbol{\delta_g}$ and $\Delta \boldsymbol{I_g}$ 6.4.2;
- Based on $\Delta \boldsymbol{V_l}$, determine $\Delta \boldsymbol{Y_l}$ 6.4.2 and A ;

end

When the additional power injection of each machine is assessed against the reference machine the disturbance vector $\boldsymbol{d}$ containing the active and reactive power mismatches is determined by a single entry related to the active power disturbance of the perturbed machine. When the power flow sensitivity is assessed in respect each of the n machines in the system the disturbance vectors are assembled into a matrix with n columns each related to one active power injection perturbation. The subset of the resulting matrix related to active power $\boldsymbol{d_P}$ is shown in (7.11).

$$\boldsymbol{d_P} = \begin{bmatrix} \Delta P_{g_1} & & \\ & \ddots & \\ & & \Delta P_{g_n} \end{bmatrix} \tag{7.11}$$

The resulting set on linear equations is then given by (7.12). This problem can efficiently be calculated by factorizing the Jacobian in terms of its $\boldsymbol{L}$ and $\boldsymbol{U}$ factors and solving for each right

hand side in parallel. For the 44 bus 18 machine system the process of obtaining the complete set of steady state sensitivities for all the 17 machines took in average $1\,\mathrm{ms}$.

$$\boldsymbol{J}\begin{bmatrix}\Delta V_{Q_{pv}}\\ \Delta V_{D_{pq}}\\ \Delta V_{Q_{pq}}\end{bmatrix} = \begin{bmatrix}\boldsymbol{d_P}\\ \mathbf{0}\\ \mathbf{0}\end{bmatrix} \tag{7.12}$$

The sensitivities of the machine currents and rotor angles are then directly derived according to (6.35) - (6.37). The load sensitvity matrices are determined based on (6.38) - (6.40).

The range of ΔP where the linear assessment provides a good approximation of the real trajectory of the power system is limited by the degree of nonlinearity of the system. The more the nonlinearities in the system dominate the trajectory of the operating point the smaller becomes the region where the linear prediction is accurate.

7.5 Eigenvalue sensitivity algorithm

The purpose of the eigenvalue sensitivity algorithm is to combine the results of the algorithm presented in the previous sections to determine for each machine the shift in eigenvalue if the power injection is increased by $1pu$ in respect to the reference machine. The relevant theory is related to section 6.6 of the thesis. It employs a first order eigenvalue sensitivity assessment of the form (4.56) to determine the element-wise eigenvalue shift. The analytically derived machine transfer function sensitivities are evaluated in respect to the steady state parameter sensitivities obtained from algorithm 3.

By exploiting the synergy between the method that initializes the system with the correct eigenvalue and the method that evaluates the eigenvalue shift due to a given redispatch scenario, some computationally expensive calculations can be avoided. The device voltage changes $\boldsymbol{\Delta V}$ as well as the machine transfer functions and their derivatives in respect to the eigenvalue are readily available as a byproduct of algorithm 2.

Algorithm 4: Algorithm for determining the eigenvalue sensitivity

Input: $\Delta \boldsymbol{V}$, $\boldsymbol{TF}$, $\frac{\partial \boldsymbol{TF}}{\partial s}$, $\boldsymbol{p}$

Output: $\frac{\Delta \boldsymbol{s}}{\Delta \boldsymbol{P}}$

Factorize the augmented admittance matrix $(\boldsymbol{Y} - \boldsymbol{G_{IV}})$ in terms of $\boldsymbol{L}$ and $\boldsymbol{U}$;

Calculate sensitivity of the system in respect to s 4.5 ;

foreach *machine except the reference* **do**

- Calculate $\frac{\Delta \boldsymbol{TF}}{\Delta P}$ using $\boldsymbol{p}$ 4.5 ;
- Determine the load sensitivity in respect to $\Delta \boldsymbol{V_{ld}}$ 4.4 ;
- Solve (6.56) to obtain the device voltage change ;
- Insert the device voltages in $eq : dTdP$ to obtain the torque changes;
- Determine the eigenvalue shift $\Delta s/\Delta P$ using (6.54) ;

end

An overview of the algorithm is presented in algorithm 4. The admittance matrix augmented by the dynamic device admittances is factorized to optimize the solution for the device voltages. The voltage sensitivities need to be determined once to consider the effect of frequency changes and $n-1$ time for the assessment of the active power injections, where n is the number of machines in the system. The result of the algorithm are the $n-1$ sensitivities that relate to an injection change in respect to the reference machine. This part is the main computationally expensive part of the algorithm since it involves factorizing the augmented admittance matrix and calculating the machine transfer function sensitivities as well as the device voltage sensitivities. The factorization only needs to be performed once since the matrix factors are constant during the iterations. Each other calculation though has to be performed $n-1$ times. Solving the same 18 machine 44 bus system as in section 7.3 took in average $8.8\,\mathrm{ms}$. Analyzing the time that is spent for certain components of the algorithm reveals that for this small system the calculation of the transfer function derivatives is the most time consuming component. Another reason for the relatively long runtime is that the code is executed sequentially assessing each machine after the other. Since the individual evaluations within the for loop are independent of each other, it should be possible to execute the code in parallel to achieve a considerable speed up.

7.6 Computational complexity

The algorithm is optimized in such a way that it makes efficient use of the synergies between the different functionalities by transferring the relevant results between the blocks. The largest part of the assessment method scales linearly with the amount of machines in the system and can for the most part be parallelized. The most computationally demanding elements in terms of how they scale with the problem size are the evaluations related to the different admittance matrices. Preordering the elements in the admittance matrix by means of an AMD algorithm reduces the number of nonzeros in the matrix factors of the admittance matrices and furthermore reduces the time spent for the factorization.
For the 44 bus system, the runtime of the algorithm to determine all the 18 critical sensitivities was in average $12.8\,\mathrm{ms}$. To investigate the scaling of the method with increasing system size, it was also applied to the WECC 179 bus system (adopted from [74]). Due to the unavailability of dynamic generator data, each generator was represented by the same sixth order dynamic model. The specific results of the assessment method are therefore not representative. However, the system was considered suitable to evaluate the performance of the method. After performing 1000 iterations of the method the average time to assess the critical margins for all 29 machines in the system was $35.4\,\mathrm{ms}$. Considering that the second system has more than 3 times the amount of nonzero elements in the admittance matrix (2172 as compared to 662) and almost 50 % more machines the scaling of the method can be considered satisfactory. Unfortunately there was no larger test system with dynamic data available at time to further investigate the performance of the method in very large power systems. It should be noted that no dedicated parallelization was implemented except for the automated parallel processes in MATLAB. Considering that one of the most time consuming processes in the solution process is the evaluation of the transfer function sensitivities for each operating point, a considerable speed up can be expected if that particular functionality is executed in parallel. Considering the current performance and the potential improvements the method can be employed in online applications to provide a fast assessment of prevailing stability and security margins.

Part IV

Test of Method

CHAPTER 8

Test case: Application of the assessment method to the Nordic Power System

This chapter describes the scenario and the results of the test performed to demonstrate the capabilities and added value of the proposed assessment method. A test case is generated based on a representation of the Nordic power system.

8.1 Description of the test system and scenario

For the purpose of validating the performance of the proposed method testing is performed on the Nordic 44 [69] which is a reduced model of the Norwegian, Swedish and Finnish system. The system is driven towards instability by generating a set of operating points that allow to illustrate the functionalities of the developed assessment algorithm. An overview of the simplified Scandinavian system is provided in figure 8.1. The system is partitioned into five different areas: South Norway (NO^S), North Norway (NO^N), South Sweden (SE^S), North Sweden (SE^N) and Finland (FI).

The inter-area mode selected for generating the test case involves machines in southern Norway that oscillate against the machines in the rest of the system, most prominently Finland and southern Sweden. The location of the machine buses and the corresponding areas are summarized in table 8.1. All generators in the system are represented by a detailed sixth order machine models. The type of machines refers to, whether the plant is either hydro based (HY) or thermal based (TH). Hydro generators are modeled as salient pole machines, while thermal generators are represented as round rotor machines. The active power component of the loads in the system are modeled as 60 % constant current and 40 % constant impedance while the reactive power component is assumed as 100 % constant impedance. The system has 7 HVDC buses which are represented as additional load buses with either positive or negative injection in the system. The particular effect of the HVDC systems on the damping of the inter-area modes, as for instance through active power modulation, is therefore not taken into account.

The system, in its initial state was very stable and only a low sensitivity of the oscillatory mode to reasonable changes in power flow could be detected. Studying the characteristics of the system in detail revealed that oscillatory stability problems could be provoked by increasing the flow of active power from Norway to Sweden through the transmission lines connecting south Norway with southern Sweden. This effect can be observed in the real system as well [75] which shows that some of the essential characteristics of the real power system are contained in the reduced model.

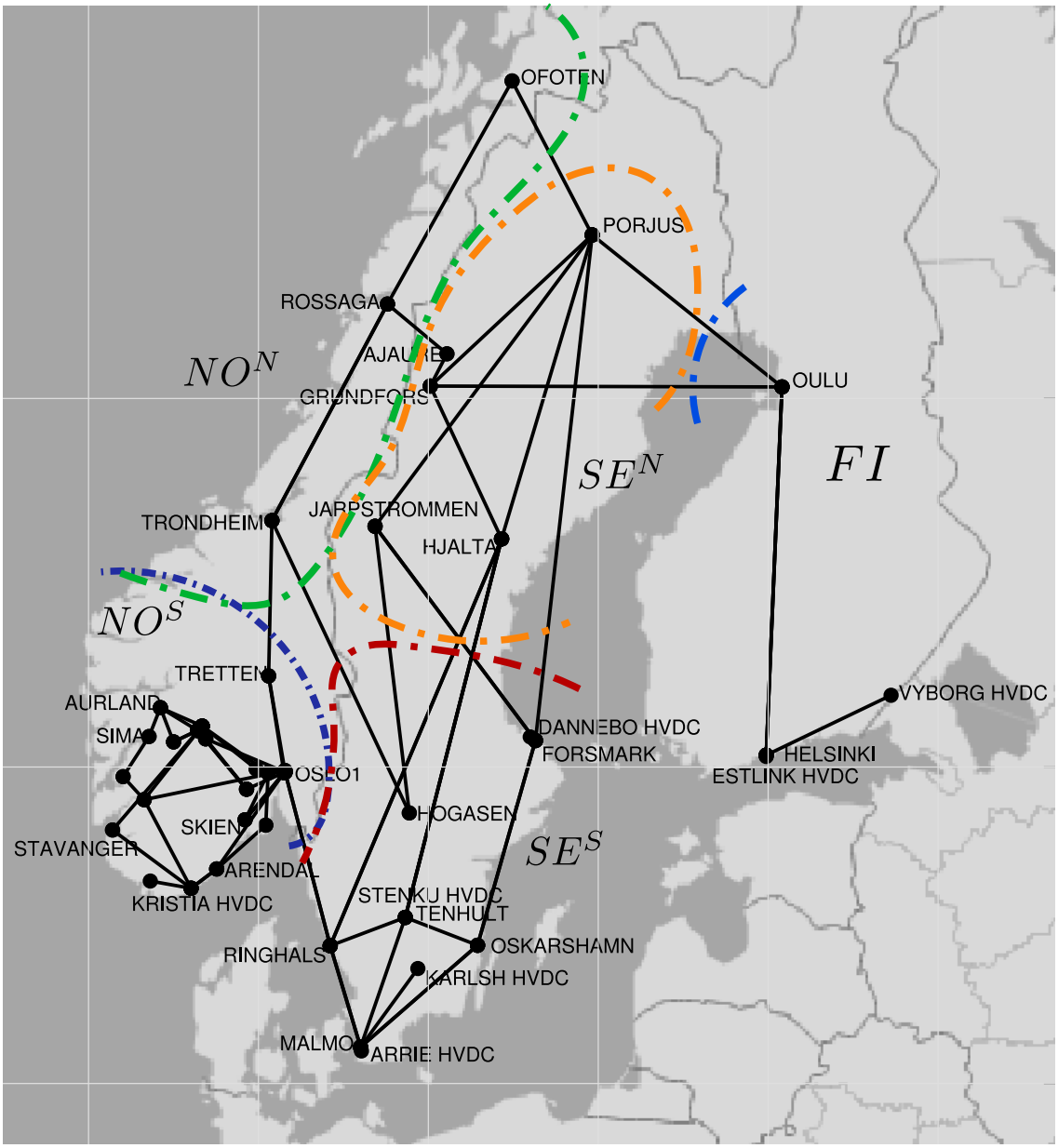

Figure 8.1: Locations of the lines and buses in the Nordic 44 test system. The system is split into five different regions: South Norway, north Norway, south Sweden, north Sweden and Finland. The colored lines indicate the boundaries between the regions.

In order to generate a case that is initially stable but is also relatively quickly driven towards instability the initial power flow scenario is adjusted.

To induce oscillatory stability problems a $n-1$ contingency is considered by disconnecting one of the lines connecting Hasle on the Norwegian side and Ringhals on the Swedish side as indicated in figure 8.2. A total of six different operating points are generated each representing the steady state conditions taken at different times. After the initial trip of the line the power export from Norway is deliberately increased in small steps to illustrate the approach and subsequent crossing of the stability boundary. The series of events that finally lead to oscillatory instability are summarized in table 8.2.

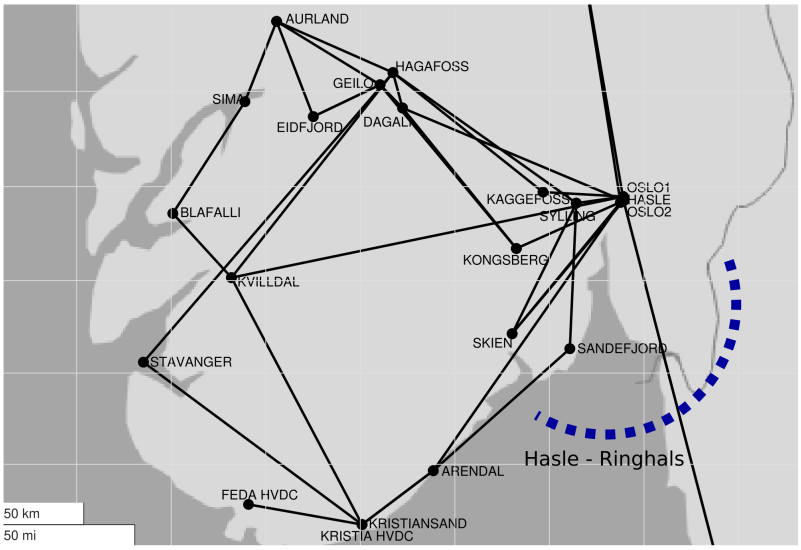

Figure 8.2: Detailed view of the network in southern Norway

Table 8.1: Generator buses and their location in the system

Gen.	Type	Location	Area	Gen	Type	Location	Area
1	TH	Forsmark	SE^S	10	HY	Oslo 2	NO^S
2	HY	Porjus	SE^N	11	HY	Kristiansand	NO^S
3	HY	Jarpstrommen	SE^N	12	HY	Kvilldal	NO^S
4	HY	Grundfors	SE^N	13	HY	Blafalli	NO^S
5	TH	Oskarshamm	SE^S	14	HY	Trondheim	NO^N
6	TH	Ringhals	SE^S	15	HY	Rossaga	NO^N
7	HY	Tretten	NO^S	16	TH	Helsinki	FI
8	HY	Sima	NO^S	17	HY	Oulu	FI
9	HY	Oslo 1	NO^S	18	TH	Malmö	SE^S

Initially after the trip of the line *Hasle - Ringhals* the damping ratio of the inter-area mode is reduced to 6.66%. This is still well above any of the practical limits reported by a number of utilities in [14]. Increasing the power flow across the weakened transmission corridor, however, quickly diminishes the damping margin and consequently leads to an oscillatory unstable system.

8.2 Results obtained by applying the assessment method

This section presents the results of the assessment method when applied to the test sequence described in section 8.1. The first part describes the results obtained from an element-wise assessment, where each machine is assessed individually. The second part then focuses on an area-wise assessment which attempts to combine the individual sensitivities to provide a representative indication of the margin of a whole subsystem.

8.2.1 Element-wise assessment of oscillatory stabilty

The assessment method is applied to each of the operating points presented in table 8.2. The numerical results of the assessment in respect to the stability boundary of the four machines

Table 8.2: Summary of the events leading to oscillatory instability of the system. All generation changes are related to an increased demand in Sweden and therefore increase the flow towards Sweden.

Scenario	Event	Effect	Damping
1	Base case characterized by large power export from Norway to Sweden		9.17%
2	Disconnection of the line Hasle-Ringhals	Decrease damping by 2.51%	6.66%
3	Increase generation by 200 MW in Kristiansand. Load @ Oskarshamm	Decrease damping by 2.59%	4.07%
4	Increase generation in Kristiansand by 200 MW. Load @ Ringhals	Decrease damping by 3.28%	0.79%
5	Increase generation in Sima by another 75 MW. Load @ Ringhals	Decrease damping by 1.46% - Crossing of the stability boundary:	-0.67%
6	Increase generation in Sima by 100 MW. Load @ Ringhals	Decrease damping by 1.68% - The mode now has a large negative damping	-2.35%

with the smallest critical percentage margin in the direction of increasing power are presented in table 8.3. These margins represent the distance to instability, i.e. when the damping of the mode is predicted to be zero. Table 8.4 additionally includes the results from an evaluation of each operating point in respect to its distance to the security boundary. The security boundary is here considered as a damping ratio of 4%.

Table 8.3: Percentage stability margin of the 4 most critical machines in increasing power direction

Machine	Operating Point					
	1	2	3	4	5	6
8	>100 %	13.58 %	6.72 %	1.09 %	-0.86 %	-2.73%
11	88.24 %	13.02 %	6.15 %	0.95 %	-0.77 %	-2.52%
12	>100 %	34.91 %	17.19 %	2.77 %	-2.23 %	-7.28%
13	>100 %	13.78 %	8.31 %	1.35 %	-1.08 %	-3.53%

Table 8.4: Percentage security margin (considered as 4% damping) of the 4 most critical machines for increasing power direction

Machine	Operating Point					
	1	2	3	4	5	6
8	73.46 %	5.94 %	0.13 %	-4.79 %	-6.45 %	-8.00%
11	59.92 %	5.67 %	0.12 %	-4.19 %	-5.73 %	-7.36%
12	>100 %	15.25 %	0.34 %	-12.21 %	-16.70 %	-21.29%
13	88.12 %	7.35 %	0.16 %	-5.94 %	-8.13 %	-10.37%

The results of the sensitivity assessment confirm the relative stability of the initial operating point since most of the margins are greater than 100 % which indicates that a machine would have to more than double its generation to cause instability. After the line trip both, the stability and the security margin, shrink considerably. While the stability margin of machine 11 was still about

88% before the fault it is now reduced to just 13%. The reduction of the stability margin already indicates emerging stability problems. Recalling that the damping ratio in this case is still above 6% there is no direct indication of these issues from observing the damping alone. A visualization of the stability margins of all the machines is provided in figure 8.3. The machines for which increasing power injections lead to instability are located within the area spanned by the stability boundary represented by the red line. Machines where a reduction of power injection in respect to their critical counterpart leads to instability are located on the other side of the boundary. If a margin of 20% was to be considered critical, as indicated here by the yellow lines surrounding the stability boundary, several machines can be regarded as being dangerously close to the emergency threshold.

Table 8.5: Active power margins in MW of all machines after the line trip (OP 2)

Gen.	Area	Margin	Gen.	Area	Margin	Gen.	Area	Margin
1	SE^S	−487.4 MW	7	NO^S	672.2 MW	14	NO^N	−489.7 MW
2	SE^N	−500.0 MW	8	NO^S	502.7 MW	15	NO^N	−496.5 MW
3	SE^N	−495.1 MW	9	NO^S	522.2 MW	16	FI	−503.3 MW
4	SE^N	−495.1 MW	10	NO^S	556.6 MW	17	FI	−503.5 MW
5	SE^S	−496.6 MW	11	NO^S	487.4 MW	18	SE^S	−494.8 MW
6	SE^S	−498.9 MW	12	NO^S	495.5 MW			
			13	NO^S	527.7 MW			

The results in terms of total active power margin for this operating point are presented in table 8.5. While only minor differences can be observed in the receiving areas, the individual machine sensitivities in the South Norway system deviate as much as ±38%. In particular machine 7 which is located close the edge of the area has a significantly larger margin than the remaining machines.

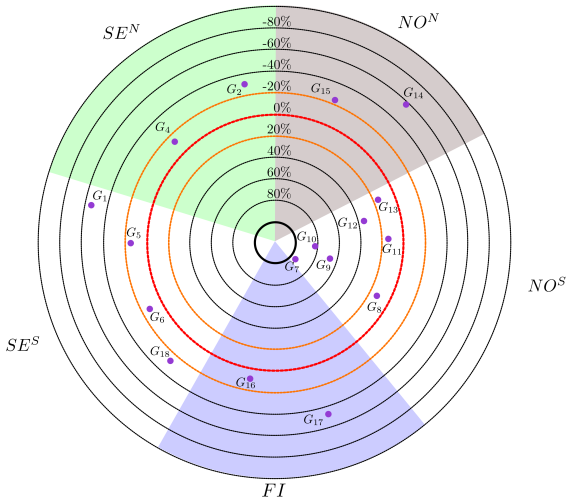

Figure 8.3: Stability margins after the line trip (OP 2). Damping ratio of the oscillation $\zeta = 6.66\%$

If the power transfer across the weakened transmission line is further increased, the system slowly approaches instability which is reflected by the shrinking margins of the machines. Between operating points 3 and 4 the damping ratio falls below the predefined security threshold of 5%, which is indicated by the negative security margins in operating points 4-6. This is reflected in

figure 8.4 where all machines except generator 3, which is a relatively small machine, are now within the critical area and about to cross the boundary.

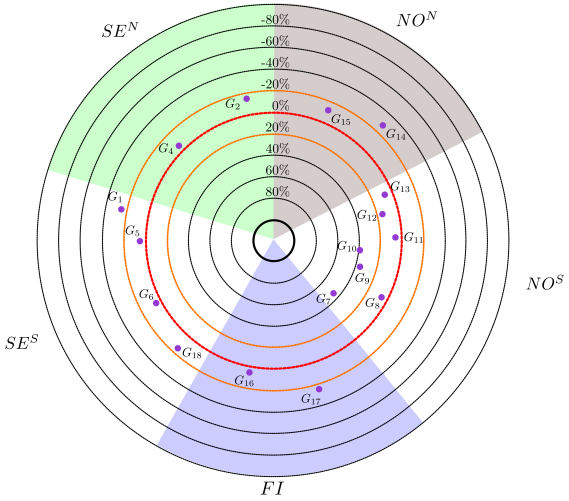

Figure 8.4: Margins after the export from Norway has increased by 200 MW (OP3). Damping ratio $\zeta = 4.07\%$

The situation after the stability boundary has been crossed is related to the margins indicated in figure 8.5. The are now located on the other side of the boundary referring to the change of sign in power direction that leads to the boundary. Instead of indicating the distance to instability the margins now rather point out the distance to stability, i.e. the active power change that leads to a marginally stable system.

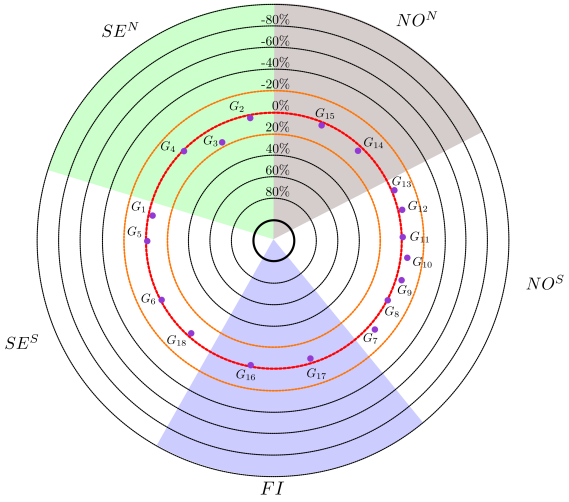

Figure 8.5: Margins after the stability boundary has been crossed (OP5) $\zeta = -2.35\%$. The change of sign of the margins indicates opposing direction towards the boundary.

To illustrate the trajectory of the margins, operating points 2, 3 and 5 are combined in a single visualization in figure 8.6. The process of emerging instability is indicated by the movement of all machines towards the boundary. While the operating points of the machines in southern Norway approach the boundary from the center, the remainder of the machines in the system moves in the opposite direction as indicated by the arrows within each area. Due to the percentage based

assessment, machines with a lower power output appear to move faster along their trajectory since all machines reach the boundary at the exact same time.

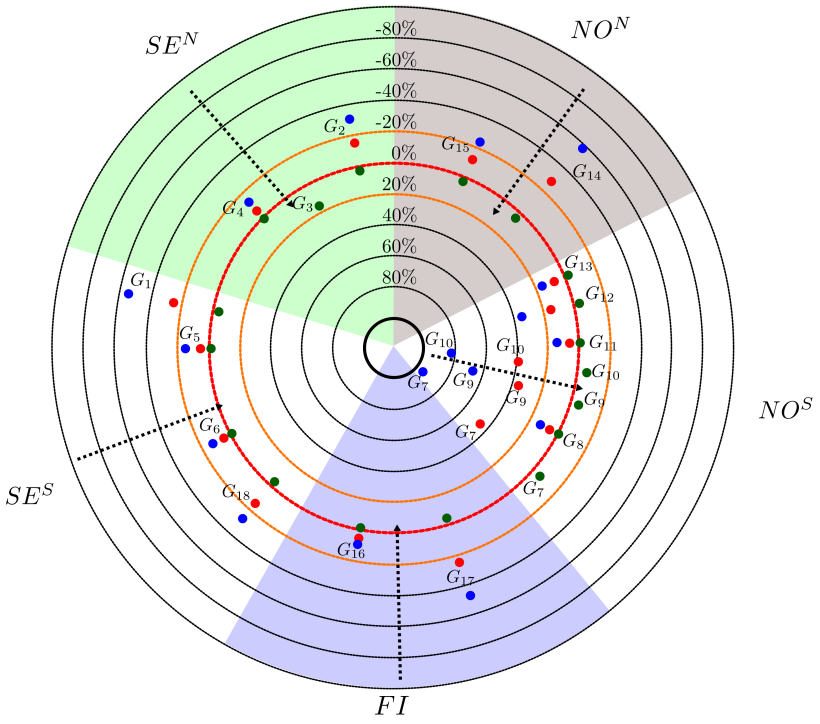

Figure 8.6: Visualization of the trajectory of the machines margins from OP2 (blue) and OP3 (red) to OP 5 (green)

8.2.2 Area-wise assessment of stability

The results of the area-wise assessment are presented in tables 8.6 and 8.7. Table 8.6 summarizes the minimum margins of all areas in percent of their active power generation. The area-wise assessment provides a good overview when export from one area into the other is the cause for oscillatory instability as it provides an overview of the area as a whole. The margin of NO^S in table 8.6 after the line trip 3.67% is a result of the combination of a small active power margin and the large generation. Since a large portion of the active power supplies the local load in the area, it might be relevant to relate the stability limit directly to the export of power. Such a measure is included in table 8.7, where the results from the perspective of the machines in Southern Norway are summarized. Additionally to the previously presented percentage based assessment, active power margins in MW and in percent of the current export are presented. The active power export is evaluated as the sum of the power flow across all the lines that leave the area. This area flow based assessment can help to identify the limitations of the critical cross-area transmission corridors, which are the typical limiting elements in respect to the oscillatory stability of the system. The development of the flow from NO^S into the system is illustrated by the black asterisks in figure 8.7.

The active power is measured at the receiving end, and the dip observed after the line trip in OP 2 results from additional losses due to the increased impedance. The estimated boundary against the machines in South Sweden is indicated by the blue asterisks for each operating point. The

Table 8.6: Area-wise active power margin for the export from Southern Norway into the remaining system

OP	NO^S	NO^N	SE^S	SE^N	FI
1	27.90 %	−141.9 %	−38.83 %	−68.77 %	−79.65 %
2	3.67 %	−17.96 %	−5.12 %	−8.97 %	−8.71 %
3	1.78 %	−8.84 %	−2.52 %	−4.41 %	−4.27 %
4	0.28 %	−1.42 %	−0.40 %	−0.71 %	−0.69 %
5	−0.23 %	1.15 %	0.33 %	0.57 %	0.55 %
6	−0.73 %	3.73 %	1.05 %	1.86 %	1.80 %

dashed red line indicates the trajectory of the estimated margins between the different operating points. The nonlinearity of the margin results from a variety of factors. One of the largest impact factors are the loads. As the assessment is performed assuming a given system load the margin is adjusted in between subsequent operating points to reflect the changing load conditions. The impact the load has on system stability varies from location to location. In the provided example it can, for instance, be concluded that the first load increase between operating points 2 and 3 has a significantly larger effect on the stability margin than the load increase between operating points 3 and 4. The magnitude is the same in both cases while the location differs. Consequently, a load increase in Oskarshamm affects the system more than an increase in loading in Ringhals. Considering that the distance to the machines in Norway is shorter in the second case, this can be expected. The load change also affects the calculated sensitivities of the machines, which in turn influences the estimated boundary. ´ The calculated margins presented in table 8.7 can therefore not directly be applied to the observed boundary between operating points 4 and 5.

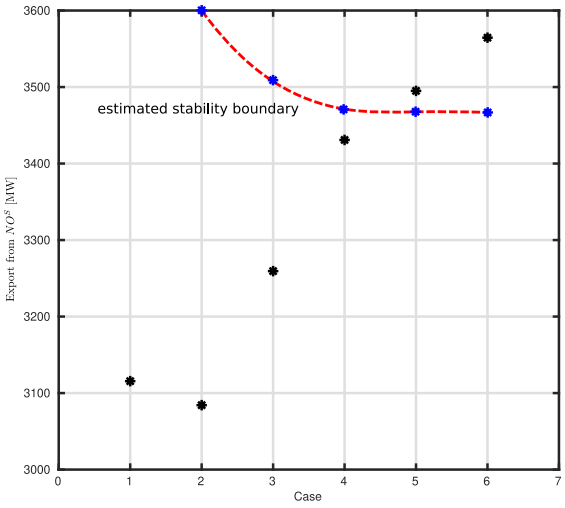

Figure 8.7: Power export from Southern Norway into the rest of the system

The margins derived from the method indicate the drastic reduction of the available stability margins as soon as the line *Hasle - Ringhals* is tripped. The available export margin reduces from around 4 GW to just above 500 MW, which is only 13 % of the initial capacity. In terms of the direction of the exported power, there are only insignificant differences between the receiving areas. The individual contributions of the receiving areas are negligible and the machines in Norway can

Table 8.7: Area-wise active power margin for the export from Southern Norway into the remaining system in MW; percent of the total generation ($\%_{tot}$) and in percent of the exported active power ($\%_{exp}$)

	NO^N			SE^S			SE^N			FI		
OP	MW	$\%_{tot}$	$\%_{exp}$	MW	$\%_{tot}$	$\%_{exp}$	MW	$\%_{tot}$	$\%_{exp}$	MW	$\%_{tot}$	$\%_{exp}$
1	4108	29.0	132	3951	27.9	127	4047	28.6	130	4857	34.3	156
2	520	3.7	16.9	523	3.7	17.0	528	3.7	17.1	531	3.8	17.2
3	256	1.8	7.8	258	1.8	7.9	260	1.8	8.0	261	1.8	8.0
4	41	0.3	1.2	42	0.3	1.2	42	0.3	1.2	42	0.3	1.2
5	−33	−0.2	−0.9	−34	−0.2	−1.0	−34	−0.2	−1.0	−34	−0.2	−1.0
6	−108	−0.7	−3.0	−109	−0.7	−3.1	−109	−0.7	−3.1	−109	−0.7	−3.0

be considered the main influence factor.
The area-wise assessment is well suited to provide an overview about the impact of flow patterns on the oscillatory stability. The derived sensitivity depends on the assigned participation factors, which provide a weighting factor for the individual sensitivities. If the local sensitivities are significantly different, the result can be misleading and the element-wise assessment needs to be taken into account.

8.3 Accuracy of the linear prediction

The method employs a first order eigenvalue sensitivity assessment in order to predict the trajectory of the operating point in respect to active power dispatch. Naturally, a linear assessment of a generally non-linear system such as the electric power system leads to some inherent inaccuracies. The region in which the linear assessment provides an accurate representation of the system trajectory is limited by a variety of factors:

- The nonlinearity of the steady state parameters in respect to power injection
- The nonlinearity of the system response in respect to the frequency of the oscillatory mode
- The nonlinearity of the machine transfer functions in respect to the initial conditions

These elements are partially system inherited and partially depend on the operating conditions. The system response in respect to changes of the eigenvalue depends to a large component on the transfer functions of the controllers, such as AVR and PSS, as well as the frequency dependent device impedance. All the aforementioned components are in principal nonlinear and large changes in the eigenvalue cannot be estimated accurately. Typically, the real part of the eigenvalue, as well as its sensitivity, is considerably smaller than the imaginary part. The accuracy of the linear prediction in respect to the real part of the eigenvalue thus depends to a large extend on how stable a mode is in respect to its frequency. Since the eigenvalue sensitivity is determined based on redispatches, it cannot be directly evaluated in respect to the results obtained in the previous sections. It is though possible to assess the linear prediction in terms of expected outcome and the accurate result when comparing a single machine-machine redispatch.
This case is illustrated in figure 8.8 *(i)* for an increase in power output of generator 11 in respect to the reference machine. Considering that the machine is already loaded by 60 % of its capacity in

the inital case it can be expected that nonlinearities influence the results for alrge injection changes. In general the accuracy can be considered sufficient taking into account that from an operational perspective it is rather irrelevant, whether the damping is exactly zero or just slightly above or below.

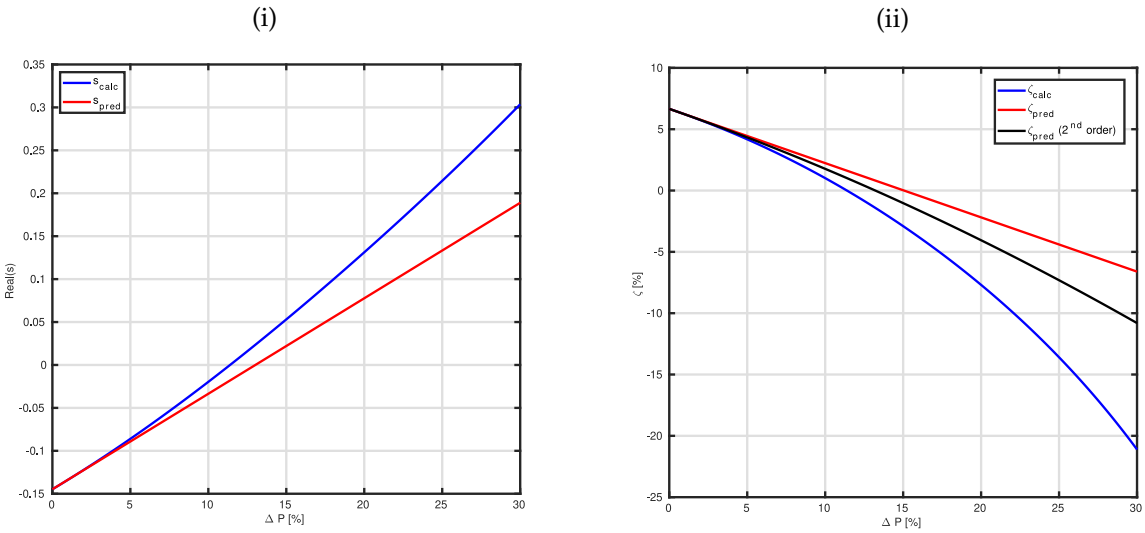

Figure 8.8: Accuracy of the linear prediction illustrated based on machine 11 in OP 2 for: (i): the real part of the eigenvalue (ii): the damping ratio

The accuracy of the prediction of the damping ratio based on the same scenario is shown in figure 8.8 *(ii)*. Two approaches are illustrated here. For obtaining the curve given by the red line, a linear evolution of the damping was considered, while the black line represents the damping estimate, when a second order approximation is employed. In both cases the estimate is based on the linear eigenvalue sensitivity but the result can be slightly improved when the nonlinearity of the damping for linear changes of the eigenvalue is taken into account. Due to the additional nonlinearities, it is more precise to base the assessment directly on the active power margin to the absolute stability limit indicated by $Re(s) = 0$.
The accuracy can be assessed in terms of the total vector error introduced in equation (3.1) as a measure of PMU accuracy. The TVE determined based on the exact result after performing the redispatch and the predicted value is illustrated in figure 8.9. In *(i)*, the TVE is calculated for the single machine-machine redispatch, while in *(ii)* the accuracy of the assessment based on the area prediction is evaluated. The range of the power dispatch is chosen such that the resulting change in eigenvalue is comparable.

The TVE increases exponentially with the distance from the initial operating point such that it can only provide accurate results when the distance to instability is relatively small compared to the size of the system. When the system is approaching the stability boundary, the results become more and more accurate. In the given case the stability boundary is crossed at a distance from the initial point of 11.2% for the single machine case, and 3.1% for the area case . The associated calculated TVEs are 1.18 and 1.33% respectively, which can be considered sufficiently small. Moreover, anything below a threshold of 4% can probably be considered accurate enough for the given application. In most cases it is sufficient to get an estimate of the distance to the boundary that indicates whether the boundary is in the reach of a small disturbance or sufficiently far away. A

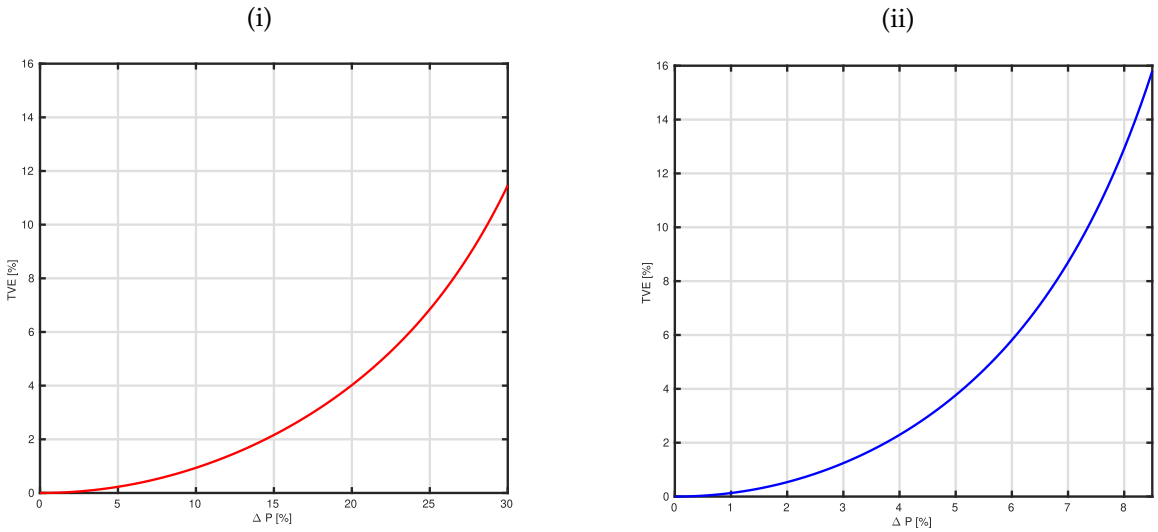

Figure 8.9: Total vector error of the eigenvalue prediction for: (i): the single machine case (G_{11} - G_5) (ii): the area assessment (NO^S - SE^S)

continuous assessment of the prediction error could be included as a separate functionality that is executed in a parallel loop with a lower rate than the main algorithm. Such an assessment could provide indicators of the confidence in the estimated margin.

Part V

Conclusion and Perspective

CHAPTER 9
Conclusion and Future Work

This chapter provides a conclusion of the thesis and presents future perspectives how the obtained results can be further exploited.

9.1 Conclusion

The overall purpose of this PhD project was to develop methods that can provide indicators for emerging oscillatory instability. The focus was to derive active power injection margins that apply to individual machines in the system and thereby provide an early-warning system that indicates when the system is operating close to its oscillatory stability boundary.

The main scope was addressed in three different development phases. Phase I relates to the derivation of an suitable stability boundary. Phase II revolves around the development of a method capable to measure the distance to the stability boundary. Finally, Phase III addresses the implementation of the method by developing algorithms that are fast enough to allow an online assessment of the applicable stability boundaries.

The stability boundary for power system oscillations is clearly defined as the point when the real part of a complex eigenvalue crosses the imaginary axis and shifts to the right half plane of the complex plane. The parameters that lead to oscillatory stability are, however, manifold. The main focus of this thesis was therefore, to limit the parameter space in such a way, that a meaningful stability margin in respect to measurable quantities can be obtained. The initial attempt focused on evaluating the element-wise contributions of individual machines to the eigenvalue. Starting from a two machine system, an equivalent representation of a multi-machine system was derived. The resulting method was able to identify the group that contributes less to the damping of the system. Furthermore, it allows to highlight the element that exhibits the worst performance within the group. The method allows to point out critical elements in the system that potentially cause instability. The shortcoming of this method is, that it does neither indicate the cause for the observed behavior, nor does it allow to determine potential system trajectories resulting from changing operating conditions.

To overcome these shortcomings a method was developed that relies on sensitivity analysis as a predictor to identify the possible system trajectories away from the current operating point. The potential trajectory was limited to the parameter space of the system quantities, that are affected by the power injections of the synchronous machines in the system. The problem was reformulated into a redispatch problem involving an arbitrary set of machines. It was shown, that by applying superposition, the redispatch can be transformed into multiple two machine equivalent systems where the complete system can be solved by calculating the power flow sensitivity of each machine against a reference machine. From the resulting sensitivity information the most critical change in active power which causes instability was derived for each machine. The sensitivity information

was extended to provide margins for a whole subsystem as well as information regarding the distance to a security boundary which can be defined as a specific damping threshold.

To determine the distance to the stability boundary of a given operating point, the eigenvalue of the oscillatory mode, that is to be assessed, needs to be known. While on-line methods can already provide a continuous estimate of the eigenvalue from measuring the ambient response of the system, the underlying system model used in the method needs to be initialized. Therefore, a torque based method that allows fast calculation of a single electromechanical eigenvalue based on machine transfer functions was implemented. The algorithm to determine the eigenvalue sensitivity was realized by using the first order derivatives of the same transfer functions exploiting the synergy between the two functionalities. Finally, sensitivity information in respect to the steady state quantities is obtained from a single evaluation of the power flow Jacobian at the current operating point.

One of the main aims of the project was to come up with solutions which could provide indicators of emerging instability in critical situations. For effectively processing such information, visualizations that allow to quickly identify the root cause are necessary. In this thesis, approaches that allow to visualize the state of each element are provided. They convey useful information regarding the available stability margin by visualizing the distance to instability for each machine based on its current loading. By incorporating area information in the visualization, the critical elements can be quickly identified and directed countermeasures can be applied immediately, since the sensitivity information simultaneously provides an estimate of the most efficient redispatch.

The assessment method was capable to identify a dangerously small margin to the stability limit, when there was no direct indication of approaching instability from an evaluation of the damping ratio. Since current applications, that provide an online monitoring of oscillatory small signal stability, mostly focus on identifying the prevailing modal parameters, frequency and damping, alone, there could be a potential gap to fill. Supplying additional information in respect to the sensitivity of the damping to changing operating conditions, can identify potential issues before they occur. When only a low sensitivity of the operating point is detected, additional transfer capacity can be activated to maximize the utilization of existing transmission corridors.

In order to be of value in real time operation of the power system, it is essential that the method is fast enough to track the constantly varying operating conditions. The developed algorithms make efficient use of the sparsity of the system admittance matrix by relying on factorization methods and an improved ordering of the elements in the matrix. Both the eigenvalue related routines rely on the same factorized form of a nodal injection problem such that the factorization can be exploited to the maximum. The time needed for an assessment of all the sensitivities in a 29 machine, 179 bus system was $35.4\,\mathrm{ms}$. Considering that the current bottleneck of the calculation was determined to be the sequential execution of the eigenvalue sensitivity algorithm, which can be easily parallelized considering some minor changes, the performance can be considered fast enough for the implementation in an online environment.

9.2 Further Work

In this section some of the potential research directions based on the work in this thesis are presented.

Extending the model database

Currently, there is only limited amount of models included in the database. The database was gradually extended based on the needs of the available dynamic test cases. Most of the dynamic test systems include only a limited amount of exciter and PSS models, while power electronically controlled devices such as TCSCs, SVCs, as well as HVDC systems are typically not included. To be able to apply the method to a real system these models need to be accurately reflected in the system model. Furthermore, the loads are typically represented by a static load model based on constant impedance, constant current and constant power characteristics. While this is sufficient in most cases, it might be necessary to include load models based on induction motor characteristics, since they can considerably affect the dynamic performance of the system.
In respect to the additional models it might as well be convenient to base the assessment method on a state space representation of the system, rather than relying on the operational impedance model of the machine. The more modular approach eases the implementation of new models in the system. The operational impedance model was applied mostly due to the computationally efficient evaluation of the steady state sensitivities. Possibly, a hybrid approach could be applied, where the control systems are implemented in their state space form, while machines are represented by operational impedance model. Each of the smaller state space models could then be evaluated in respect to its relevant transfer function for each operating point.

Improving the computational efficiency

Work can be carried out to improve the calculation time of the algorithm. Some of the computationally expensive portions of the code can be parallelized. This includes the calculation of the device transfer functions, as well as the sensitivities of the eigenvalue to the perturbations of the steady state conditions. Furthermore, it might be beneficial to investigate whether some optimization can be achieved by ordering the nodes of the dynamic system in an optimized manner. Currently, the voltage changes are calculated for all system nodes, while for the presented method only the voltage changes of the dynamic devices are needed. Considering that the current injections are also limited to the dynamic devices, there might be a possibility to apply an improved ordering strategy, that exploits the sparse structure of the underlying equations even further.

Interfacing the method with PMU measurements

A function is needed that continuously reads the data stream of measurements and forwards the relevant quantities to initialize the method. Here, a platform, that is already available, can be exploited. The existing platform provides a continuous stream of system snapshots, which can be accessed either locally or through the network. By interfacing the method with the platform, the real-time performance of the method can be evaluated.

Implementing the visualization in the loop

In this thesis, the visualization was performed independent of the main algorithm by plotting the obtained results. A dynamic visualization based on the assessment results could provide continuous information regarding the system state.

Efficient contingency screening

Oscillatory stability often occurs as a result of unexpected contingencies. As illustrated in the test case applied in this thesis, the stability margin can be reduced considerably when the impedance connecting the oscillatory groups increases. A fast contingency could be achieved, by supplying the method with relevant post-fault steady state operating points. The method could then be applied to the post-fault conditions, to provide a fast assessment of the distance to instability of the post fault system, and quickly determine whether a current operating state is n-1 secure.

Bibliography

[1] Prabha Kundur, John Paserba, Venkat Ajjarapu, Göran Andersson, Anjan Bose, Claudio Canizares, Nikos Hatziargyriou, David Hill, Alex Stankovic, Carson Taylor, Thierry Van Cursem, and Vijay Vittal. Definition and classification of power system stability. *IEEE Transactions on Power Systems*, 2004.

[2] ENTSO-E SG SPD. Analysis of CE inter-area oscillations of 19 and 24 february 2011, 2011.

[3] K. E. Martin, D. Hamai, M. G. Adamiak, S. Anderson, M. Begovic, G. Benmouyal, G. Brunello, J. Burger, J. Y. Cai, B. Dickerson, V. Gharpure, B. Kennedy, D. Karlsson, A. G. Phadke, J. Salj, V. Skendzic, J. Sperr, Y. Song, C. Huntley, B. Kasztenny, and E. Price. Exploring the IEEE Standard C37.118-2005 Synchrophasors for Power Systems. *IEEE Transactions on Power Delivery*, 23(4):1805–1811, 2008.

[4] Bahtiyar Can Karatas, Hjortur Johannsson, and Arne Hejde Nielsen. Improved Voltage Stability Boundary Monitoring by Accounting for Variations in Thevenin Voltage Magnitude. In *Proceedings - 2018 IEEE PES Innovative Smart Grid Technologies Conference Europe, ISGT-Europe 2018*, 2018.

[5] Hjörtur Jóhannsson, Arne Hejde Nielsen, and Jacob Østergaard. Wide-Area Assessment of Aperiodic Small Signal Rotor Angle Stability in Real-Time. *IEEE Transactions on Power Systems*, 28(4):4545–4557, 2013.

[6] Tilman Weckesser, Hjörtur Jóhannsson, Jacob Østergaard, and Thierry Van Cutsem. Derivation and application of sensitivities to assess transient voltage sags caused by rotor swings. *International Journal of Electrical Power and Energy Systems*, 72:75–82, 2015.

[7] Jakob Glarbo Moller, Hjortur Johannsson, and Jacob Ostergaard. Super-Positioning of Voltage Sources for Fast Assessment of Wide-Area Thévenin Equivalents. *IEEE Transactions on Smart Grid*, 8(3):1488–1493, 2017.

[8] Evgenia Dmitrova, Martin Lindholm Wittrock, Hjörtur Johannsson, and Arne Hejde Nielsen. Early Prevention Method for Power System Instability. *IEEE Transactions on Power Systems*, 30(4):1784–1792, 2015.

[9] S. Arash Nezam Sarmadi and Vaithianathan Venkatasubramanian. Inter-area resonance in power systems from forced oscillations. *IEEE Transactions on Power Systems*, 2016.

[10] North American Electric Reliability Corporation (NERC). Eastern Interconnection Oscillation Disturbance January 11, 2019 Forced Oscillation Event, 2019.

[11] J. Follum, F. Tuffner, L. Dosiek, and J. Pierre. Power System Oscillatory Behaviors: Sources, Characteristics, & Analyses, May 2017.

[12] North American Electric Reliability Corporation (NERC). Reliability Guideline - Forced Oscillation Monitoring & Mitigation, 2017.

[13] Prabha Kundur. *Power System Stability And Control*. McGraw-Hill, Inc, 1994.

[14] CIGRE Task Force 07.01.38. Analysis and Control of Power System Oscillations. *CIGRE Technical Brochure No. 111*, 1996.

[15] P. Kundur, M. Klein, G. J. Rogers, and M. S. Zywno. Application of power system stabilizers for enhancement of overall system stability. *IEEE Transactions on Power Systems*, 4(2):614–626, 1989.

[16] Graham Rogers. *Power System Oscillations*. Springer US, Boston, MA, 2000.

[17] M. J. Gibbard and D. J. Vowles. Reconciliation of methods of compensation for PSSs in multimachine systems. *IEEE Transactions on Power Systems*, 19(1):463–472, 2004.

[18] D. R. Ostojic. Stabilization of multimodal electromechanical oscillations by coordinated application of power system stabilizers. *IEEE Transactions on Power Systems*, 6(4):1439–1445, 1991.

[19] A. Elices, L. Rouco, H. Bourles, and T. Margotin. Design of robust controllers for damping interarea oscillations: application to the European power system. *IEEE Transactions on Power Systems*, 19(2):1058–1067, 2004.

[20] Narain G. Hingoranl, Laszlo Gyugyi, and Mohamed E. El-Hawary. *Understanding FACTS: Concepts and technology of flexible ac transmission systems*. IEEE Press, Piscataway, NJ, 2000.

[21] M.J. Gibbard, P. Pourbeik, and D.J. Vowles. *Small-signal stability, control and dynamic performance of power systems*. University of Adelaide Press, Adelaide, 2015.

[22] T. Smed and G. Andersson Member. Utilising HVDC to Damp Power Oscillations. *IEEE Transactions on Power Delivery*, 1993.

[23] Brian J. Pierre, Felipe Wilches-Bernal, David A. Schoenwald, Ryan T. Elliott, Daniel J. Trudnowski, Raymond H. Byrne, and Jason C. Neely. Design of the Pacific DC Intertie Wide Area Damping Controller. *IEEE Transactions on Power Systems*, 2019.

[24] S. K. M. Kodsi and C. A. Canizares. Application of a Stability-Constrained Optimal Power Flow to Tuning of Oscillation Controls in Competitive Electricity Markets. *IEEE Transactions on Power Systems*, 22(4):1944–1954, 2007.

[25] R. Zarate-Minano, F. Milano, and A. J. Conejo. An OPF Methodology to Ensure Small-Signal Stability. *IEEE Transactions on Power Systems*, 26(3):1050–1061, 2011.

[26] L. Halilbašić, F. Thams, A. Venzke, S. Chatzivasileiadis, and P. Pinson. Data-driven Security-Constrained AC-OPF for Operations and Markets. In *2018 Power Systems Computation Conference (PSCC)*, pages 1–7, 2018.

[27] C. Y. Chung, Lei Wang, Frederic Howell, and Prabhashankar Kundur. Generation Rescheduling Methods to Improve Power Transfer Capability Constrained by Small-Signal Stability. *Ieee Transactions on Power Systems*, 19(1):524–530, 2004.

[28] Yuri V. Makarov, David J. Hill, and E. Zhao-Yang Dong. Computation of bifurcation boundaries for power systems: A new a-plane method. *Ieee Transactions on Circuits and Systems I: Fundamental Theory and Applications*, 47(4):536–544, 2000.

[29] Sarai Mendoza-Armenta and Ian Dobson. Applying a Formula for Generator Redispatch to Damp Interarea Oscillations Using Synchrophasors. *Ieee Transactions on Power Systems*, 31(4):7305841, 2016.

[30] T. J.M.A. Parreiras, S. Gomes, G. N. Taranto, and K. Uhlen. Closest security boundary for improving oscillation damping through generation redispatch using eigenvalue sensitivities. *Electric Power Systems Research*, 160:119–127, 2018.

[31] Chongtao Li, Hsiao Dong Chiang, and Zhengchun Du. Investigation of an Effective Strategy for Computing Small-Signal Security Margins. *Ieee Transactions on Power Systems*, 33(5):8303722, 2018.

[32] Ruisheng Diao, Zhenyu Huang, Ning Zhou, Yousu Chen, Francis Tuffner, Jason Fuller, Shuangshuang Jin, and Jeff E. Dagle. Deriving optimal operational rules for mitigating inter-area oscillations. *2011 Ieee/pes Power Systems Conference and Exposition, Psce 2011*, page 5772564, 2011.

[33] Chongtao Li, Hsiao Dong Chiang, and Zhengchun Du. Network-Preserving Sensitivity-Based Generation Rescheduling for Suppressing Power System Oscillations. *Ieee Transactions on Power Systems*, 32(5):7811213, 2017.

[34] Draitry N. Kosterev, Carson W. Taylor, and William A. Mittelstadt. Model validation for the august 10,1996 wscc system outage. *IEEE Transactions on Power Systems*, 1999.

[35] ENTSO-E SG SPD. Analysis of CE inter-area oscillations of 1st december 2016, 2017.

[36] ENTSO-E SG SPD. Oscillation Event 03.12.2017, 2018.

[37] C. Steinmetz. Complex Quantities and their Use in Electrical Engineering. In *AIEE Proceedings of International Electrical Congress*, pages 33–74, Chicago, 1894.

[38] IEEE standard for synchrophasors for power systems. *IEEE Std C37.118-2005 (Revision of IEEE Std 1344-1995)*, pages 1–65, 2006.

[39] A. G. Phadke, H. Volskis, R. M. de Moraes, T. Bi, R. N. Nayak, Y. K. Sehgal, S. Sen, W. Sattinger, E. Martinez, O. Samuelsson, D. Novosel, V. Madani, and Y. A. Kulikov. The Wide World of Wide-area Measurement. *IEEE Power and Energy Magazine*, 6(5):52–65, 2008.

[40] I. Kamwa, J. Béland, G. Trudel, R. Grondin, C. Lafond, and D. McNabb. Wide-area monitoring and control at hydro-Québec: Past, present and future. *2006 Ieee Power Engineering Society General Meeting, Pes*, page 1709097, 2006.

[41] K. Uhlen, Tor Rolv Time, Øystein Kirkeluten, and J. Gjerde. Raising stability limits in the nordic power transmission system. In *Proceedings of the 14th Power System Computation Conference (PSCC'02)*, 2002.

[42] R. Majumder, B. Chaudhuri, and B. C. Pal. Implementation and test results of a wide-area measurement-based controller for damping interarea oscillations considering signal-transmission delay. *Iet Generation Transmission and Distribution*, 1(1):1–7, 2007.

[43] Balarko Chaudhuri, Rajat Majumder, and Bikash C. Pal. Wide-area measurement-based stabilizing control of power system considering signal transmission delay. *Ieee Transactions on Power Systems*, 19(4):1971–1979, 2004.

[44] AG PHADKE, JS THORP, and KJ KARIMI. STATE ESTIMATION WITH PHASOR MEASUREMENTS. *Ieee Transactions on Power Systems*, 1(1):233–241, 1986.

[45] Reynaldo F. Nuqui and Arun G. Phadke. Phasor measurement unit placement techniques for complete and incomplete observability. *Ieee Transactions on Power Delivery*, 20(4):2381–2388, 2005.

[46] JF HAUER, CJ DEMEURE, and LL SCHARF. INITIAL RESULTS IN PRONY ANALYSIS OF POWER-SYSTEM RESPONSE SIGNALS. *Ieee Transactions on Power Systems*, 5(1):80–89, 1990.

[47] D. J. Trudnowski, J. M. Johnson, and J. F. Hauer. Making prony analysis more accurate using multiple signals. *Ieee Transactions on Power Systems*, 14(1):226–231, 1999.

[48] M. L. Crow and A. Singh. The matrix pencil for power system modal extraction. *IEEE Transactions on Power Systems*, 20(1):501–502, 2005.

[49] Jean Michel Papy, Lieven De Lathauwer, and Sabine Van Huffel. Common pole estimation in multi-channel exponential data modeling. *Signal Processing*, 86(4):846–858, 2006.

[50] Ning Zhou, Zhenyu Huang, Francis Tuffner, John Pierre, and Shuangshuang Jin. Automatic implementation of prony analysis for electromechanical mode identification from phasor measurements. *Ieee Pes General Meeting, Pes 2010*, page 5590169, 2010.

[51] J. W. Pierre. Initial results in electromechanical mode identification from ambient data. *Ieee Transactions on Power Systems*, 12(3):1245–1251, 1997.

[52] Daniel J. Trudnowski, John W. Pierre, Ning Zhou, John F. Hauer, and Manu Parashar. Performance of three mode-meter block-processing algorithms for automated dynamic stability assessment. *Ieee Transactions on Power Systems*, 23(2):680–690, 2008.

[53] Ning Zhou, John Pierre, and John Hauer. Initial results in power system identification from injected probing signals using a subspace method. *2008 Ieee Power and Energy Society General Meeting*, page 1 pp., 2008.

[54] J. W. Pierre. Initial results in electromechanical mode identification from ambient data. *Ieee Transactions on Power Systems*, 12(3):1245–1251, 1997.

[55] Richard W. Wies, John W. Pierre, and Daniel J. Trudnowski. Use of ARMA block processing for estimating stationary low-frequency electromechanical modes of power systems. *Ieee Transactions on Power Systems*, 18(1):167–173, 2003.

[56] R. W. Wies and J. W. Pierre. Use of least-mean squares (LMS) adaptive filtering technique for estimating low-frequency electromechanical modes in power systems. *Proceedings of the American Control Conference*, 6:4867–4873, 2002.

[57] Ning Zhou, Daniel J. Trudnowski, John W. Pierre, and William A. Mittelstadt. Electromechanical mode online estimation using regularized robust RLS methods. *Ieee Transactions on Power Systems*, 23(4):1670–1680, 2008.

[58] Luke Dosiek, Ning Zhou, John W. Pierre, Zhenyu Huang, and Daniel J. Trudnowski. Mode shape estimation algorithms under ambient conditions: A comparative review. *Ieee Transactions on Power Systems*, 28(2):6299000, 2013.

[59] D. H. Wilson, K. Hay, and G. J. Rogers. Dynamic model verification using a continuous modal parameter estimator. In *2003 IEEE Bologna Power Tech Conference Proceedings,*, volume 2, pages 6 pp. Vol.2–, 2003.

[60] Ning Zhou, John W. Pierre, and John F. Hauer. Initial results in power system identification from injected probing signals using a subspace method. *Ieee Transactions on Power Systems*, 21(3):1296–1302, 2006.

[61] John W. Pierre, Ning Zhou, Francis K. Tuffner, John F. Hauer, Daniel J. Trudnowski, and William A. Mittelstadt. Probing signal design for power system identification. *Ieee Transactions on Power Systems*, 25(2):5338001, 2010.

[62] Sjoerd Boersma, Xavier Bombois, Luigi Vanfretti, Juan Carlos Gonzalez-Torres, and Abdelkrim Benchaib. Probing signal design for enhanced damping estimation in power networks. *International Journal of Electrical Power and Energy Systems*, 129:106640, 2021.

[63] A. Semerow, S. Höhn, M. Luther, W. Sattinger, H. Abildgaard, A. D. Garcia, and G. Giannuzzi. Dynamic Study Model for the interconnected power system of Continental Europe in different simulation tools. In *2015 IEEE Eindhoven PowerTech*, pages 1–6, 2015.

[64] I. A. Hiskens. Nonlinear dynamic model evaluation from disturbance measurements. *IEEE Transactions on Power Systems*, 16(4):702–710, 2001.

[65] Zhenyu Huang, M. Kosterev, R. Guttromson, and T. Nguyen. Model validation with hybrid dynamic simulation. *2006 Ieee Power Engineering Society General Meeting*, page 9 pp., 2006.

[66] ZY Huang, RT Guttromson, and JF Hauer. Large-scale hybrid dynamic simulation employing field measurements. *2004 Ieee Power Engineering Society General Meeting, Vols 1 and 2*, pages 1570–1576, 2004.

[67] Paul C. Krause, Oleg Wasynczuk, and Scott D. Sudhoff. *Machine Equations in Operational Impedances and Time Constants*, chapter 7, pages 271–298. John Wiley Sons, Ltd, 2013.

[68] M. Klein, G. J. Rogers, and P. Kundur. A fundamental study of inter-area oscillations in power systems. *IEEE Transactions on Power Systems*, 6(3):914–921, 1991.

[69] L. Vanfretti, T. Rabuzin, M. Baudette, and M. Murad. iTesla Power Systems Library (iPSL): A Modelica library for phasor time-domain simulations. *SoftwareX*, 2016.

[70] D. Y. Wong, G. J. Rogers, B. Porretta, and P. Kundur. Eigenvalue analysis of very large power systems. *IEEE Transactions on Power Systems*, 1988.

[71] D. M. Lam, H. Yee, and B. Campbell. An efficient improvement of the aesops algorithm for power system Eigenvalue calculation. *IEEE Transactions on Power Systems*, 9(4):1880–1885, 1994.

[72] Joe H. Chow and Kwok W. Cheung. A Toolbox for Power System Dynamics and Control Engineering Education and Research. *IEEE Transactions on Power Systems*, 7(4):1559–1564, 1992.

[73] Patrick R. Amestoy, Timothy A. Davis, and Iain S. Duff. Algorithm 837: AMD, an approximate minimum degree ordering algorithm, 2004.

[74] S. Maslennikov, B. Wang, Q. Zhang, a. Ma, a. Luo, a. Sun, and E. Litvinov. A test cases library for methods locating the sources of sustained oscillations. In *2016 IEEE Power and Energy Society General Meeting (PESGM)*, pages 1–5, 2016.

[75] Kjetil Uhlen, Tor Rolv Time, and Jan Ove Gjerde. Raising Stability Limits in the Nordic Power. In *14th Power System Computation Conference (PSCC)*, 2002.

Appendix

A. Derivatives of the load admittances

A.1. Constant admittance load

$$\frac{\partial \boldsymbol{Y_{ll}}}{\partial V_D} = -\frac{2V_D}{|V|^4}\begin{bmatrix} P_l & Q_l \\ -Q_l & P_l \end{bmatrix} \tag{9.1}$$

$$\frac{\partial \boldsymbol{Y_{ll}}}{\partial V_Q} = -\frac{2V_Q}{|V|^4}\begin{bmatrix} P_l & Q_l \\ -Q_l & P_l \end{bmatrix} \tag{9.2}$$

A.2. Constant current load

$$\frac{\partial Y_{DD}}{\partial VD} = -\frac{2\,CIP\,V_D + CIQ\,V_Q}{|V|^4} + 4\,V_D^2\,\frac{CIP\,V_D + CIQ\,V_Q}{|V|^5} \tag{9.3}$$

$$\frac{\partial Y_{DQ}}{\partial VD} = -\frac{CIP\,V_Q}{|V|^4} + 4\,V_D\,V_Q\,\frac{CIP\,V_D + CIQ\,V_Q}{|V|^5} \tag{9.4}$$

$$\frac{\partial Y_{QD}}{\partial VD} = -\frac{CIP\,V_Q - 2\,CIQ\,V_D}{|V|^4} + 4\,V_D^2\,\frac{CIP\,V_Q - CIQ\,V_D}{|V|^5} \tag{9.5}$$

$$\frac{\partial Y_{QQ}}{\partial VD} = \frac{CIQ\,V_Q}{|V|^4} + 4\,V_D\,VQ\,\frac{CIP\,V_Q - CIQ\,V_D}{|V|^5} \tag{9.6}$$

$$\frac{\partial Y_{DD}}{\partial VQ} = -\frac{CIQ\,V_D}{|V|^4} + 4\,V_D\,V_Q\,\frac{CIP\,V_D + CIQ\,V_Q}{|V|^5} \tag{9.7}$$

$$\frac{\partial Y_{DQ}}{\partial VQ} = -\frac{CIP\,V_D + 2\,CIQ\,V_Q}{|V|^4} + 4\,V_Q^2\,\frac{CIP\,V_D + CIQ\,V_Q}{|V|^5} \tag{9.8}$$

$$\frac{\partial Y_{QD}}{\partial VQ} = -\frac{CIP\,V_D}{|V|^4} + 4\,V_D\,V_Q\,\frac{CIP\,V_Q - CIQ\,V_D}{|V|^5} \tag{9.9}$$

$$\frac{\partial Y_{QQ}}{\partial VQ} = -\frac{2\,CIP\,V_Q - CIQ\,V_D}{|V|^4} + 4\,V_Q^2\,\frac{CIP\,V_Q - CIQ\,V_D}{|V|^5} \tag{9.10}$$

A.3. Constant power load

$$\frac{\partial Y_{DD}}{\partial VD} = -2\left(\frac{2\,CP\,V_D + CQ\,V_Q}{|V|^4} + 4\,V_D^2\,\frac{CP\,V_D + CQ\,V_Q}{|V|^5}\right) \tag{9.11}$$

$$\frac{\partial Y_{DQ}}{\partial VD} = -2\left(\frac{CP\,V_Q}{|V|^4} + 4\,V_D\,V_Q\,\frac{CP\,V_D + CQ\,V_Q}{|V|^5}\right) \tag{9.12}$$

$$\frac{\partial Y_{QD}}{\partial VD} = -2\left(\frac{CP\,V_Q - 2\,CQ\,V_D}{|V|^4} + 4\,V_D^2\,\frac{CP\,V_Q - CQ\,V_D}{|V|^5}\right) \tag{9.13}$$

$$\frac{\partial Y_{QQ}}{\partial VD} = -2\left(\frac{CQ\,V_Q}{|V|^4} + 4\,V_D\,V_Q\,\frac{CP\,V_Q - CQ\,V_D}{|V|^5}\right) \tag{9.14}$$

$$\frac{\partial Y_{DD}}{\partial VQ} = -2\left(\frac{CQ\,V_D}{|V|^4} + 4\,V_D\,V_Q\,\frac{CP\,V_D + CQ\,V_Q}{|V|^5}\right) \tag{9.15}$$

$$\frac{\partial Y_{DQ}}{\partial VQ} = -2\left(\frac{CP\,V_D + 2\,CIQ\,V_Q}{|V|^4} + 4\,V_Q^2\,\frac{CIP\,V_D + CIQ\,V_Q}{|V|^5}\right) \tag{9.16}$$

$$\frac{\partial Y_{QD}}{\partial VQ} = -2\left(\frac{CP\,V_D}{|V|^4} + 4\,V_D\,V_Q\,\frac{CP\,V_Q - CQ\,V_D}{|V|^5}\right) \tag{9.17}$$

$$\frac{\partial Y_{QQ}}{\partial VQ} = -2\left(\frac{2\,CP\,V_Q - CQ\,V_D}{|V|^4} + 4\,V_Q^2\,\frac{CP\,V_Q - CQ\,V_D}{|V|^5}\right) \tag{9.18}$$

B. Derivatives of the machine transfer functions

B.1. Derivatives of the machine transfer functions in respect to s

$$\frac{G_{IV}}{\partial s} = \begin{bmatrix} \frac{1}{2}\sin(2\delta) & -\cos^2\delta \\ \sin^2\delta & -\frac{1}{2}\sin(2\delta) \end{bmatrix} \frac{\partial dx}{\partial s} + \begin{bmatrix} -\frac{V_D \sin\delta}{x_{ds}} & \frac{V_Q \sin\delta}{x_{ds}} \\ \frac{V_D \cos\delta}{x_{ds}} & \frac{V_Q \cos\delta}{x_{ds}} \end{bmatrix} \frac{\partial K_1}{\partial s} + \begin{bmatrix} \frac{K_1 V_D \sin\delta}{x_{ds}^2} & \frac{1+K_1 V_Q \sin\delta}{x_{ds}^2} \\ -\frac{1+K_1 V_D \cos\delta}{x_{ds}^2} & -\frac{K_1 V_Q \cos\delta}{x_{ds}^2} \end{bmatrix} \frac{\partial x_{ds}}{\partial s} \tag{9.19}$$

$$\frac{\partial G_{I\delta}}{\partial s} = \begin{bmatrix} -\frac{V_d \sin\delta}{x_{ds}^2} \\ \frac{V_d \cos\delta}{x_{ds}^2} \end{bmatrix} \frac{\partial x_{ds}}{\partial s} - \begin{bmatrix} \frac{V_q \cos\delta}{x_{qs}^2} \\ \frac{V_q \sin\delta}{x_{qs}^2} \end{bmatrix} \frac{\partial x_{qs}}{\partial s} \tag{9.20}$$

$$\frac{\partial G_{IVr}}{\partial s} = \begin{bmatrix} \frac{G_{avr}}{x_{ds}} \sin\delta \\ \frac{G_{avr}}{x_{ds}} \cos\delta \end{bmatrix} \frac{\partial G_s}{\partial s} + \begin{bmatrix} \frac{G_s}{x_{ds}} \sin\delta \\ \frac{G_s}{x_{ds}} \cos\delta \end{bmatrix} \frac{\partial G_{avr}}{\partial s} - \begin{bmatrix} \frac{G_{avr} G_s}{x_{ds}^2} \sin\delta \\ \frac{G_{avr} G_s}{x_{ds}^2} \cos\delta \end{bmatrix} \frac{\partial x_{ds}}{\partial s} \tag{9.21}$$

$$\frac{\partial G_{TV}}{\partial s} = \begin{bmatrix} V_q \sin\delta \\ -V_q \cos\delta \end{bmatrix}^T \frac{\partial dx}{\partial s} + \begin{bmatrix} \frac{V_D V_d}{x_{ds}} \\ -\frac{V_Q V_d}{x_{ds}} \end{bmatrix}^T \frac{\partial K_1}{\partial s} + \begin{bmatrix} -\frac{V_Q - K_1 V_D V_d}{x_{ds}^2} \\ \frac{V_D + K_1 V_D V_d}{x_{ds}^2} \end{bmatrix}^T \frac{\partial x_{ds}}{\partial s} \tag{9.22}$$

$$\frac{\partial G_{T\delta}}{\partial s} = -\frac{V_d^2}{x_{ds}^2} \frac{\partial x_{ds}}{\partial s} - \frac{V_q^2}{x_{ds}^2} \frac{\partial x_{qs}}{\partial s} \tag{9.23}$$

$$\frac{\partial G_{TVr}}{\partial s} = \frac{V_d}{x_{ds}} G_{avr} \frac{\partial G_s}{\partial s} + \frac{V_d}{x_{ds}} G_s \frac{\partial G_{avr}}{\partial s} - \frac{V_d G_s G_{avr}}{x_{ds}^2} \frac{\partial x_{ds}}{\partial s} \tag{9.24}$$

With

$$\frac{\partial dx}{\partial s} = \frac{1}{x_{ds}^2} \frac{\partial x_{ds}}{\partial s} - \frac{1}{x_{qs}^2} \frac{\partial x_{qs}}{\partial s} \tag{9.25}$$

$$\frac{\partial K_1}{\partial s} = \frac{G_{avr}}{V_t} \frac{\partial G_s}{\partial s} + \frac{G_s}{V_t} \frac{\partial G_{avr}}{\partial s} \tag{9.26}$$

$$\frac{\partial G_s}{\partial s} = \frac{T_{kd} - G_s(T_{1d} + T_{2d} + 2T_{1d}T_{3d}\, s)}{1 + (T_{1d} + T_{2d})s + T_{1d}T_{3d}\, s^2} \tag{9.27}$$

$$\frac{\partial x_{ds}}{\partial s} = \frac{1}{D_d}\left(\frac{\partial N_d}{\partial s}\, x_d - x_{ds} \frac{\partial D_d}{\partial s}\right) \tag{9.28}$$

$$\frac{\partial x_{qs}}{\partial s} = \frac{1}{D_q}(\frac{\partial N_q}{\partial s}\, x_q - x_{qs}\frac{\partial D_q}{\partial s}) \tag{9.29}$$

$$x_{ds} = \frac{N_d}{D_d}\, x_d = \frac{1 + (T_{4d} + T_{5d})\, s + T_{4d}T_{6d}\, s^2}{1 + (T_{1d} + T_{2d})\, s + T_{1d}T_{3d}\, s^2}\, x_d \tag{9.30}$$

$$x_{qs} = \frac{N_q}{D_q}\, x_q = \frac{1 + (T_{4q} + T_{5q})\, s + T_{4q}T_{6q}\, s^2}{1 + (T_{1q} + T_{2q})\, s + T_{1q}T_{3q}\, s^2}\, x_q \tag{9.31}$$

$$\frac{\partial N_d}{\partial s} = T_{4d} + T_{5d} + 2T_{4d}T_{6d}\, s; \tag{9.32}$$

$$\frac{\partial D_d}{\partial s} = T_{1d} + T_{2d} + 2T_{1d}T_{3d}\, s \tag{9.33}$$

$$\frac{\partial N_q}{\partial s} = T_{4q} + T_{5q} + 2T_{4q}T_{6q}\, s \tag{9.34}$$

$$\frac{\partial D_q}{\partial s} = T_{1q} + T_{2q} + 2T_{1q}T_{3q}\, s \tag{9.35}$$

B.2. Derivatives of the machine transfer functions in respect to steady state quantities

$$\frac{\Delta G_{IV}}{\Delta P} = \begin{bmatrix} dx\cos(2\delta) - \frac{K_1 V_D \cos\delta}{x_{ds}} & dx\sin(2\delta) - \frac{K_1 V_Q \cos\delta}{x_{ds}} \\ dx\sin(2\delta) - \frac{K_1 V_D \sin\delta}{x_{ds}} & -dx\cos(2\delta) - \frac{K_1 V_Q \sin\delta}{x_{ds}} \end{bmatrix} \frac{\Delta\delta}{\Delta P} + \begin{bmatrix} \frac{-K_1\sin\delta}{x_{ds}} & -\frac{K_1\sin\delta}{x_{ds}} \\ \frac{K_1\cos\delta}{x_{ds}} & \frac{K_1\cos\delta}{x_{ds}} \end{bmatrix} \begin{bmatrix} \frac{\Delta V_D}{\Delta P} \\ \frac{\Delta V_Q}{\Delta P} \end{bmatrix} \tag{9.36}$$

$$\frac{\Delta G_{I\delta}}{\Delta P} = \begin{bmatrix} \frac{\sin\delta}{x_{ds}} & \frac{\cos\delta}{x_{qs}} \\ \frac{-\cos\delta}{x_{ds}} & \frac{\sin\delta}{x_{qs}} \end{bmatrix} \begin{bmatrix} \frac{\Delta V_d}{\Delta P} \\ \frac{\Delta V_q}{\Delta P} \end{bmatrix} + \begin{bmatrix} \frac{V_d\cos\delta}{x_{ds}} + \frac{-V_q\sin\delta}{x_{qs}} \\ \frac{V_d\sin\delta}{x_{ds}} + \frac{V_q\cos\delta}{x_{qs}} \end{bmatrix} \frac{\Delta\delta}{\Delta P} + \begin{bmatrix} \frac{-\Delta I_Q}{\Delta P} \\ \frac{\Delta I_D}{\Delta P} \end{bmatrix} \tag{9.37}$$

$$\frac{\Delta G_{IVr}}{\Delta P} = \begin{bmatrix} \frac{G_s G_{avr}\cos\delta}{x_{ds}} \\ \frac{G_s G_{avr}\sin\delta}{x_{ds}} \end{bmatrix} \frac{\Delta\delta}{\Delta P} \tag{9.38}$$

$$\frac{\Delta G_{TV}}{\Delta P} = \left[\begin{bmatrix} dxV_q\cos\delta \\ dxV_q\sin\delta \end{bmatrix} \frac{\Delta\delta}{\Delta P} + \begin{bmatrix} \frac{\Delta I_D}{\Delta P} \\ \frac{\Delta I_Q}{\Delta P} \end{bmatrix} + \begin{bmatrix} \frac{-K_1 V_D}{x_{ds}} & dx\sin\delta \\ \frac{-K_1 V_Q}{x_{ds}} & -dx\cos\delta \end{bmatrix} \begin{bmatrix} \frac{\Delta V_d}{\Delta P} \\ \frac{\Delta V_q}{\Delta P} \end{bmatrix} \right]^T - \left[\begin{bmatrix} \frac{K_1 V_d}{x_{ds}} & \frac{1}{x_{ds}} \\ -\frac{1}{x_{ds}} & \frac{K_1 V_d}{x_{ds}} \end{bmatrix} \begin{bmatrix} \frac{\Delta V_D}{\Delta P} \\ \frac{\Delta V_Q}{\Delta P} \end{bmatrix} \right]^T \tag{9.39}$$

$$\frac{\Delta G_{T\delta}}{\Delta P} = \begin{bmatrix} \frac{2V_d}{x_{ds}} \\ \frac{2V_q}{x_{ds}} \end{bmatrix}^T \begin{bmatrix} \frac{\Delta V_d}{\Delta P} \\ \frac{\Delta V_q}{\Delta P} \end{bmatrix} + \begin{bmatrix} -I_Q \\ I_D \end{bmatrix}^T \begin{bmatrix} \frac{\Delta V_D}{\Delta P} \\ \frac{\Delta V_Q}{\Delta P} \end{bmatrix} + \begin{bmatrix} V_Q \\ -V_D \end{bmatrix}^T \begin{bmatrix} \frac{\Delta I_D}{\Delta P} \\ \frac{\Delta I_Q}{\Delta P} \end{bmatrix} \tag{9.40}$$

$$\frac{\Delta G_{TVr}}{\Delta P} = \frac{G_s G_{avr}}{x_{ds}} \frac{\Delta V_d}{\Delta P} \tag{9.41}$$

$$\begin{bmatrix} \frac{\Delta V_d}{\Delta P} \\ \frac{\Delta V_q}{\Delta P} \end{bmatrix} = \begin{bmatrix} V_q \\ -V_d \end{bmatrix} \frac{\Delta \delta}{\Delta P} + \begin{bmatrix} \sin\delta & -\cos\delta \\ \cos\delta & \sin\delta \end{bmatrix} \begin{bmatrix} \frac{\Delta V_D}{\Delta P} \\ \frac{\Delta V_Q}{\Delta P} \end{bmatrix} \tag{9.42}$$

Department of Electrical Engineering
Center for Electric Power and Energy (CEE)
Technical University of Denmark
Elektrovej, Building 325
DK-2800 Kgs. Lyngby
Denmark

www.elektro.dtu.dk/cee
Tel: (+45) 45 25 35 00
Fax: (+45) 45 88 61 11
E-mail: cee@elektro.dtu.dk